STATIC AND ROTORDYNAMIC CHARACTERISTICS OF LIQUID ANNULAR SEALS WITH A CIRCUMFERENTIALLY-GROOVED STATOR AND SMOOTH ROTOR USING THREE LEVELS OF CIRCUMFERENTIAL INLET-FLUID ROTATION

A Thesis

by

JOSE MARIA TORRES

Submitted to the Office of Graduate and Professional Studies of
Texas A&M University
in partial fulfillment of the requirements for the degree of

MASTER OF SCIENCE

Chair of Committee,	Dara W. Childs
Committee Members,	Gerald L. Morrison
	Douglas M. Kingman
Head of Department,	Andreas Polycarpou

December 2016

Major Subject: Mechanical Engineering

ABSTRACT

Original Equipment Manufacturers (OEMs) increase pump efficiency by reducing process fluid leakage from high-pressure stages into low-pressure ones. Smooth, liquid annular seals are used between pump stages to achieve this goal. In an effort to reduce leakage, OEMs sometimes machine circumferential grooves in the stators of annular liquid seals. Unfortunately, grooved seals do more than improve pump efficiency; they sometimes help degrade the system's (pump, motor) rotordynamics, causing adverse effects that overshadow its helpful qualities. The rotordynamic community recognizes that fluid rotating in the shaft direction, at the entrance of the seal, is a source instability. The relevant literature lacks test results showing how high levels of inlet-fluid rotation affect a grooved seal's performance, and how this effect changes as the shaft operates very close to the stator. The present study addresses this lack.

Supplied with VG2 oil @ 46 °C (115 °F), the grooved seal used for this investigation has a length-to-diameter ratio L/D of 0.5, and a minimum radial clearance C_r of 203 µm (8 mil). It features 15 circumferential grooves with a length G_l, and depth G_d of 1.52 mm (60 mils), which are equally-spaced by a land length of 1.52 mm (60 mils). The experimenter conducts tests at shaft angular speeds ω of 2, 4, and 6 krpm, eccentricity ratios ϵ_0 of 0.00, 0.27, 0.53, and 0.80, and axial pressure drops ΔP of 2.1, 4.1, 6.2, 8.3 bar (30, 60, 90, 120 PSI). Using 3 distinct inlet-fluid rotation inserts, the author induces increasing levels of circumferential fluid velocity at the seal's inlet. Pre-swirl ratio (PSR) and outlet swirl ratio (OSR) are defined as the ratio of circumferential velocity at the seal's inlet and outlet, respectively, to the rotor's tangential surface velocity.

To assess the seal's static performance, the author measures leakage rate $\dot{Q}$, eccentricity ratio ϵ_0, PSR, and OSR. To assess the seal's dynamic performance, the author measures stator-rotor relative displacement, stator acceleration, and dynamic excitations. The author uses the dynamic measurements to calculate the seal's rotordynamic coefficients and Whirl Frequency Ratio (WFR). Finally, the author calculates effective stiffness and damping coefficients to compare the grooved seal's rotordynamic performance to that of a smooth seal with the same C_r, L/D, and operating conditions.

In regards to static performance, the grooved seal's leakage rate ranges from a low 15.64 LPM (4.13 GPM) at ω = 6 krpm, and ΔP = 2 bar (30 PSI), to a high 56.36 LPM (14.16 GPM) at ω = 2 krpm, and ΔP = 8 bar (120 PSI). When compared to the smooth seal, the grooved seal provides a 20% $\dot{Q}$ reduction at ω = 2 krpm, and a 6% reduction at ω = 6 krpm.

Test results show all of the smooth seal's rotordynamic coefficients increase markedly for ϵ_0 > 0.50, while those of the grooved seal generally remain unchanged through the entire eccentricity range. In essence, the grooves eliminate the seal's dependency on eccentricity. Next, the grooved seal generally produces lower-magnitude cross-coupled stiffness and damping coefficient values than the smooth seal. Furthermore, the only positive effective stiffness values arise from the smooth seal operating at ω = 2 krpm. The smooth seal consistently produces higher K_{eff} than the grooved seal. Specifically, the smooth seal's effective stiffness is higher than that of the grooved seal by at least 30% at ω = 6 krpm, across the ΔP range, for ϵ_0 = 0.00. Also, the grooved seal's measured OSR is lower than that of the smooth seal by at least 10%, across the test matrix, suggesting that the grooves effectively slow down circumferential flow. For the grooved seal, the test program measures PSR values ranging from ~0 to 0.98, and OSR values bounded between 0.21 and 0.34. At ω = 2 krpm, increasing PSR across its range reduces the grooved seal's direct stiffness and damping, drives its cross-coupled stiffness and damping away from zero, increases its whirl frequency ratio (WFR) from ~0 to 0.8, and reduces its effective damping by a factor of approximately 3.5 when operating at ΔP = 8.3 bar [120 PSI]. In general, the smooth seal produces larger effective stiffness and damping coefficients than the grooved seal, highlighting the grooves' adverse effect on seal rotordynamics.

Using XLCGvr®, a code that calculates $\dot{Q}$ and rotordynamic coefficients for centered, circumferentially-grooved annular seals, the author performs a measurement-vs.-prediction comparison. The code over predicts $\dot{Q}$ by at least 15%. The stiffness, damping, and virtual mass coefficients are all under predicted by at least 50%. While the author used the code's default empirical parameters, modifying them could have improved its accuracy.

DEDICATION

I dedicate this work to you: the motivated, knowledge-hungry scholar who will continue advancing and expanding our scientific understanding.

ACKNOWLEDGEMENTS

Alex J. Moreland, Joshua T. Bullock: Thanks for turning endless obstacles into countless victories. Without exaggerating, I could not have done this without you.

Jesus Salas, Ivan Cortez, Matthew Kluitenberg, Clay Norrbin, Jimmy McLean, and Andrew Crandall: Your work and mentorship was essential to the completion of this work; your unique personalities made this journey enjoyable and unforgettable.

Stephen Phillips, Dr. Luis San Andres, Dr. Morrison, and Ray Mathews: Thanks for sharing your technical expertise, providing valuable support, and guiding me throughout this project.

Dr. Dara Childs: Working at the Turbomachinery Lab improved my engineering judgment, and prepared me for the next stage in my career. More importantly, you demonstrated that no matter how successful, honesty and humbleness should always shine bright in our character. Thank you!

My dear Family: Mom, Dad, Brother and Sister: Your support, motivation, love, and most importantly… your persistent example of self-improvement, were the engines propelling me towards the completion of this work.

The following also deserve profound acknowledgments:

- I was looking to rent a room; instead, I found a home with Eric and Mindy.
- I feel fortunate to have employment at ExxonMobil.
- Music…music was the lubrication for this work.

NOMENCLATURE

$\boldsymbol{A}_{ij}$	Frequency domain stator acceleration [L/T^2]
c	Seal cross-coupled damping coefficient as used in Eq. (2). When C_{xy} != C_{yx}, c becomes their average [FT/L]
C	Seal direct damping coefficient as used in Eq. (2). When C_{xx} != C_{yy}, C becomes their average [FT/L]
C_{eff}	Seal effective damping coefficient [FT/L]
C_{ij}	Damping coefficients [FT/L]
C_r	Minimum seal radial clearance [L]
C_r/R	Clearance-to-radius ratio [-]
D	Seal inner diameter [L]
$\boldsymbol{D}_{ij}$	Frequency domain stator displacement [L]
F_r	Fluid-film reaction force [F]
f_{sx}, f_{sy}	Fluid-film reaction-force components in the *x* and *y* directions [F]
F_s	Applied static load [F]
f_x, f_y	Applied dynamic forces in the *x* and *y* directions [F]
$\boldsymbol{F_x}$, $\boldsymbol{F_y}$	Frequency domain excitation forces in the *x* and *y* directions [F]
G_d	Seal groove depth [L]
G_l	Seal groove axial length [L]
$\boldsymbol{H}_{ij}$	Frequency domain impedance, or dynamic stiffness [F/L]
k	Seal cross-coupled stiffness coefficient as used in Eq. (2). When K_{xy} != K_{yx}, k becomes their average [F/L]
K	Seal direct stiffness coefficient as used in Eq. (2). When K_{xx} != K_{yy}, K becomes their average [F/L]
K_{eff}	Seal effective stiffness coefficient [F/L]
K_{eq}	Seal Equivalent stiffness coefficient [F/L]
K_{ij}	Seal stiffness coefficients [F/L]
L	Seal axial length [L]

m	Seal cross-coupled virtual mass coefficient as used in Eq. (2). When M_{xy} != M_{yx}, m becomes their average [M]
M	Seal direct virtual mass coefficient as used in Eq. (2). When M_{xx} != M_{yy}, M becomes their average [M]
M_{ij}	Seal virtual mass coefficients [M]
M_s	Stator mas [M]
$\dot{Q}$	Individual Seal volumetric leakage rate (1/2 of total measured flow-rate) [L^3/T]
R	Shaft radius [L]
Re	Vector Reynolds number, defined in Eq. (23) [-]
Re_θ	Circumferential Reynolds number, defined in Eq. (24) [-]
Re_z	Axial Reynolds number, defined in Eq. (25) [-]
v_{inlet}	Average circumferential velocity at the inlet of the seal [L/T]
v_{outlet}	Average circumferential velocity at the outlet of the seal [L/T]
$\ddot{x}, \ddot{y}$	Stator accelerations in the x, and y directions [L/T^2]

Greek Symbols

ϵ_0	Eccentricity ratio [-]
ΔP	Axial pressure-drop across the seal [F L^2]
$\Delta x, \Delta y$	Stator-rotor relative displacement [L]
ρ	Fluid density [M/L^3]
ω	Angular shaft speed [T^{-1}]
Ω	Excitation frequency [T^{-1}]

Subscripts

i	Direction of system response, $i = x, y$
j	Direction of perturbation, $j = x, y$

Abbreviations

CGS/SR	Circumferentially-grooved seal/smooth rotor. “grooved seal”
DE	Drive end
ESP	Electrical submersible pump
FFT	Fast Fourier Transform
NDE	Non drive end
OEM	Original equipment manufacturer
OSR	Outlet swirl ratio, defined in Eq. (8)
PSR	Pre-swirl ratio, defined in Eq. (7)
SS/SR	Smooth Seal/Smooth Rotor. “smooth seal”
SSS	Spring stabilization system
VFD	Variable frequency drive
WFR	Whirl frequency ratio, defined in Eq. (3)

TABLE OF CONTENTS

Page

LIST OF FIGURES

Page

LIST OF TABLES

Page

1. INTRODUCTION

Faced with increasingly challenging reservoir environments, today's upstream companies could benefit from an improved understanding of pump rotordynamics. From a production standpoint, for example, increasing the reliability of Electrical Submersible Pumps (ESPs) would facilitate the development of subsea oil reservoirs [1]. Common to most pumps, liquid annular seals originally designed to control leakage across stages also affect the pump's response and stability [2].

Portraying a typical ESP configuration, Fig. 1 reveals a commonality across all pump seals: a thin film of process fluid forms in the annulus between a stationary (stator) and a rotating (rotor) component. While minute in thickness, this fluid film plays a noticeable role on the system's stability and response [2].

Throughout its history, the pump industry has experimented with various seal geometries and configurations. Having the simplest geometry, plain annular seals feature a smooth rotor operating on a smooth stator. Additionally, some OEMs machine circumferential grooves on the stator or rotor in an effort to further decrease leakage rates, and increase component durability [3].

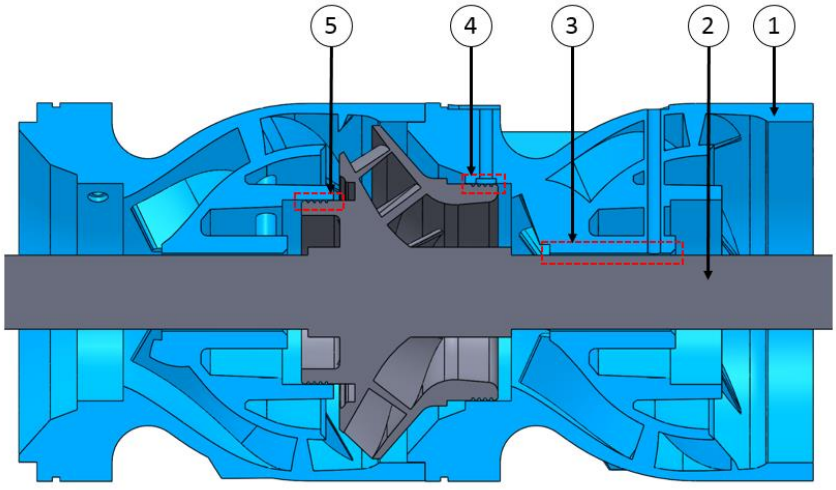

Item	Description
1	Housing (Stator)
2	Shaft/Impeller (Rotor)
3	Interstage Seal
4	Front wear ring seal
5	Rear wear seal

Figure 1. Cross-section view of typical pump stage with seal locations. Adapted from [3].

With a typical clearance-to-radius ratio C_r/R of 0.003, annular liquid seals develop reaction forces via the hydrodynamic bearing effect, and the Lomakin effect [4]. San Andres [5] attributes the appearance of the bearing effect to the interaction between the rotating shaft, the thin fluid film, and the stationary component. In short, when a bearing operates eccentrically, the shaft's angular speed ω forces fluid into a converging wedge, generating a positive pressure gradient around the location of minimum clearance, while the maximum-clearance region cavitates into a low pressure field. The combination of these two events creates a bearing restoring force that supports the rotor.

In contrast to plain journal bearings, annular seals have large supply pressures that preclude cavitation, and hinder the hydrodynamic lift effect [2]. Next, arising from axial pressure drops ΔP at the inlet and through the land of the seal, the Lomakin effect provides a restoring force. Childs [2] summarizes Lomakin's 1958 [4] explanation of a direct stiffness in annular seals.

Headlining the following seal-rotordynamics primer, Table 1 summarizes typical rotordynamic coefficients, and Fig. 2 shows their arrangement on a generic shaft-fluid-seal configuration.

Table 1. Summary of typical rotordynamic coefficients in turbomachines.

Coefficient name	Sym.	Physical representation
Direct stiffness	K_{ii}	Proportional to the reaction force *parallel* to a *displacement*.
Cross-coupled stiffness	K_{ij}	Proportional to the reaction force *perpendicular* to a *displacement*.
Direct damping	C_{ii}	Proportional to the reaction force *parallel* to a *velocity*.
Cross-coupled damping	C_{ij}	Proportional to the reaction force *perpendicular* to a *velocity*.
Direct virtual mass	M_{ii}	Proportional to the reaction force *parallel* to an *acceleration*.
Cross-coupled virtual mass	M_{ij}	Proportional to the reaction force *perpendicular* to an *acceleration*.

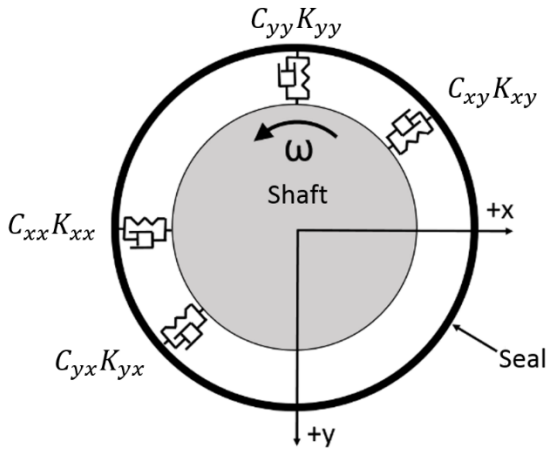

Figure 2. Typical rotordynamic coefficients emerging from the fluid-structure interaction between the seal, the lubricant, and the shaft. Adapted from [6].

Rotordynamic coefficients are used to model the seal's reaction force components f_{sx}, f_{sy} for small perturbations about an equilibrium position in the following reaction-force model:

$$-\begin{Bmatrix} f_{sx} \\ f_{sy} \end{Bmatrix} = \begin{bmatrix} K_{xx} & K_{xy} \\ K_{yx} & K_{yy} \end{bmatrix} \begin{Bmatrix} \Delta x \\ \Delta y \end{Bmatrix} + \begin{bmatrix} C_{xx} & C_{xy} \\ C_{yx} & C_{yy} \end{bmatrix} \begin{Bmatrix} \Delta \dot{x} \\ \Delta \dot{y} \end{Bmatrix} + \begin{bmatrix} M_{xx} M_{xy} \\ M_{yx} M_{yy} \end{bmatrix} \begin{Bmatrix} \Delta \ddot{x} \\ \Delta \ddot{y} \end{Bmatrix} \quad (1)$$

where $\Delta x, \Delta y$; $\Delta \dot{x}, \Delta \dot{y}$; and $\Delta \ddot{x}, \Delta \ddot{y}$, are the relative displacement, velocity, and acceleration components, respectively, between the seal and the shaft, in their corresponding x and y directions. Also, the K_{ij}, C_{ij}, and M_{ij} coefficients are a function of ϵ_0. For small motion about a centered position, the eccentricity-dependent model of Eq. (1) is frequently replaced by the following simplified reaction-force model:

$$-\begin{Bmatrix} f_{sx} \\ f_{sy} \end{Bmatrix} = -\begin{bmatrix} K & k \\ -k & K \end{bmatrix} \begin{Bmatrix} \Delta x \\ \Delta y \end{Bmatrix} - \begin{bmatrix} C & c \\ -c & C \end{bmatrix} \begin{Bmatrix} \Delta \dot{x} \\ \Delta \dot{y} \end{Bmatrix} - \begin{bmatrix} M & m \\ -m & M \end{bmatrix} \begin{Bmatrix} \Delta \ddot{x} \\ \Delta \ddot{y} \end{Bmatrix} \quad (2)$$

where $K = K_{xx} = K_{yy}$, $k = K_{xy} = -K_{yx}$, $C = C_{xx} = C_{yy}$, $c = C_{xy} = -C_{yx}$, $M = M_{xx} = M_{yy}$, $m = M_{xy} = -M_{yx}$.

The model of Eq. (2) is generally assumed to be valid for $\epsilon_0 < 0.5$.

To continue, first developed by Lund [7], and used to compare bearing stability across different operating conditions, the whirl-frequency ratio WFR is

$$WFR^2 = \frac{\left(K_{eq} - K_{xx}\right)\left(K_{eq} - K_{yy}\right) - \left(K_{xy}K_{yx}\right)}{\omega^2(C_{xx}C_{yy} - C_{xy}C_{yx})} \tag{3}$$

where K_{eq} is

$$K_{eq} = \frac{K_{xx}C_{yy} + K_{yy}C_{xx} - K_{xy}C_{yx} - K_{yx}C_{xy}}{C_{xx} + C_{yy}} \tag{4}$$

While San Andres [8] developed a WFR model that accounts for significant cross-coupled virtual mass magnitudes, Eq.(4) is adequate for the grooved seals studied here since their cross-coupled mass terms are small relative to the direct virtual mas terms.

Next, the author uses effective stiffness K_{eff} and effective damping C_{eff} to determine how machining circumferential grooves into a smooth seal affect its rotordynamic performance. K_{eff} tells how centering forces compare, and is defined as

$$K_{eff} = -K + C\omega - M\omega^2 \tag{5}$$

C_{eff} tells how damping forces compare, and is defined as

$$C_{eff} = C\left(1 - \frac{K}{C\omega}\right) \tag{6}$$

Note that the effective stiffness and damping coefficient equations only apply for centered orbits where ϵ_0 is approximately equal to zero.Typically, rotordynamically stable annular seals feature high values of C, K_{eff}, C_{eff}, and low values of WFR. Conversely, high, opposite values of K_{xy} and K_{yx} are often found on systems plagued with instabilities [2]. Defining the circumferential fluid velocity at the seal's inlet as v_{inlet} and at its outlet as v_{outlet}, the author calculates the seal's PSR and OSR as

$$PSR = \frac{v_{inlet}}{\omega R} \tag{7}$$

$$OSR = \frac{v_{outlet}}{\omega R} \tag{8}$$

In terms of predictions for grooved seals, Florjancic and McCloskey [9] developed a three-control-volume model for a circumferentially-grooved-stator (CGS) seal operating on a

smooth rotor in 1990, generating acceptable predictions for centered configurations with high ΔPs (60 bar), and a low pre-swirl ratio (PSR) of 0.25. Six years later, Marquette and Childs [10] expanded their three-control-volume approach by introducing diverging flow in the groove sections. When compared to Florjancic and McCloskey's original three-control-volume approach, their expansion offered increased consistency and a prediction of lower direct damping values. In 2004, Arghir and Frene [11] used the SIMPLE algorithm to model CGS annular seals with ϵ_0 up to 0.50. When compared to Marquette and Childs' [12] experimental data at ΔPs greater than 40 bar (580.15 PSI), and ω greater than 10.2 krpm, Arghir's model yielded adequate predictions.

In terms of testing, Iwatsubo et al. [13] measured the static and dynamic characteristics of turbulent-flow plain annular seals using water as the fluid medium. They varied ω from 0.5 to 3.5 krpm, ΔP from 1.9 to 8.8 bars (27.6 to 127.5 PSI), and PSR values from 0 to approximately 1.7. They conclude that while increasing PSR doesn't affect leakage performance, it tends to noticeably destabilize the system. Next, Kilgore and Childs [14] measured leakage rates and K_{eff}, C_{eff} values for six CGS liquid-seals in 1990, while varying ω from 1 to 7.2 krpm, and ΔP from 2.5 to 27.5 bars (36.26 to 399.85 PSI), under turbulent flow conditions. Their tests were centered and did not induce fluid rotation at the seal's inlet. Their test results suggest that the Hirs' friction model poorly predicts the friction factor of grooved seals with orbiting-rotors, which significantly lowers the leakage rate prediction accuracy. Despite this poor friction correlation, they obtain reasonable predictions for rotordynamic stiffness. Also in 1990, Florjancic and McCloskey [9] measured results for centered, smooth and CGS seals under turbulent conditions, with a max ΔP of 60 bar (870.2 PSI), and an inlet-swirl ratios of 0.15. They used these results to validate their own three-control-volume model. In 1996, Marquette et al [12] used a similar test rig to the one described in here to measure leakage and rotordynamic performance of CGS seals while varying ΔP from 41 to 64 bar (594.66 to 928.45 PSI), ω from 10.2 to 24.6 krpm, and ϵ_0 from 0.00 to 0.50. They concluded that the grooves provide an increase in sealing capacity at the cost of small and even negative direct stiffness coefficients, and acknowledge the lack of control or measurement of inlet-fluid rotation as drawback of their test program. In 2007, Childs et al. [15] conducted experiments with laminar-flow seals having different groove

depths, and determined that while increasing groove depth reduces all rotordynamic coefficients, except M_{ii}, it played a negligible effect on seal leakage.

2. STATEMENT OF WORK

While literature exists on models and test programs regarding CGS, liquid annular seals, the author is unaware of any that measure inlet and outlet-fluid rotation across a complete range of ϵ_0, and PSRs. Consequently, the present test program uses hardware and instrumentation to induce and record three levels of PSR, ranging from approximately 0.0 to 0.98, over ϵ_0 ranging from 0.0 to 0.8. As the main objective, the author aims to measure the effects of increasing inlet-fluid rotation on the rotordynamic performance of CGS liquid annular seals. Additionally, the author uses the test matrix shown in Table 2 to determine how seal performance reacts to changes in ΔP, ω, and ϵ_0, for each level of inlet-fluid rotation. Also, the author uses smooth-seal results from an unpublished thesis available at Texas A&M's Turbomachinery Lab, and compares them to those of the grooved seal. Finally, the author quantifies the effectiveness of XLCGrv® in matching the results of this experiment.

Table 2. Program test matrix – one completed for each level of inlet-fluid rotation.

ω [krpm]	ΔP [bar]	ϵ_0 [-]	ω [krpm]	ΔP [bar]	ϵ_0 [-]	ω [krpm]	ΔP [bar]	ϵ_0 [-]
2	2.07	0.00	4	2.07	0.00	6	2.07	0.00
		0.27			0.27			0.27
		0.53			0.53			0.53
		0.80			0.80			0.80
	4.14	0.00		4.14	0.00		4.14	0.00
		0.27			0.27			0.27
		0.53			0.53			0.53
		0.80			0.80			0.80
	6.21	0.00		6.21	0.00		6.21	0.00
		0.27			0.27			0.27
		0.53			0.53			0.53
		0.80			0.80			0.80
	8.27	0.00		8.27	0.00		8.27	0.00
		0.27			0.27			0.27
		0.53			0.53			0.53
		0.80			0.80			0.80

The grooved seal used here features a grooved pattern similar to those found on industrial pumps. Figure 3 shows the grooved seal featuring 15 equally spaced grooves, each 1.52 mm (60.00 mil) deep, with entrance and exit land lengths of 3.30 mm (130 mil), and a minimum radial clearance C_r of 203 µm (8 mil). The grooved seal's performance was compared to that of a smooth seal featuring the same L and D as the grooved seal, and whose nominal radial clearance equalls the grooved seal's C_r. Note that the smooth seal mentioned here was the test subject of a currently unpusblished thesis at Texas A&M's Turbomachinery lab.

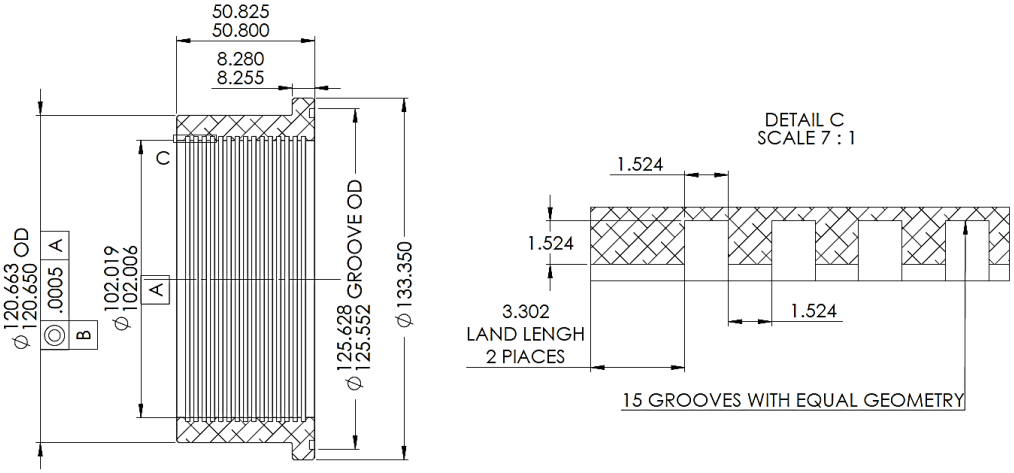

(a) **(b)**

Figure 3. (a) Grooved seal geometry. (b) Grooves details. All dimensions are in mm.

As discussed in the introduction, fluid rotation strengthens cross-coupled destabilizing forces, often limiting the applicability of turbomachines in challenging environments. Thus, increasing our understanding of this phenomena propels the industry towards improving pump reliability, ultimately aiding operators in developing challenging reservoirs, such as deep subsea oil fields.

3. TEST RIG DESCRIPTION

3.1 Test Rig

Initially designed to determine leakage and rotordynamic properties of annular bushing oil seals by Kaul in 1999 [16], the current test rig underwent several modifications, while maintaining the fundamental "shake-the-stator" elements innovated by Glienicke in 1966 [17]. Kleutinberg [18] and others carefully describe the rig's working principles for testing fluid-film bearings, hardware, and operational procedures. Thus, this section focuses on its fundamental features, and highlights the recent upgrades required for testing annular seals.

Shown in Fig. 4, the main elements of the test rig are the driver, the coupling, the shaft, the shaker system, the pedestal, the test section, the static loader, and the spring stabilization system (SSS). Note that the test section attaches to the bedplate via the Spring Stabilization System (SSS).Originally driven with an air turbine, the test rig was upgraded to a VFD-controlled electric motor capable of reaching 8 krpm, and resulting in significantly improved ω control.

Supported by angular-contact hybrid ceramic ball bearings, the AISI 4041 steel shaft attaches to the electric motor via a disk-pack hybrid coupling and a hydraulic hub. The shaft was precision machined to a diameter of 101.600 mm (4.000 in.) at the test seal film lands and uses six pitch stabilizers to achieve axial alignment with respect to the seals [16]. Additionally, the bearings supporting the rotor are lubricated using an oil mist system and supported by rigid pedestals. Air buffer seals prevent axial oil leakage from the test section into the ball bearing chambers. Figure 5 shows a close up of the main rotor-assembly components.

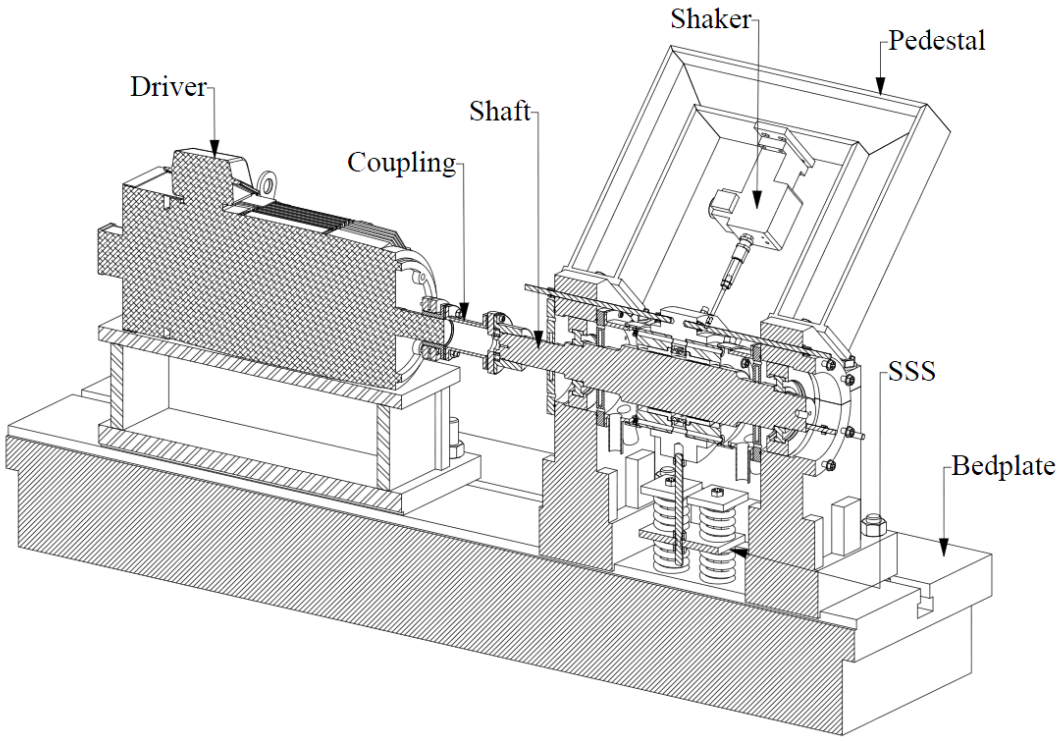

Figure 4. Main test rig components.

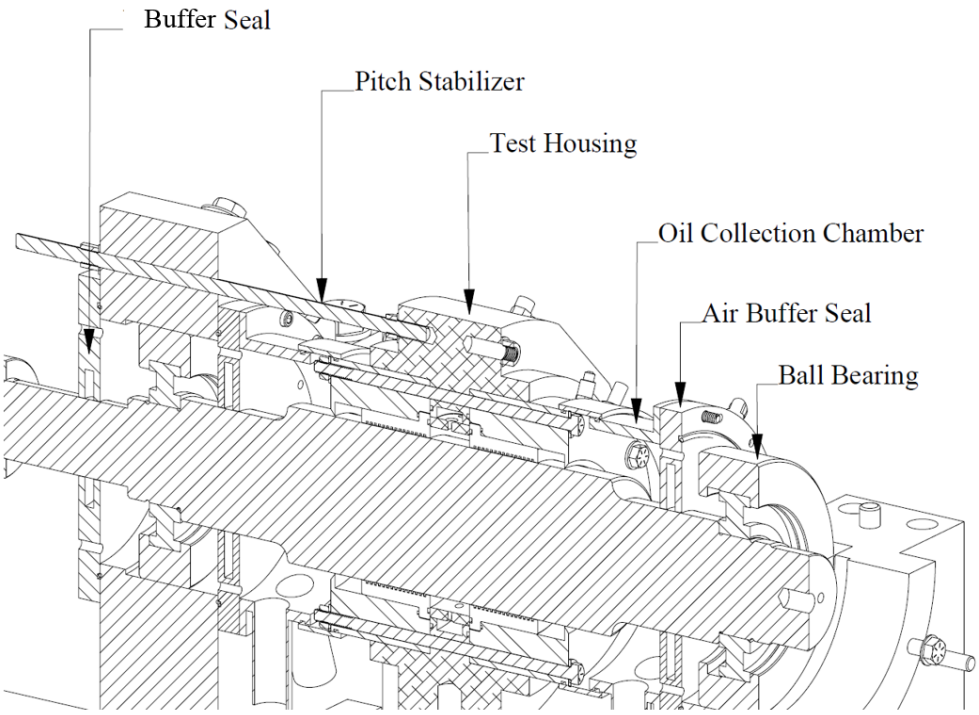

Figure 5. Main rotor-assembly components.

Figure 6 shows a cross-section of the test section's core. Oil enters the test section through two ports placed 180° from each other and then accelerates thought the pre-swirl insert nozzles to achieve the desired circumferential velocities before reaching the seal inlet. After squeezing through the seal-rotor clearance, the oil accumulates in the cavity between the seal holder and rotor, finally exiting the test section through the collection chambers at near atmospheric pressure. The oil inlet temperature is controlled by mixing hot and cold oil, and a pneumatically actuated control valve regulates its flow-rate.

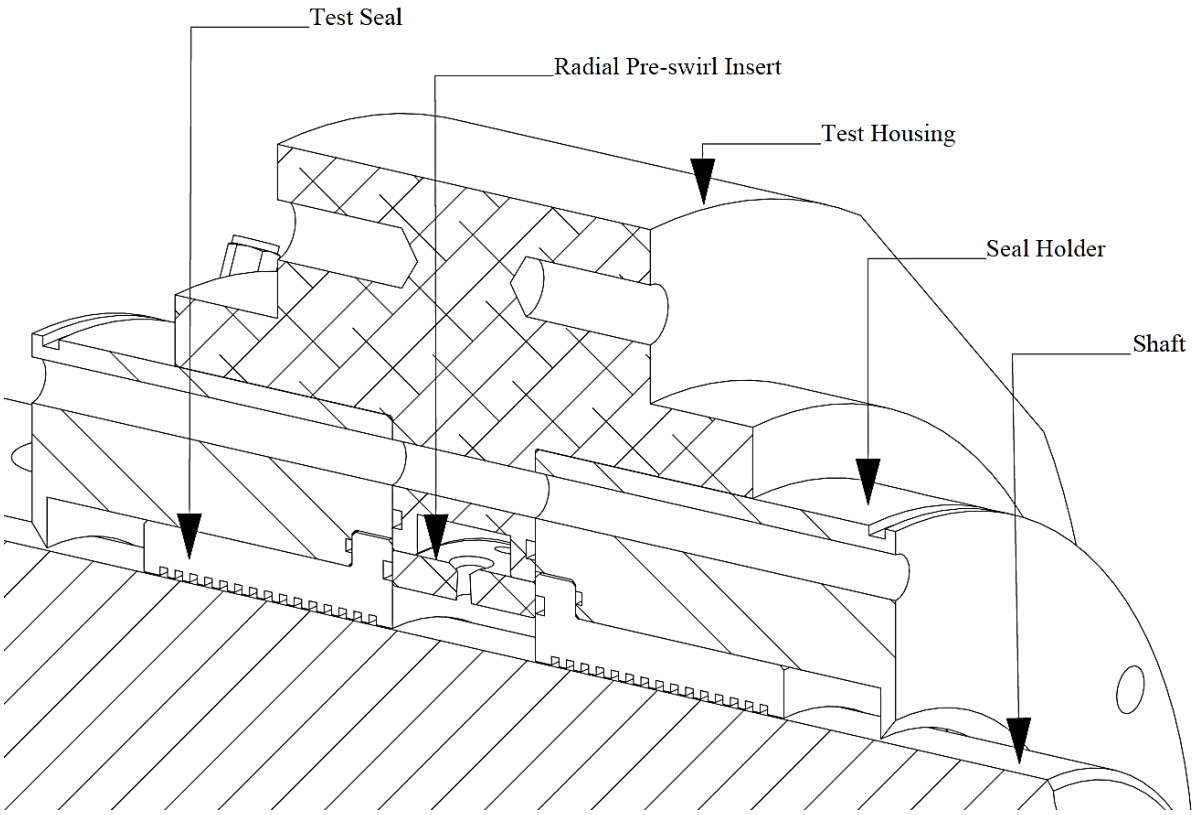

Figure 6. Cross-section view of test section's core fitted with the low PSR insert.

Shown in Fig. 7, the static loader was not used for this test program as a result of the seal's low resistance to eccentric displacements. Next, the dynamic shakers aid in defining the system rotordynamics by perturbing the test section at high frequencies and low amplitudes. Shown in Fig. 8, the x and y-shakers are mounted orthogonal, and parallel to the static load direction, respectively, and can apply dynamic loads at frequencies up to 1 kHz. In addition, adjusting the shaker static loads to center the rotor and support the weight of the test section allows for zero-load condition measurements, and the negation of gravity. Finally, the rotor and pedestal's high rigidity ensures minimal deflection under the applied loads, isolating the fluid film properties from the supporting structures.

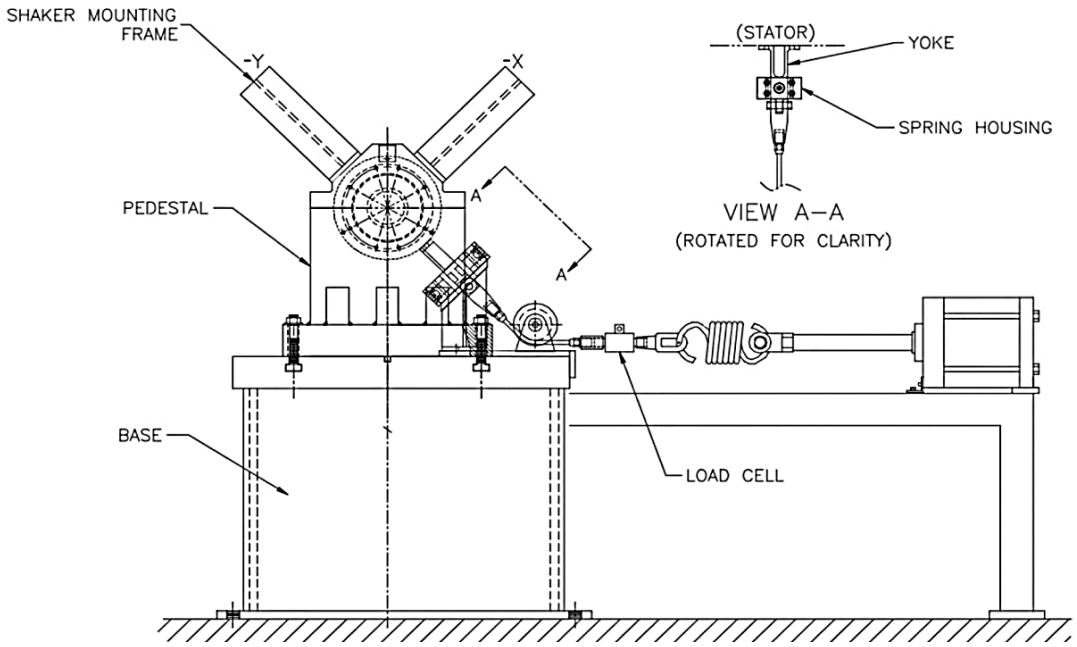

Figure 7. Non-Drive end (NDE) side of test rig displaying the static loader system. Adapted from [19].

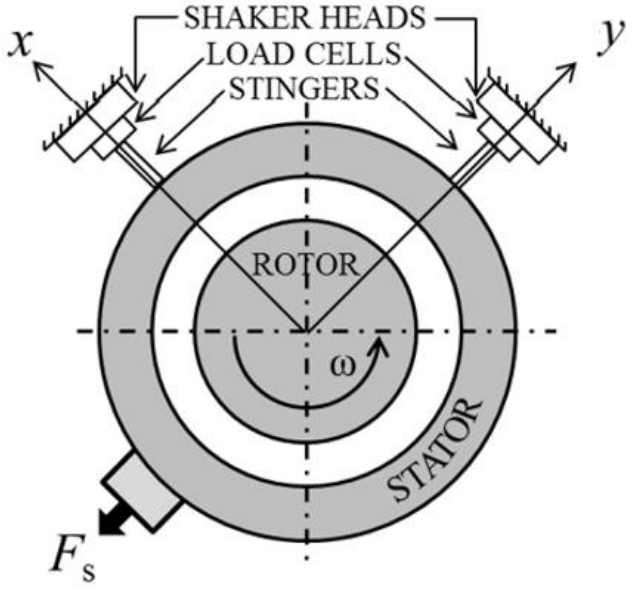

Figure 8. Drive Side (DS) view of the shaker assembly with static load f_s. Adapted from [18].

3.2 Instrumentation

Figure 9 shows that the test section houses the grooved seal elements, accommodates most of the instrumentation, and accepts oil inlet, static loader, and dynamic shaker connections. Also described in detail by Kleutinberg [18], and shown in Fig. 9, the instrumentation used to measure and record the test variables is summarized in Table 3. Appendix B offers an instrumentation uncertainty analysis.

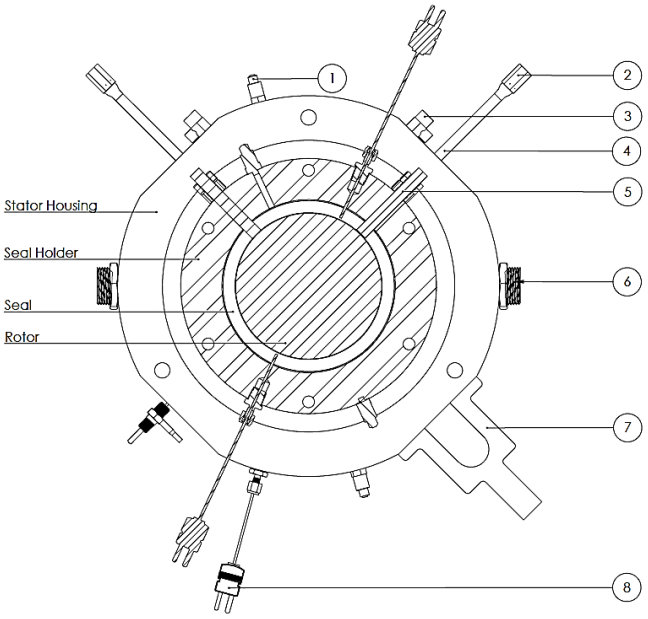

Item	Description
1	Pressure Probe
2	Load Cell
3	Accelerometer
4	Dynamic Shaker
5	Proximity Probe
6	Oil Inlet
7	Static Loader
8	Thermocouple

Table 3. Summary of main instrumentation used.

Parameter	Instrument
Shaft Rotational speed	Tachometer
Total oil Flow rate	Turbine flow meter
Inlet oil temperature	Type J thermocouple
Relative displacement between rotor and seals	Eddy current proximity probes
Inlet and Outlet pressure	Pressure transducers
Absolute acceleration of the seals	Piezoelectric accelerometers
Force applied by each shaker	Load Cells
Circumferential flow velocity before and after seal	Differential pressure transducer and pitot tubes

3.3 Pre Swirl Inserts and Pitot Tubes

Inducing and recording a wide range of inlet-fluid rotation is one of the features of this investigation. Consequently, the pre-swirl-inserts shown in Fig. 10 were designed to achieve low, medium, and high circumferential fluid velocity at the inlet of the seal. Both medium and high-velocity inserts feature nozzles that direct flow in the circumferential direction of the shaft's rotation. Additionally, the high-velocity insert features smaller nozzles to achieve higher inlet-fluid rotation than the medium-velocity insert.

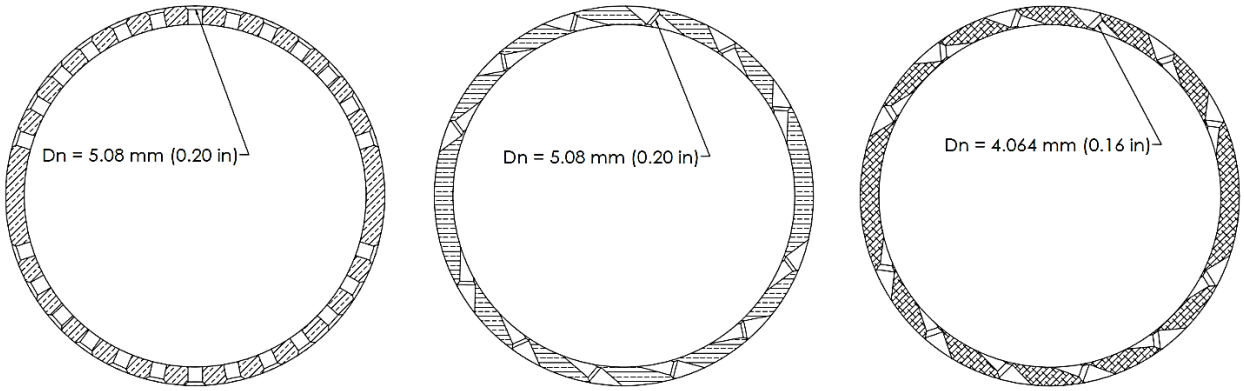

(a) **(b)** **(c)**

Figure 10. Pre-swirl-inserts. (a) Low PSR. (b) medium PSR. (c) high PSR. Note the reduced nozzle diameter on the high PSR insert.

Figure 11 shows that the test section accepts pitot tubes upstream and downstream of the seal to enable pre and post-fluid rotation measurements. Connecting each Pitot tube to a differential pressure transducer allowed for the calculation of the dynamic pressure and ultimately, the circumferential fluid velocity. Using custom gage blocks, the pitot tubes are aligned to point in the shaft's circumferential direction.

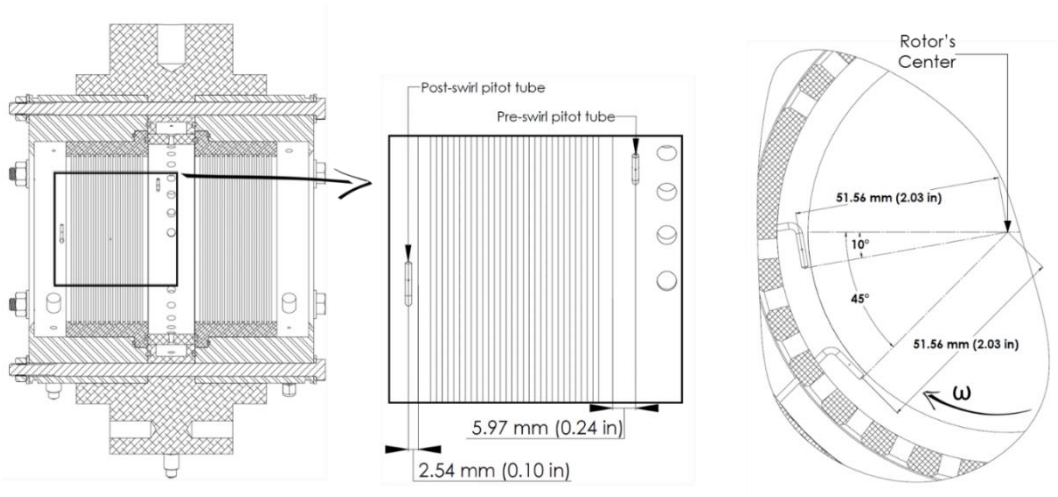

(a) **(b)** **(c)**

Figure 11. Pitot tubes. (a) Stator housing cross-section. (b) Pitot tube axial position relative to entrance and exit of the seal. (c) Pitot tube radial position relative to the seal's center.

3.4 Spring Stabilization System (SSS)

The CGS seals tested in this program provided minimal direct stiffness, causing excessive stator subsynchronous vibration for ω > 4 krpm. Consequently, a set of vertical and diagonal springs were attached to the stator housing, increasing the system's stiffness and allowing safe operation for ω up to 6 krpm. Shown in Fig. 12, the SSS consists of a diagonal and vertical set of springs connecting the stator to the base plate. The diagonal springs are aligned perpendicular to the applied load, and the vertical springs are angled 45° relative to the applied load. As detailed in Section 4 (Experimental procedure and Data Analysis), the forces contributed by the springs during testing are later subtracted from the raw data, leaving the forces from the fluid-film only.

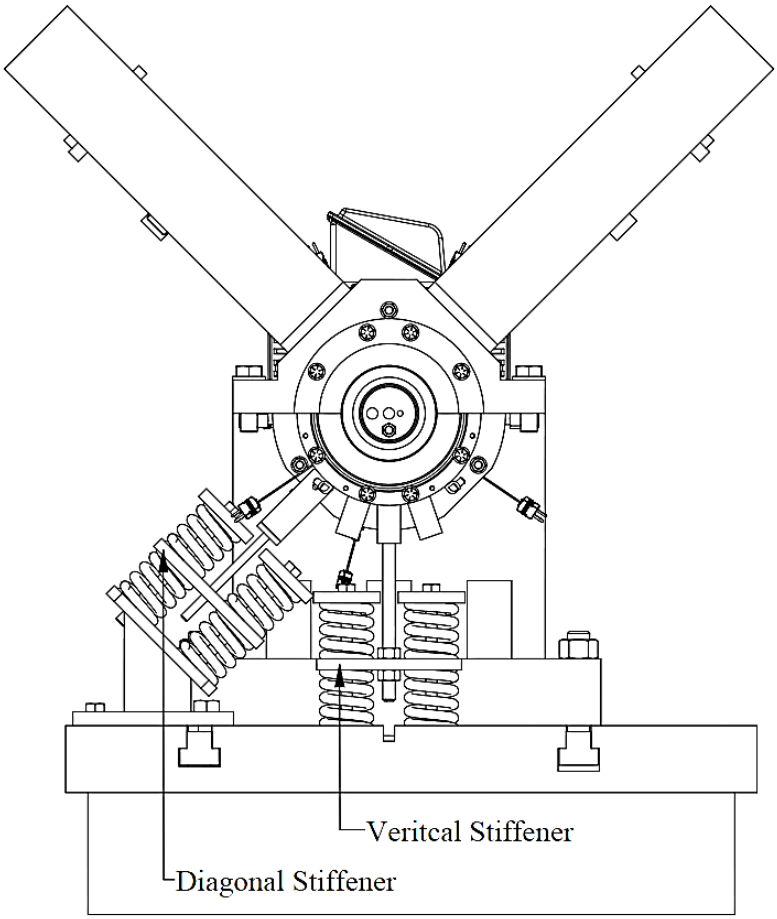

Figure 12. Non-Drive End (NDE) view of test rig showing the vertical and diagonal stiffeners, which make up the Spring Stabilization System (SSS).

4. EXPERIMENTAL PROCEDURE AND DATA ANALYSIS

The following discussion presents a summary of the procedure conducted for this investigation. Goghlan [20] offers a detailed operating procedure description of the test rig as configured for bearing tests in his 2014 thesis. Defining the seal location and coordinate system, section 4.1(Seal location and coordinate system) helps the reader paint a picture of the experimental procedures outlined in section 4.2 (Process overview). The remaining sections highlight important steps of the experimental procedure.

4.1 Seal Location and Coordinate System

The seal's location relative to the shaft is tracked using the eccentricity ratio,

$$\epsilon_0 = \frac{\sqrt{\epsilon_{x0}^2 + \epsilon_{y0}^2}}{R} \tag{9}$$

where ϵ_{x0} and ϵ_{y0} are:

$$\epsilon_{x0} = \frac{\Delta x_0}{C_r};\ \ \epsilon_{y0} = \frac{\Delta y_0}{C_r} \tag{10}$$

and Δx_0, and, Δy_0, are the static horizontal and vertical relative displacement components, respectively, between the center of the shaft, O_j, and the center of the seal, O_s. Figure 13 shows the coordinate system defined in this investigation with the load applied in the negative y-direction. Note that ϵ_0 values of 0.0 and 1.0 respectively correspond to a perfectly centered seal, and one contacting the shaft.

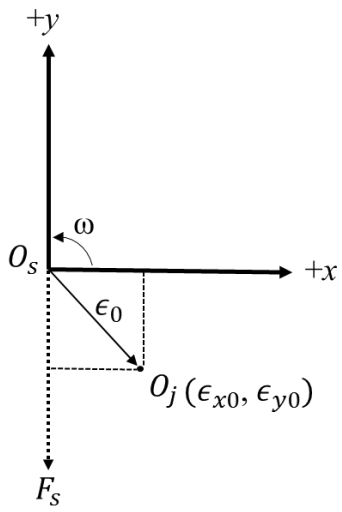

Figure 13. Coordinate system used in this investigation.

4.2 Process Overview

The following procedure serves to extract the test seal rotordynamic coefficients:

1. **Record a dry baseline**. The dry baseline consists of recording a test point with the rotor stationary and centered, and prior to any oil presence. Lacking fluid-film forces, this test point reflects only the dynamic characteristics of the supporting structures, and SSS.
2. **Record spring deflection baseline**. With the shaft stationary, and the absence of oil precluding ΔP development, the y-direction shaker moves the stator through the eccentricity range while the data acquisition system continually records the corresponding load at each eccentric position.
3. **Record hot Clearance**. The experimenter introduces oil into the system, and runs the rotor until the inlet oil temperature reaches a constant 46°C (115°F). Quickly after reaching a constant operating temperature, the experimenter turns off the rotor, and records a hot clearance by displacing the stator about the rotor, creating a circular profile accounting for thermal growth.

4. **Record dynamic test points**. During this step, the experimenter records a test point at each operating condition outlined in Table 2. Each test point yields impedance data used to define the rotordynamic coefficients. The impedances are divided by two, to produce coefficients for an individual test-seal.
5. **Subtract dry baseline from each test point**. Subtracting the dry baseline from each test point eliminates the structures' and SSS's contribution, and yields results ideally corresponding to the fluid-film between the rotor and test seal.
6. **Extract rotordynamic coefficients from impedance data**. The experimenter extracts the actual rotordynamic coefficients: stiffness, damping, and virtual mass, from the impedance data. This step is detailed in section 4.4 (Curve fits).

As the final step in the procedure, the experimenter enters the testing conditions as inputs to Marquette and Childs' XLCGrv® rotordynamic code [12], and uses the following formula to evaluate its effectiveness in matching the results of this test program:

$$\%\, deviation = \left|\frac{Predictions - Results}{Results}\right| * 100 \tag{11}$$

4.3 Measuring Impedances

Following Childs and Hale [21], and Rouvas et al. [22] approach to obtain rotordynamic coefficients, the process begins by stating the stator-system's equation of motion (EOM) as

$$M_s \begin{Bmatrix} \Delta\ddot{x} \\ \Delta\ddot{y} \end{Bmatrix} = \begin{Bmatrix} f_x \\ f_y \end{Bmatrix} + \begin{Bmatrix} f_{sx} \\ f_{sy} \end{Bmatrix} \tag{12}$$

where M_s is the stator mass, f_{sx}, and f_{sy} are the fluid-film reaction-force components, and f_x, and f_y are the shaker system's applied dynamic forces. Solving for the reaction-forces of Eq. (1), and inserting them into Eq. (12) yields:

$$-\begin{Bmatrix} f_{sx} - M_s\ddot{x} \\ f_{sy} - M_s\ddot{y} \end{Bmatrix} = \begin{bmatrix} K_{xx} & K_{xy} \\ K_{yx} & K_{yy} \end{bmatrix} \begin{Bmatrix} \Delta x \\ \Delta y \end{Bmatrix} + \begin{bmatrix} C_{xx} & C_{xy} \\ C_{yx} & C_{yy} \end{bmatrix} \begin{Bmatrix} \Delta\dot{x} \\ \Delta\dot{y} \end{Bmatrix} + \begin{bmatrix} M_{xx} M_{xy} \\ M_{yx} M_{yy} \end{bmatrix} \begin{Bmatrix} \Delta\ddot{x} \\ \Delta\ddot{y} \end{Bmatrix} \tag{13}$$

The displacement, acceleration, and input force components are recorded in the time domain and transformed to the frequency domain using a Fast Fourier Transform (FFT),

resulting in a frequency-domain set of displacements ($\boldsymbol{D}_x$, $\boldsymbol{D}_y$), accelerations ($\boldsymbol{A}_x$, $\boldsymbol{A}_y$) and excitation forces, ($\boldsymbol{F}_x$, $\boldsymbol{F}_y$), ultimately yielding

$$\begin{Bmatrix} \boldsymbol{F}_x - M_s\boldsymbol{A}_x \\ \boldsymbol{F}_y - M_s\boldsymbol{A}_y \end{Bmatrix} = -\begin{bmatrix} \boldsymbol{H}_{xx} & \boldsymbol{H}_{xy} \\ \boldsymbol{H}_{yx} & \boldsymbol{H}_{yy} \end{bmatrix} \begin{Bmatrix} \boldsymbol{D}_x \\ \boldsymbol{D}_y \end{Bmatrix} \tag{14}$$

where $\boldsymbol{H}_{ij}$ is the impedance

$$\boldsymbol{H}_{ij} = \left(K_{ij} - M_{ij}\Omega^2\right) + \boldsymbol{j}(\Omega C_{ij}) \tag{15}$$

In Eq. (15), Ω is the excitation frequency, and $\boldsymbol{j}$ is $\sqrt{-1}$. Next, shaking the system in two orthogonal directions allows for the impedance calculation by extending Eq.(14) to

$$\begin{bmatrix} \boldsymbol{F}_{xx} - M_s\boldsymbol{A}_{xx} & \boldsymbol{F}_{xy} - M_s\boldsymbol{A}_{xy} \\ \boldsymbol{F}_{yx} - M_s\boldsymbol{A}_{yx} & \boldsymbol{F}_{yy} - M_s\boldsymbol{A}_{yy} \end{bmatrix} = -\begin{bmatrix} \boldsymbol{H}_{xx} & \boldsymbol{H}_{xy} \\ \boldsymbol{H}_{yx} & \boldsymbol{H}_{yy} \end{bmatrix} \begin{bmatrix} \boldsymbol{D}_{xx} & \boldsymbol{D}_{xy} \\ \boldsymbol{D}_{yx} & \boldsymbol{D}_{yy} \end{bmatrix} \tag{16}$$

4.4 Curve Fits

Using a linear curve fit in Ω^2 from the real part of Eq.(15), the experimenter can extract the stiffness and virtual mass coefficients. Specifically, the stiffness and virtual mass coefficients are the y-intercept and slope of the curve fit, respectively. Finally, the damping coefficient results from a linear curve fit of Ω in the imaginary part of the dynamic stiffness. The author uses the curve fit for frequencies up to 200 Hz, twice the maximum running speed of 6 krpm (100 Hz).

To start, the experimenter linearizes the 2nd order, real part of Eq. (15) by replacing Ω^2 with Λ, yielding the following dynamic stiffness equation

$$\boldsymbol{H}_{ij} = \left(K_{ij} - M_{ij}\Lambda\right) + \boldsymbol{j}(\Omega C_{ij}) \tag{17}$$

Then, the following least-squares regression analysis, as detailed by Beckwith [23], serves to extract the rotordynamic coefficients when applied separately to the real and imaginary parts of Eq. (14):

Assuming that the curve fit has a linear relationship between input and output yields the form

$$O_i = aP_i + a_1 \tag{18}$$

where O_i represents calculated outputs from a set of input measurements, P_i. Thus the slope, a, and the y-intercept, a_1, are

$$a = \frac{\sum O_i \sum P_i^2 - \sum P_i \sum P_i O_i}{n \sum P_i^2 - \left(\sum P_i\right)^2} \tag{19}$$

$$a_1 = \frac{n \sum P_i O_i - \sum P_i \sum O_i}{n \sum P_i^2 - \left(\sum P_i\right)^2} \tag{20}$$

4.5 Circumferential Fluid Velocity

To calculate the circumferential fluid velocities used in the PSR and OSR definitions of Eqs. (7) and (8), the experimenter installs pitot tubes at the inlet and outlet of the seal, and connects each to a differential pressure transducer. With the pitot tube differential pressure, ΔP_v, and the fluid density, ρ, the experimenter uses the following equation to calculate circumferential velocity:

$$v = \sqrt{\frac{2\Delta P_v}{\rho}} \tag{21}$$

4.6 Reynolds Number

To characterize the flow regime within the grooved seal annulus, the author uses the maximum clearance, C_{max}, between the rotor and the seal:

$$C_{max} = C_r + G_d \tag{22}$$

and defines the Reynolds number, Re, as

$$Re = \sqrt{Re_\theta^2 + Re_z^2} \tag{23}$$

where Re_θ, and Re_z are the circumferential and axial Reynolds number, respectively, and defined as

$$Re_\theta = 2\rho R\omega C_{max}/\mu \tag{24}$$

$$Re_z = 2\rho\, wC_{max}/\mu \tag{25}$$

Note that the hydraulic radius used in the definition is $2C_{max}$. In Eq.(24), w represents the axial fluid velocity and is defined as

$$w = \dot{Q}/A \tag{26}$$

where, using the annulus area, A, becomes

$$A = 2\pi RC_{max} + \pi C_{max}^2 \tag{27}$$

In regards to the smooth seals, its circumferential and axial Reynolds number, and annulus area are defined as

$$Re_{\theta\_Smooth} = \rho R\omega C_{r\_s}/\mu \tag{28}$$

$$Re_{z\_Smooth} = 2\rho\, wC_{r\_s}/\mu \tag{29}$$

$$A = 2\pi RC_{r\_s} + \pi C_{r\_s}^2 \tag{30}$$

Finally, fluid flow is categorized as laminar if it features a Reynolds number less than 2,000, in the transitional regime if between 2,300 and 4,000, and in the turbulent regime if more than 4,000. [24]

5. STATIC RESULTS

As a preface to this section, recall that the term "grooved seal" refers to a circumferentially-grooved stator/smooth rotor (CGS/SR) liquid annular seal, while the term "smooth seal" refers to a smooth stator/smooth rotor (SS/SR) liquid annual seal. *Additionally, all presented static and dynamic results correspond to the low PSR configuration, unless stated otherwise.*

This section presents the measured clearance for each configuration, a leakage comparison between the grooved and smooth seals, the measured pre and post-swirl ratios, and the calculated Reynolds number.

While the SSS enabled testing at $\omega > 4$ krpm, it tainted the fluid-film reaction force, F_r, static results, even after subtracting the static-load baselines from the results. In a more noticeable fashion, the SSS markedly deformed the seal loci measurements by modifying the seal's natural displacement tendencies. Consequently, load deflection and seal loci data offer little insight and are omitted from this section.

5.1 Clearance

As summarized in section 4.2 (Process Overview), gently pushing the stator around the seal yields a clearance as recorded by the proximity probes. Table 4 reports the clearance information for each configurations.

Table 4. Measured average radial hot clearances.

Configuration	Clearance [μm]
Low PSR	183.9
Med. Tangential injection	190.67
High Tangential injection	190.43

5.2 Leakage

Displaying the leakage performance of the grooved seal, Fig. 14a shows $\dot{Q}$ markedly increasing with increasing ΔP and slightly increasing with ϵ_0. Figure 14b shows $\dot{Q}$ modestly decreasing with increasing ω. Overall, a minimum $\dot{Q}$ of 15.64 LPM (4.13 GPM) occurs at ω = 6 krpm, and ΔP = 2.1 bar (30 PSI), and a maximum $\dot{Q}$ of 56.36 LPM (14.89 GPM) at ω = 2 krpm, and ΔP = 8.3 bar (120 PSI).

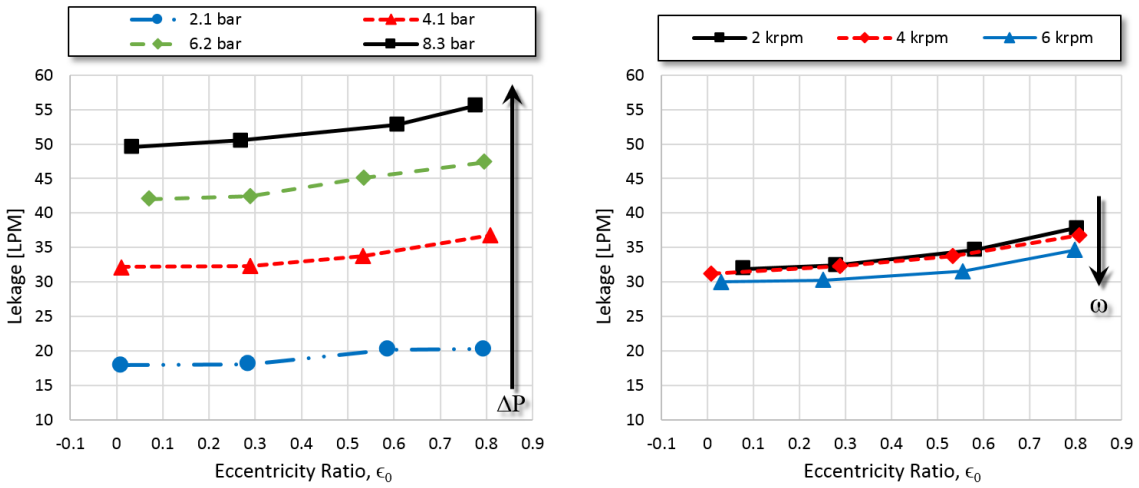

(a) **(b)**

Figure 14. $\dot{Q}$ versus ϵ_0 for (a) ω = 2 krpm over the ΔP range, and (b) ΔP = 2.1 bar over the ω range.

Next, highlighting the effects of circumferential grooves on leakage performance, Fig. 15 shows $\dot{Q}$ as a function of ϵ_0 for the grooved and smooth seals. Figure 15a shows that at ω = 2 krpm, and ΔP = 8.3 bar (120 PSI), the grooved seal leaks approximately 20% less than the smooth seal, across the ϵ_0 range. However, Fig. 15b shows this benefit diminishing to approximately 6% when increasing ω to 6 krpm. Additionally, the groove's leakage-reducing ability appears only at high ΔPs, yielding negligible improvement over the smooth seal at ΔP = 2 bar [30 PSI].

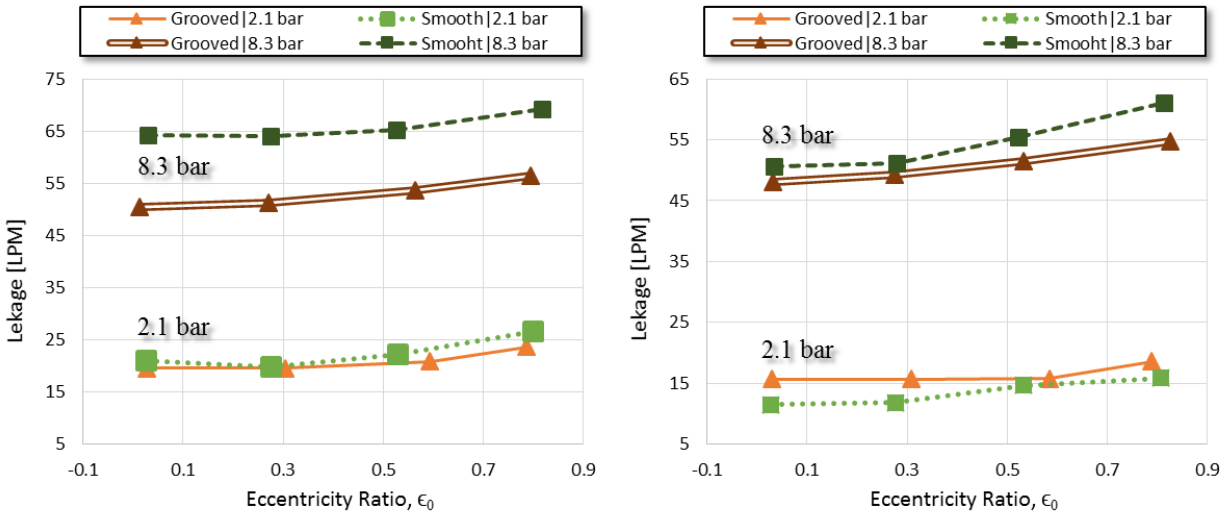

Figure 15. Comparison of $\dot{Q}$ between the grooved and smooth seals. $\dot{Q}$ versus ϵ_0 for (a) ω = 2 krpm and (b) ω = 6 krpm.

5.3 Pre-swirl Ratio (PSR), defined in Eq. (7)

Figure 16 shows PSR as a function of ω and ΔP, while Table 5 summarizes its range. For the low PSR configuration shown in Fig. 16a, increasing ΔP strengthens the axial flow, and hinders the development of the PSR. In contrast, increasing ΔP enhances circumferential flow through the high PSR configuration, markedly increasing PSR, as show in Fig. 16b. Additionally, increasing ω lowers PSR in the high PSR configuration, as suggested by ω's appearance in the denominator of Eq. (7). PSR is largely indifferent to increasing ϵ_0.

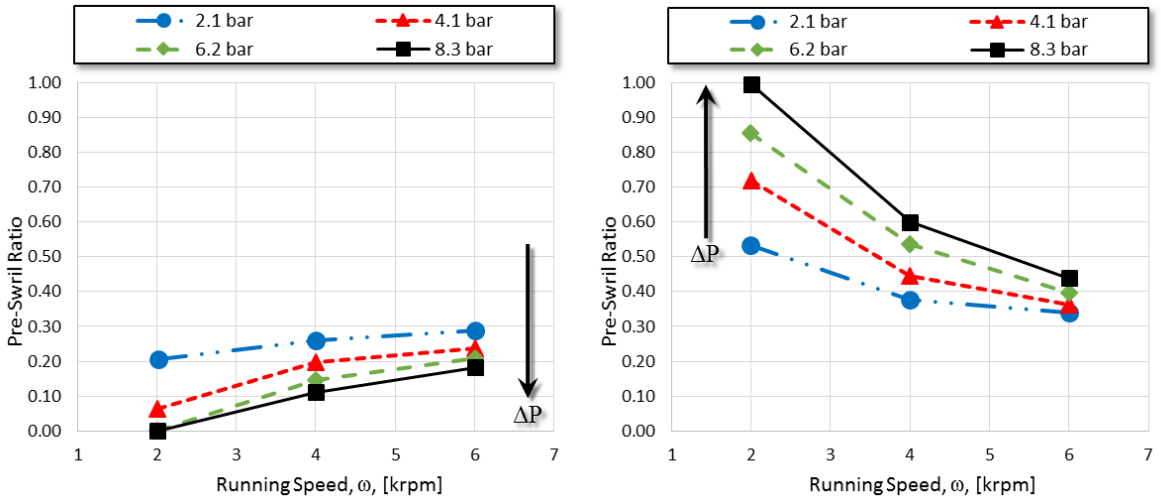

Figure 16. Grooved seal's PSR versus ω at $\epsilon_0 = 0.00$ over the ΔP range for the (a) low PSR, and (b) high PSR configurations of Fig. 10.

Table 5. Minimum and maximum values of PSR for each ω.

Running Speed, ω [krpm]	Minimum PSR [-]	Maximum PSR [-]
2	0.00	0.95
4	0.11	0.60
6	0.18	0.44

5.4 Outlet-swirl Ratio (OSR), defined in Eq. (8)

Contained between 0.2 and 0.3 across the test matrix, the OSR shown in Fig. 17a decreases with increasing ω, and increases with increasing ΔP. Figure 17b shows it increasing with ϵ_0.

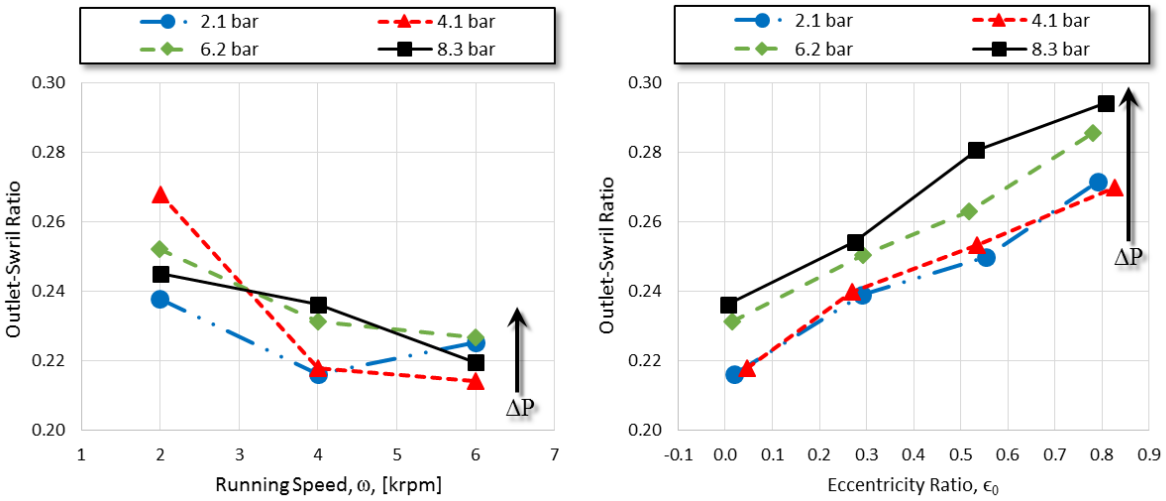

(a) **(b)**

Figure 17. Grooved seal's OSR versus (a) ω at $\epsilon_0 = 0.00$, and (b) ϵ_0 at 4 krpm across the ΔP range for the high PSR configuration.

Next, Fig. 18 shows OSR as a function of measured PSR. Specifically, Fig. 18a shows OSR decreasing with increasing PSR values below 0.3, and Fig. 18b shows this trend flip for PSR values larger than 0.3. Notice that these are all modest changes, as the entire OSR range resides between 0.2 and 0.3 for the grooved seal.

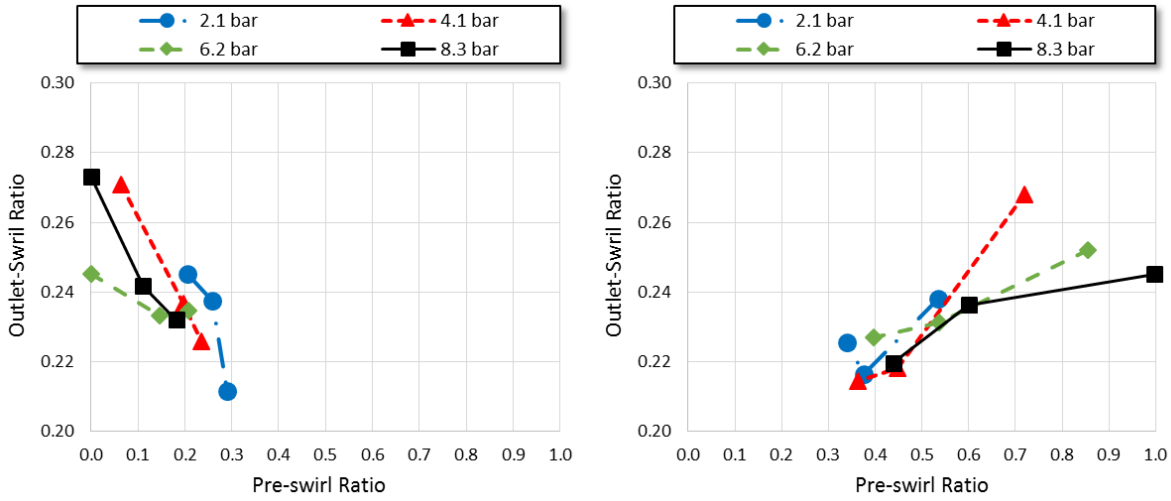

(a) **(b)**

Figure 18. Grooved seal's OSR versus PSR at $\epsilon_0 = 0.00$ over the ΔP range for (a) low PSR, and (b) high PSR configurations.

Figure 19 reveals that the grooved seal produces lower OSR values relative to its smooth seal counterpart. While Fig. 19a shows an average reduction of 9% at ΔP = 2.1 bar (30 PSI), Fig. 19b shows this average reduction increase to approximately 24% at ΔP = 8.3 bar (120 PSI). Note that the OSR remains between 0.2 and 0.4 across all test points in both the smooth and grooved seal configurations. The smooth seal's higher OSR represents higher average circumferential velocity within the seal and is reflected by higher cross-coupled stiffness and damping magnitudes relative to the grooved seal, as shown in section 7.2 (Rotordynamic Stiffness Coefficients) and 7.3 (Rotordynamic Damping Coefficients)

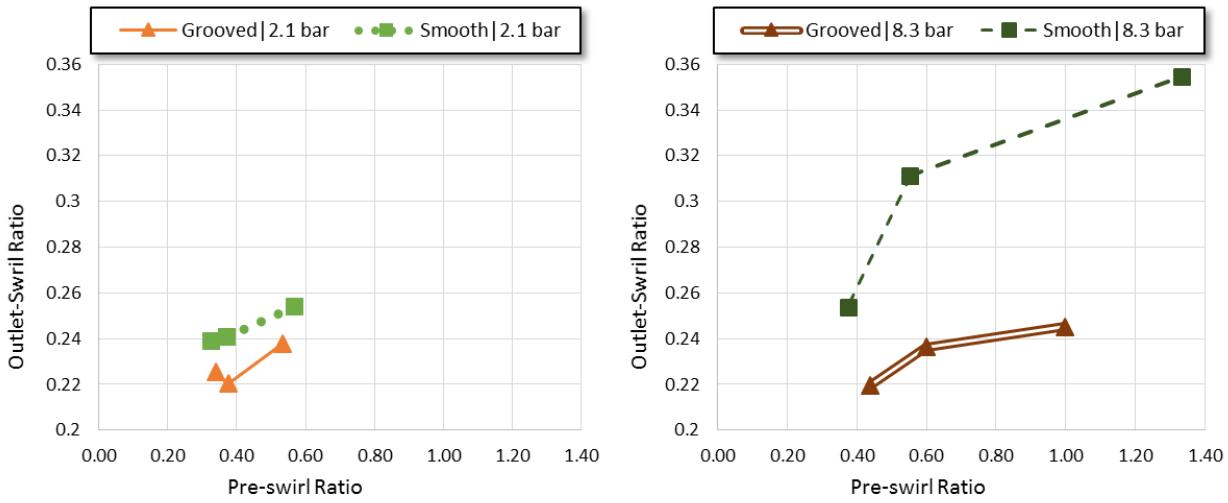

(a) **(b)**

Figure 19. Comparison of OSR between the grooved and smooth seals. OSR vs PSR for the high PSR configuration, and ϵ_0 = 0.00 at (a) ΔP = 2.1 bar, and (b) ΔP = 8.3 bar.

5.5 Reynolds Number

Figures 20a and 20b show the grooved seal's circumferential and axial Reynolds number, respectively, versus running speed. While Fig. 20a shows Re_θ's linear dependence on ω, and its indifference to ΔP, Fig. 20b shows Re_z increasing with ΔP, and remaining approximately constant throght the ω range. Note that circumferential flow clearly dominates with in the grooved seal annulus. Next, Fig. 20c compares the grooved seal's total Reynolds number to that of the smooth seal. Notice that the grooved seal operates in the turbulent flow regime across the entire ΔP and ω range with Reynolds number ranging from 7.91 x 10^3 to 2.43 x 10^4. On the other hand, the smooth seal operates in the laminar flow regime only for ΔP = 2.1bar (30 PSI) and ω = 2 krpm, and in the transitional flow regime across all other operating conditions. The smooth's seal Reynolds number is bounded between 1.18 x 10^3 and 3.82 x 10^3.

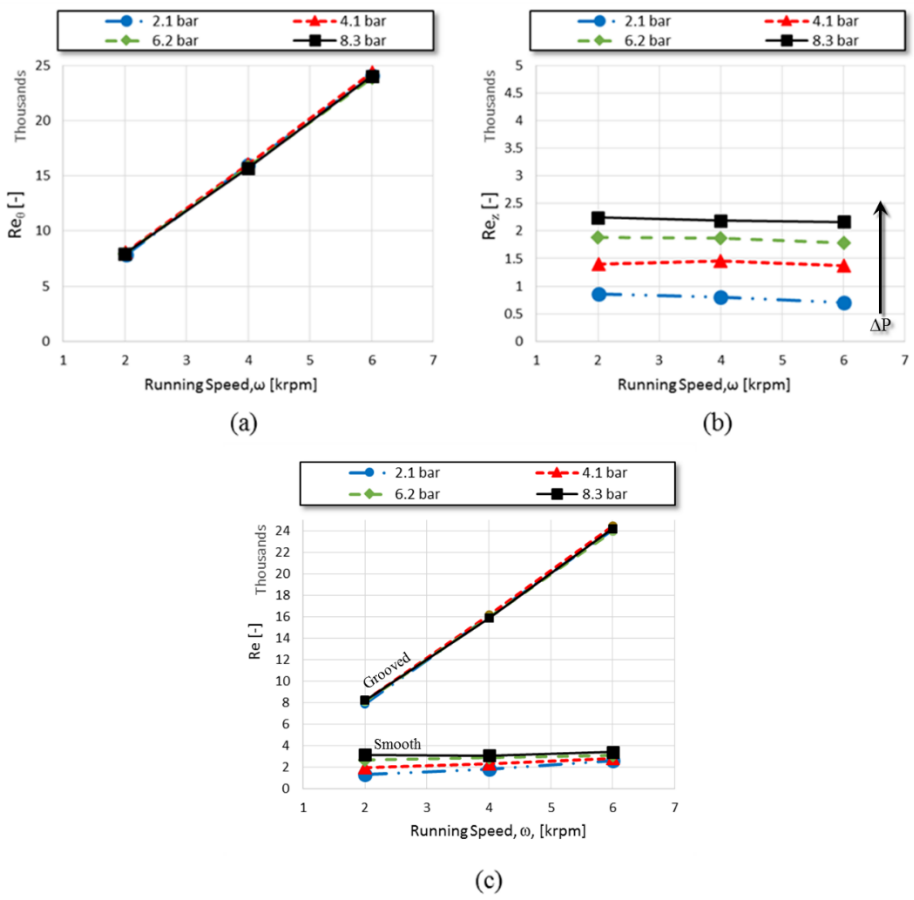

Figure 20. Grooved seal's (a) Re_θ, (b) Re_z versus ω at ϵ = 0.00 over the ΔP range. (C) Comparison between grooved and smooth seal. Re versus ω at ϵ = 0.00 over the ΔP range.

6. DYNAMIC RESULTS

6.1 Dynamic Stiffness Coefficients

Characteristic of the entire data set, Figs. 21 and 22 show the fluid-film's real and imaginary dynamic stiffness components, respectively, as a function of Ω, for an arbitrary test point. With the exception of a few outliers at Ω > 140 Hz, the dynamic stiffness shows good agreement with the model in Eq. (15). Figure 21a shows $Re(\boldsymbol{H}_{xx})$ and $Re(\boldsymbol{H}_{yy})$ decreasing with Ω, and Fig. 21b shows that $Re(\boldsymbol{H}_{xy})$ and $Re(\boldsymbol{H}_{yx})$ have a low dependence on Ω. Figure 22a shows $Im(\boldsymbol{H}_{xx})$ and $Im(\boldsymbol{H}_{yy})$ also increasing with Ω, and Fig. 22b shows $Im(\boldsymbol{H}_{xy})$ and $Im(\boldsymbol{H}_{yx})$ diverging away from zero with increasing Ω. For comparison, Fig. 23 shows the smooth seal's real dynamic stiffness for the same operating point as Fig. 21.

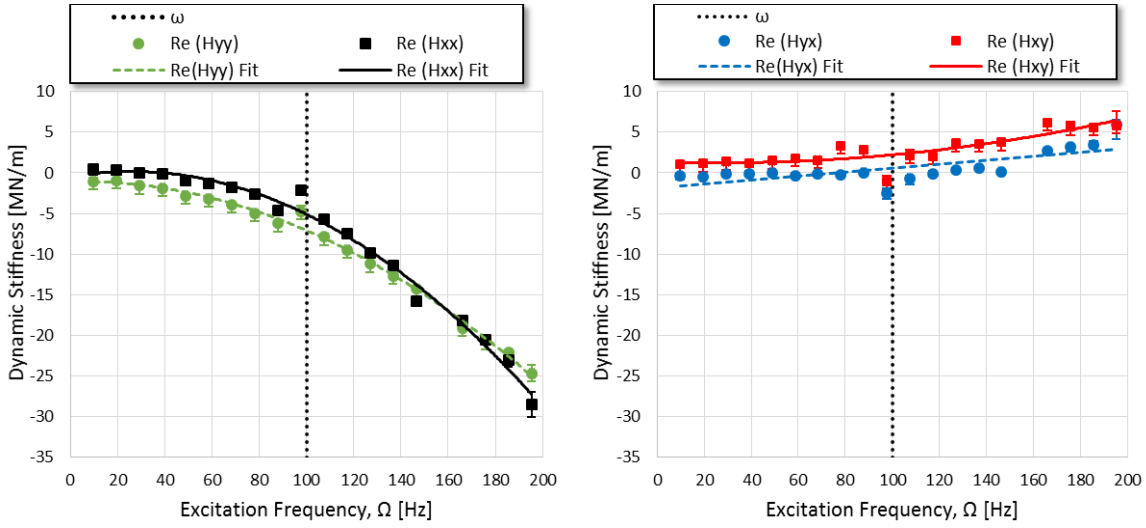

(a) **(b)**

Figure 21. Real component of the grooved seal's (a) direct and (b) cross-coupled dynamic stiffness versus Ω, for ω = 6 krpm, ΔP = 6.2 bar, ϵ_0 = 0.27, and PSR = 0.21.

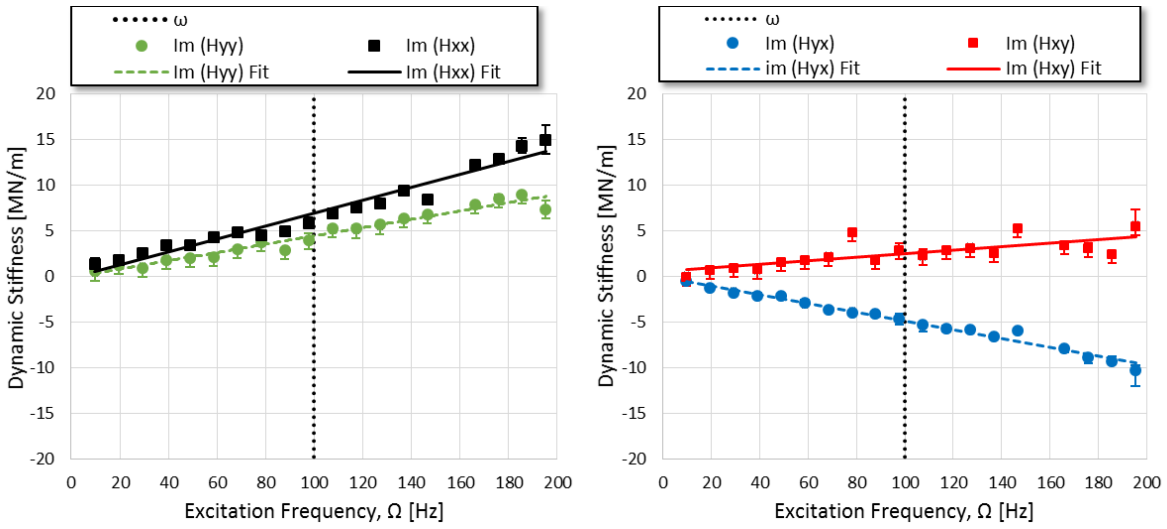

(a) **(b)**

Figure 22. Imaginary component of the grooved seal's (a) direct and (b) cross-coupled dynamic stiffness versus Ω, for ω = 6 krpm, ΔP = 6.2 bar ϵ_0 = 0.27, and PSR = 0.21.

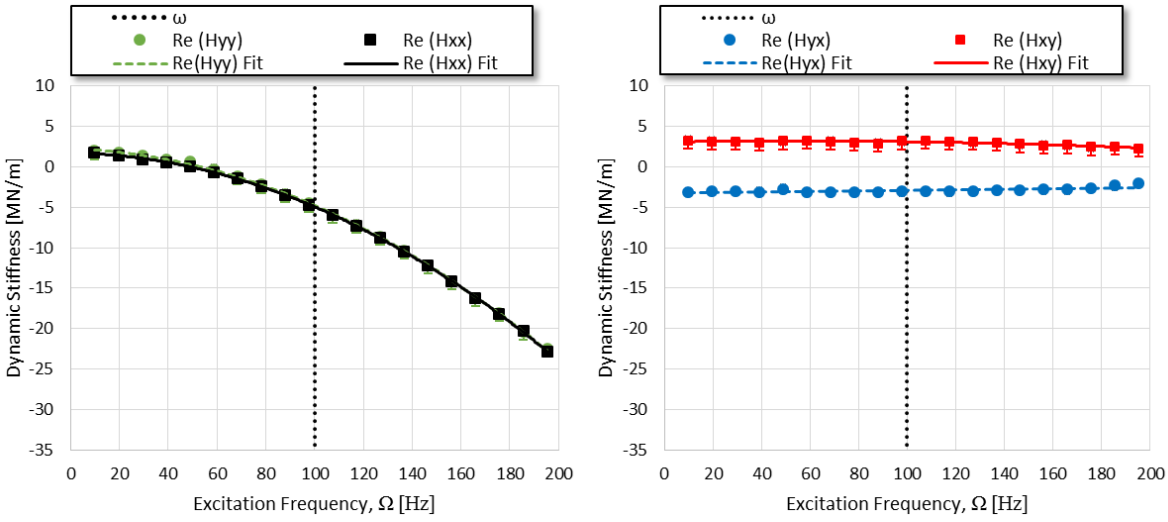

(a) **(b)**

Figure 23 - Real component of the smooth seal's (a) direct and (b) cross-coupled dynamic stiffness versus Ω, for ω = 6 krpm, ΔP = 6.2 bar, ϵ_0 = 0.27, and PSR = 0.20.

6.2 Rotordynamic Stiffness Coefficients

Recall that the applied load acts in the negative y-directtion. Bounded between -0.038 and 2.13 MN/m (-2.17 x 10^5 to 1.22 x 10^7 lbf/in) for all test cases, the grooved seal's direct stiffness generally decreases with increasing ω, as shown in Fig. 24. Figure 24a shows K_{xx} modestly increasing with increasing ϵ_0. Figure 24b shows K_{yy} increasing with increasing ϵ_0 at $\omega = 6$ krpm , but indifferent to increasing ϵ_0 at ω = 2, 4 krpm. Figures 25a, and Fig. 25b show K_{xx} and K_{yy} increasing as a function of ΔP. For $\omega >$ 4 krpm, K_{xx} values are generally close to zero, and K_{yy} values are negative, which would lower a pump's natural frequency. Finally, note that $K_{xx} \neq K_{yy}$ as suggested by Eq. (2), which applies for centered operation.

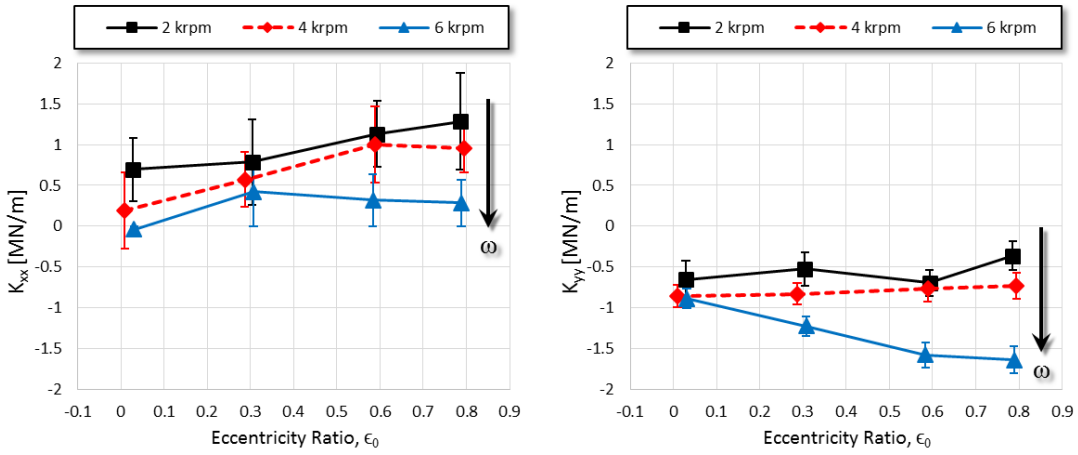

(a) **(b)**

Figure 24. Grooved seal's (a) K_{xx} and (b) K_{yy} versus ϵ_0, at ΔP = 2.1 bar for the ω range.

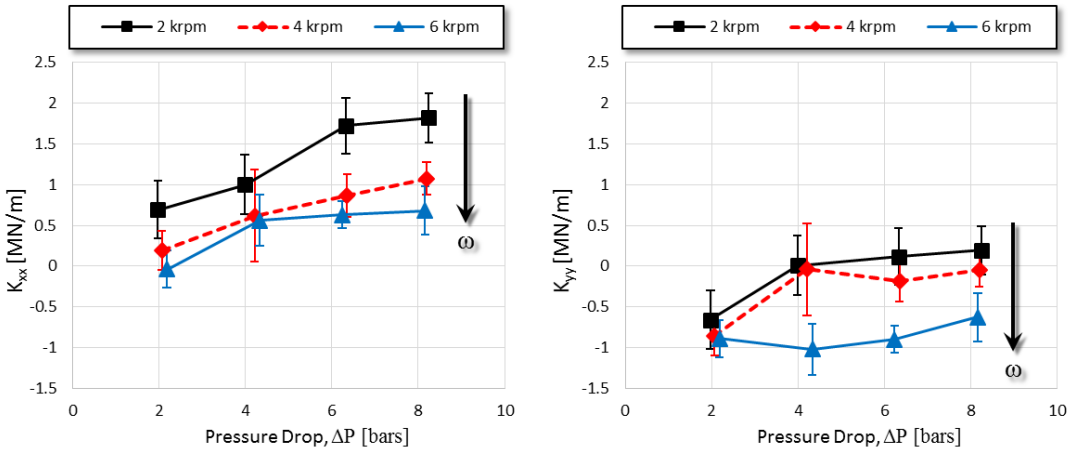

(a) **(b)**

Figure 25. Grooved seal's (a) K_{xx} and (b) K_{yy} versus ΔP, at ϵ_0 = 0.0 for the ω range.

Recalling that large values of $|K_{xy} - K_{yx}|$ are detrimental to seal stability, Figs. 26a and 26b show that increasing ω forces the K_{xy}, K_{yx} values away from zero, reducing the seal's stability. Increasing ΔP did not have a consistent effect on the cross-coupled stiffness coefficients.

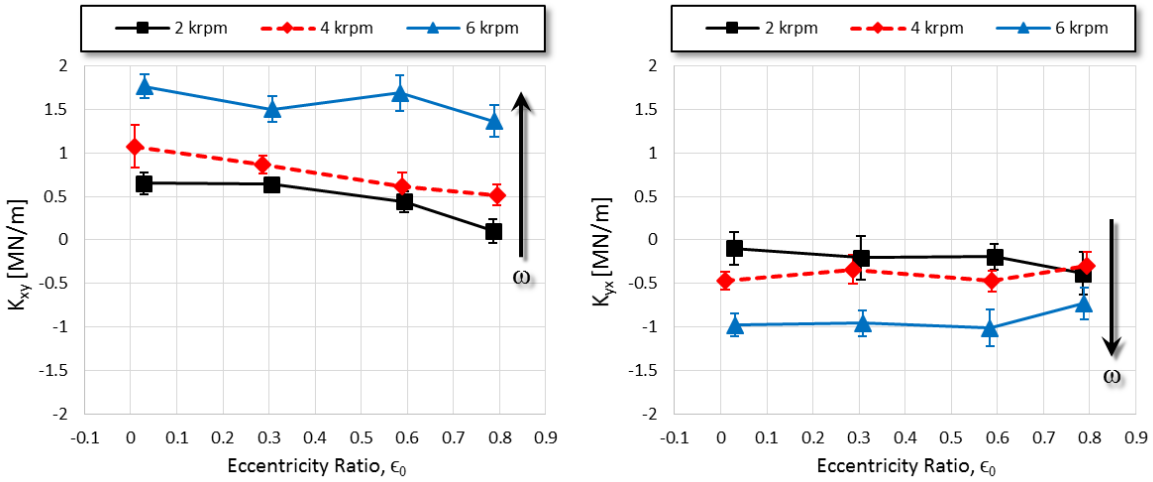

(a) **(b)**

Figure 26. Grooved seal's (a) K_{xy} and (b) K_{yx} versus ϵ_0 at ΔP = 2.1 bar over the ω range. Measured PSR values range from 0.0 to 0.29.

Comparing stiffness coefficients between grooved and smooth seals, Fig. 27 shows that changes in ϵ_0 have a greater impact on the smooth seal than the grooved seal. Specifically, Figs. 27a and 27b show the smooth seal's direct and cross-coupled stiffness, respectively, markedly departing from zero as a function of ϵ_0, especially at $\epsilon_0 > 0.50$. Note that the grooved seal's stiffness coefficients remain largely unchanged by increasing ϵ_0 across its range. As a possible physical explanation for this phenomenon, consider the following: In the smooth seals, increasing ϵ_0 creates strongly converging and diverging flow fields, altering its dynamic coefficients. In contrast, increasing ϵ_0 in the grooved seal "displaces" the fluid-film into the grooves, having little impact on its actual stiffness characteristics.

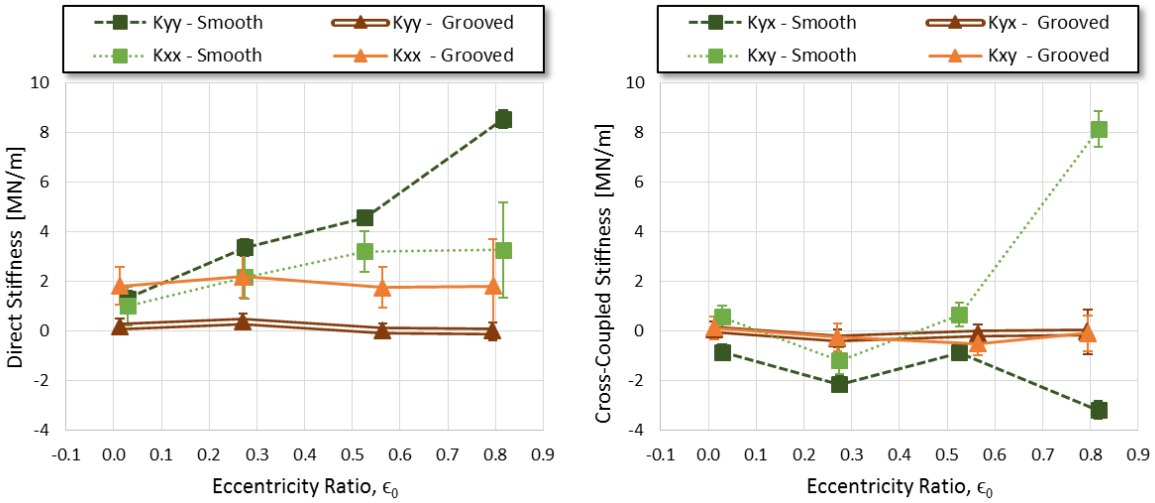

(a) **(b)**

Figure 27. Comparison between grooved and smooth seals. (a) direct and (b) cross-coupled stiffness versus ϵ_0 at ω = 2 krpm and ΔP = 8.3 bar. Measured PSR values range from 0.0 to 0.31.

Figure 28 shows that the grooved seal's direct and cross-coupled damping coefficients remain largely unaffected by increasing ΔP across its range. Figure 28a shows the smooth seal's direct stiffness clearly increasing with increasing ΔP, and Fig. 28b shows its cross-coupled damping terms sharply increase in magnitude at ϵ_0 = 0.80.

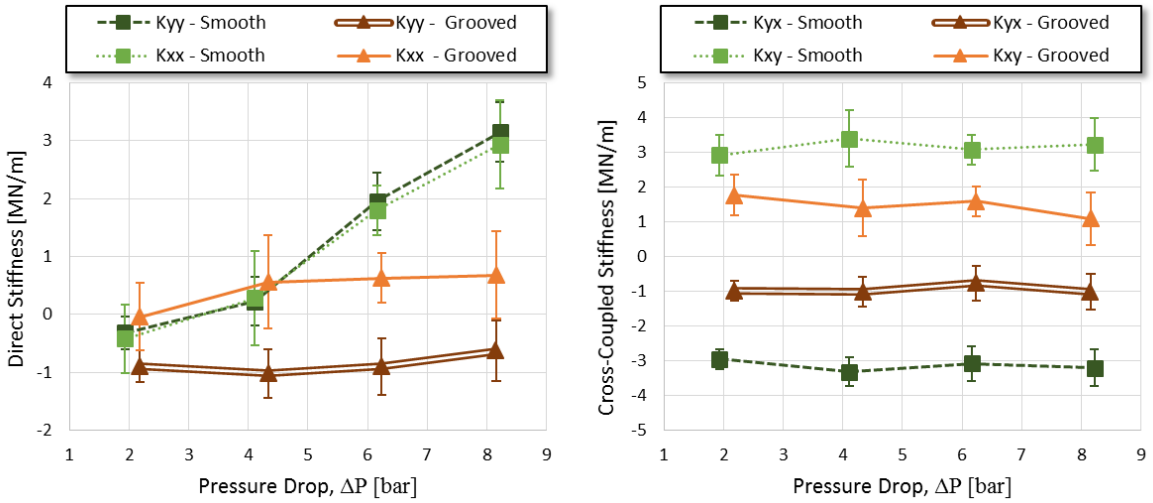

(a) **(b)**

Figure 28. Comparison between grooved and smooth seals. (a) direct and (b) cross-coupled stiffness versus ΔP at ϵ_0 = 0.00, and ω = 6 krpm. Measured PSR values range from 0.16 to 0.30.

Finally, Fig. 29 shows that increasing PSR has a detrimental effect on both seal geometries: Fig. 29a shows direct stiffness coefficients diminish with increasing PSR, and Fig. 29b shows the cross-coupled stiffness magnitude steadily increase as a with increasing PSR.

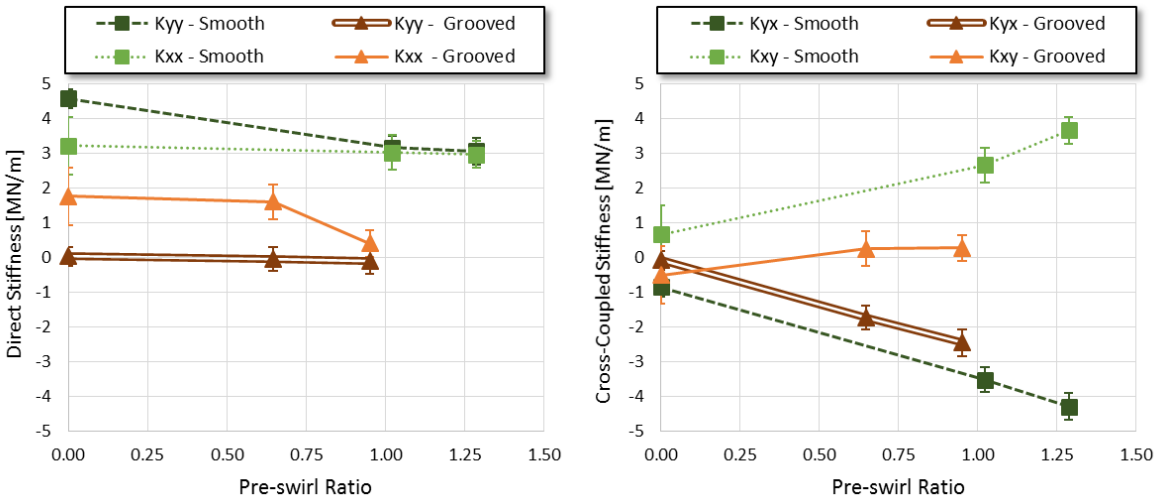

(a) **(b)**

Figure 29. Comparison between grooved and smooth seals. (a) Direct and (b) cross-coupled stiffness versus measured PSR at ϵ_0 = 0.53, ΔP = 8.3 bar, and ω = 2 krpm.

6.3 Rotordynamic Damping Coefficients

Figures 30 and 31 show the grooved seal's direct and cross-coupled damping coefficients, respectively. Figure 30a shows C_{xx} markedly increasing with increasing ΔP and slightly increasing with increasing ω. Figure 30b shows C_{yy} following a similar trend.

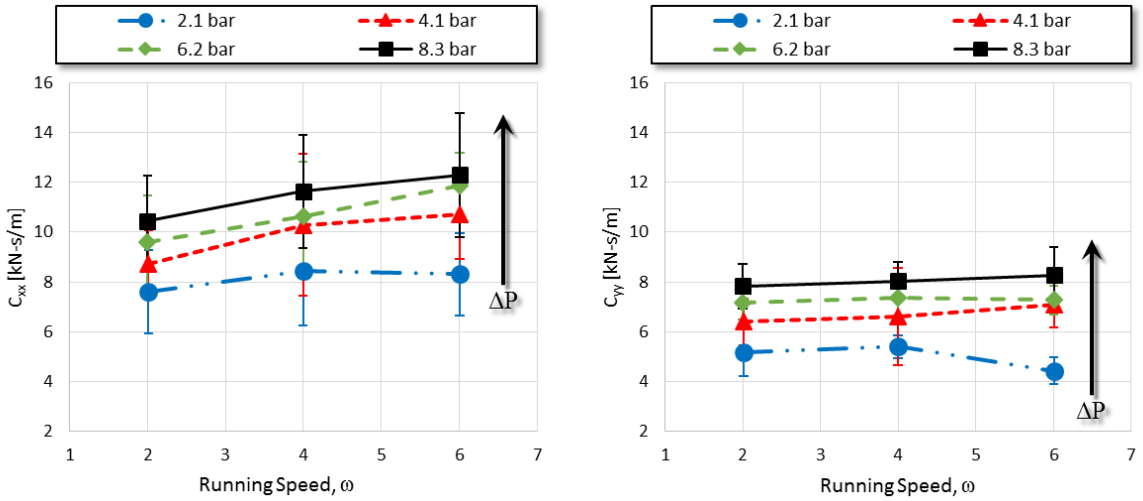

(a) **(b)**

Figure 30. Grooved seal's (a) C_{xx} and (b) C_{yy} versus ω at ϵ_0 = 0.00 over the ΔP range.

In contrast to its direct damping terms, the grooved seal's cross-coupled damping terms clearly increase in magnitude with increasing ω, and remaining mostly unchanged by increasing ΔP, as shown in Figs. 31a and 31b. Also, notice the C_{xy} and C_{yx} diverging from zero with increasing ω.

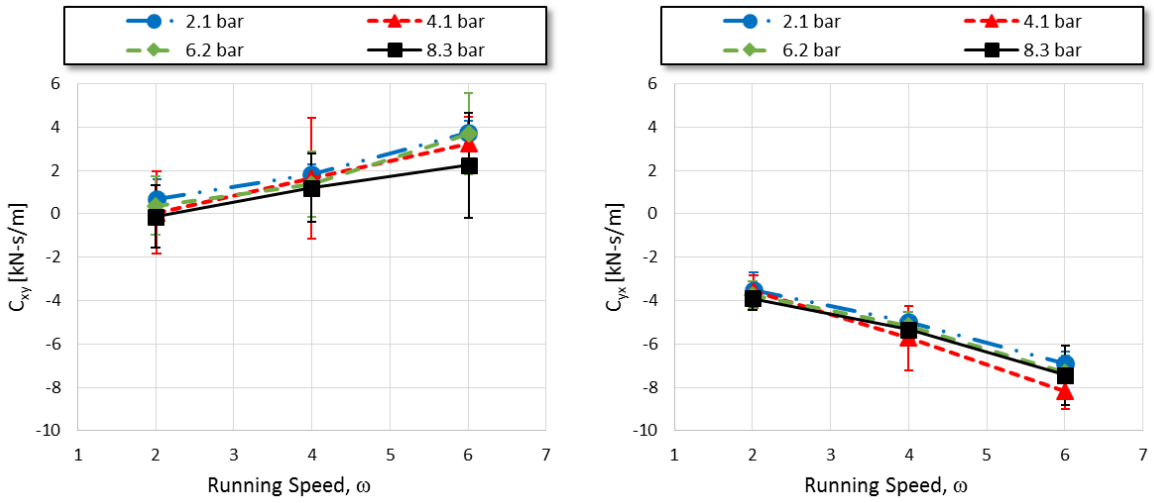

(a) **(b)**

Figure 31. Grooved seal's (a) C_{xy} and (b) C_{yx} versus ω at ϵ_0 = 0.00 over the ΔP range.

To continue, Figs. 32, 33, and 34 compare the grooved and smooth seal's damping terms as a function of ϵ_0, PSR and ω, respectively. In terms of ϵ_o, Fig. 32 shows the grooved seal's damping coefficients remaining largely unchanged over the entire ϵ_0 range. While the smooth seal follows this trend for ϵ_0 up to 0.50, both its direct and cross-coupled damping terms sharply increase in magnitude at ϵ_0 = 0.80. Note that for ϵ_0 < 0.5, the smooth seal's direct damping nearly doubles that of the grooved seal. The smooth seal's cross-coupled damping generally follows the model in Eq. (2) by having opposite signs for ϵ_0 < 0.5. However, at ϵ_0 =0.80, where said model is no longer valid, they both take a sharp dive to the negative side. The author is unsure of what causes this same-sing phenomenon.

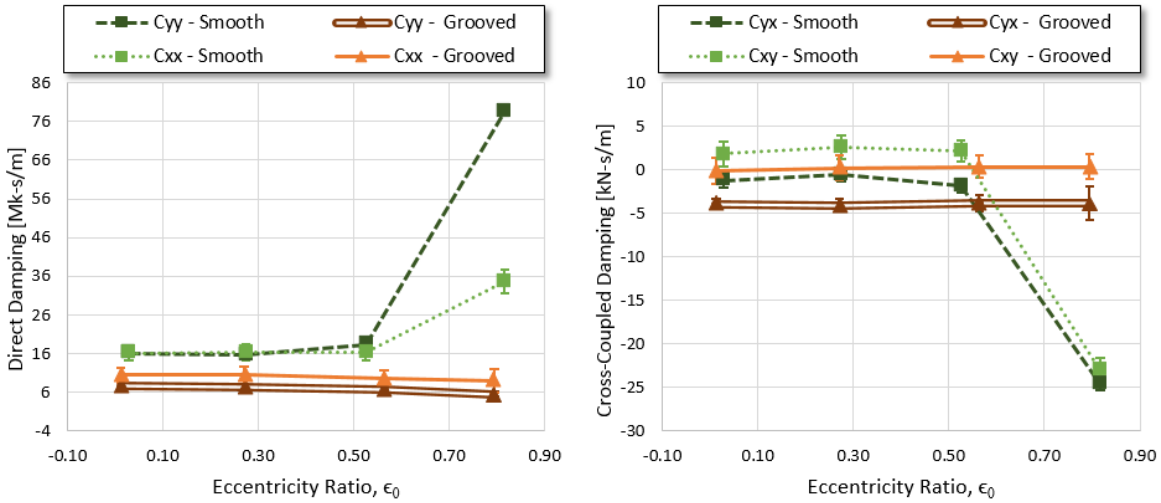

(a) **(b)**

Figure 32. Comparison between grooved and smooth seals. (a) Direct and (b) cross-coupled damping versus ϵ_0 at ΔP = 8.3 bar, and ω = 2 krpm. Measured PSR values range from 0.0 to 0.18.

Figure 33a suggests that both seals' direct damping terms are a weak function of PSR. Figure 33b shows the grooved seal's cross-coupled damping terms remaining generally unchanged across the PSR range. In contrast, the smooth seal's C_{xy}, C_{yx} clearly increase in magnitude with increasing PSR.

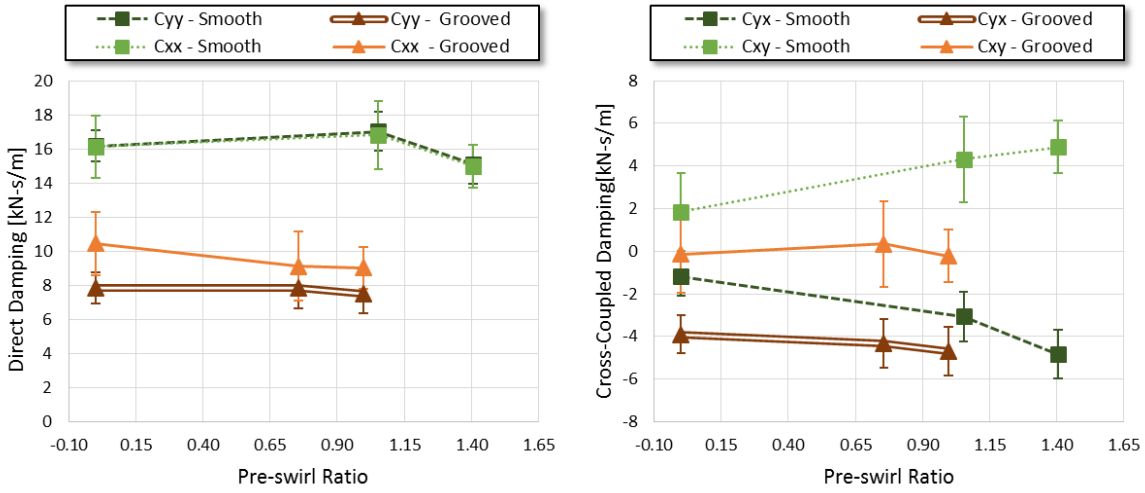

(a) **(b)**

Figure 33. Comparison between grooved and smooth seals. (a) Direct and (b) cross-coupled damping versus measured PSR at ϵ_0 = 0.0, ΔP = 8.3 bar, and ω = 2 krpm.

In Fig. 34a, the direct damping values slightly increase and decrease for the grooved and smooth seals, respectively, with increasing ω. Figure 34b shows both seals' cross-coupled damping increase in magnitude with increasing ω.

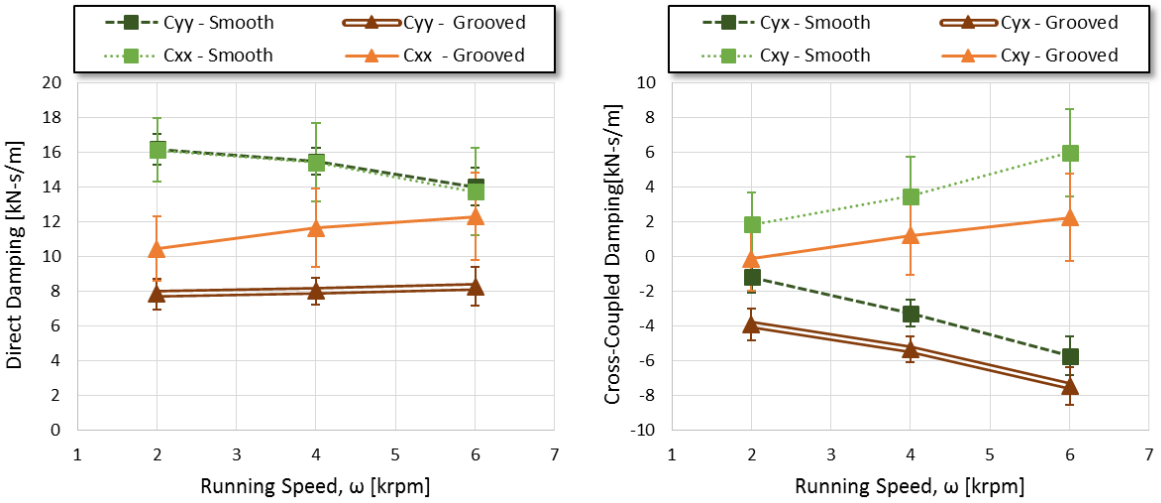

(a) **(b)**

Figure 34. Comparison between grooved and smooth seals. (a) Direct and (b) cross-coupled damping versus ω at ϵ_0 = 0.00, and ΔP = 8.3 bar. Measured PSR values range from 0.0 to 0.29.

For centered positions (ϵ_0 = 0.00), the smooth seal generally develops higher direct damping coefficients than the grooved seal by a factor of approximately 1.5, on average, enabling it to better withstand perturbations.

6.4 Rotordynamic Virtual Mass Coefficients

Figures 35 and 36 show the grooved seal's direct, and cross-coupled virtual mass terms, respectively, as a function of ϵ_0. Figures 35a and 35b show the M_{xx}, M_{yy} values increasing slightly with increasing ω and increasing ϵ_0, but do not display a clear trend with increasing ΔP. Note that the grooved seal's direct virtual mass terms remain above 10 kg [22.05 lbs]. In contrast, the M_{xy} and M_{yx} terms shown in Fig. 36 are both slightly negative. In general, the grooved seal's cross-coupled virtual mass terms remain above -2 kg [-4.41 lbs]. Recalling Eq. (15), negative virtual mass terms generally result in a dynamic stiffness (Re($\boldsymbol{H}_{ij}$)) that increases with increasing Ω. In this case, however, M_{xy} and M_{yx} are generally at least 4 times smaller in magnitude than the M_{xx} and M_{yy} terms, ultimately having little

impact on the seal's stability characteristics.

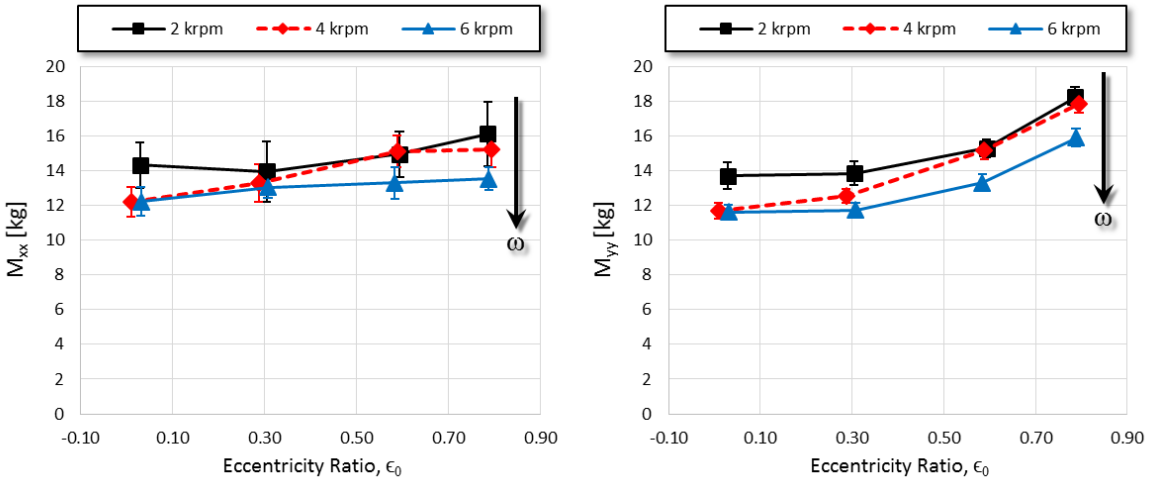

(a) **(b)**

Figure 35. Grooved seal (a) M_{xx} and (b) M_{yy} versus ϵ_0 at ΔP = 2.1 bar, over the ω range.

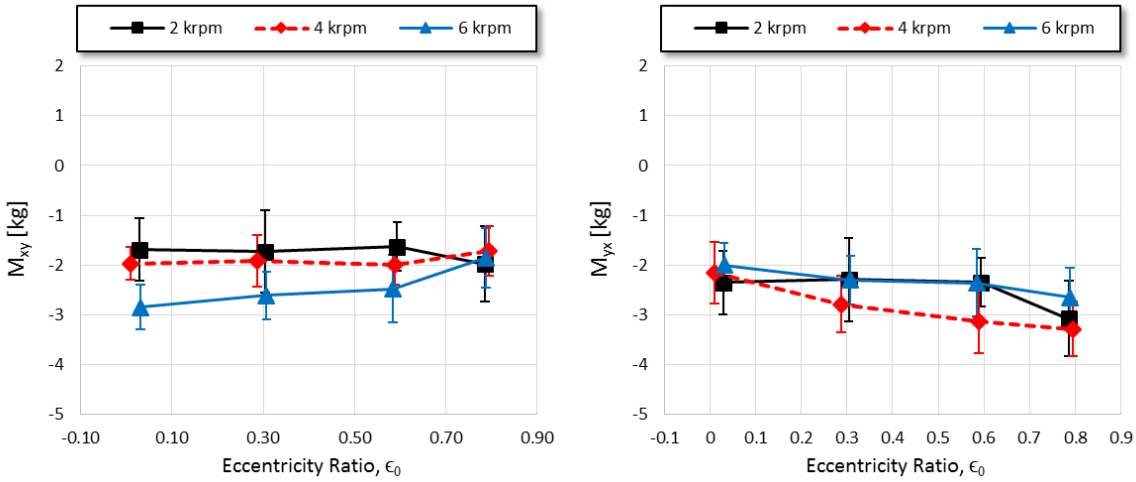

(a) **(b)**

Figure 36. Grooved seal (a) M_{xy} and (b) M_{yx} versus ϵ_0 at ΔP = 2.1 bar, over the ω range.

Figures 37a and 37b show that the grooved seal's mass terms are largely independent of increasing ϵ_0 through its entire range. The smooth seal follows this same trend for ϵ_0 up to 0.50, but show a significant magnitude increase in their direct and cross-coupled visual mass terms for ϵ =0.80. The smooth seal's virtual mass increase at ϵ_0 = 0.80 is common across the ω and ΔP range. As with the smooth seal's cross-coupled damping terms, the Author does not know what causes the smooth seal's virtual mass terms to have the same sign at ϵ_0 = 0.80. In his 2015 thesis work [6], J. Salas also encounters large, negative virtual mass terms in smooth seals operating at similar conditions to those here, but is unable to account for their source. Recall that the grooved seal's cross-coupled virtual mass terms are small when comparted to its direct virtual mass terms, and have little impact on its performance.

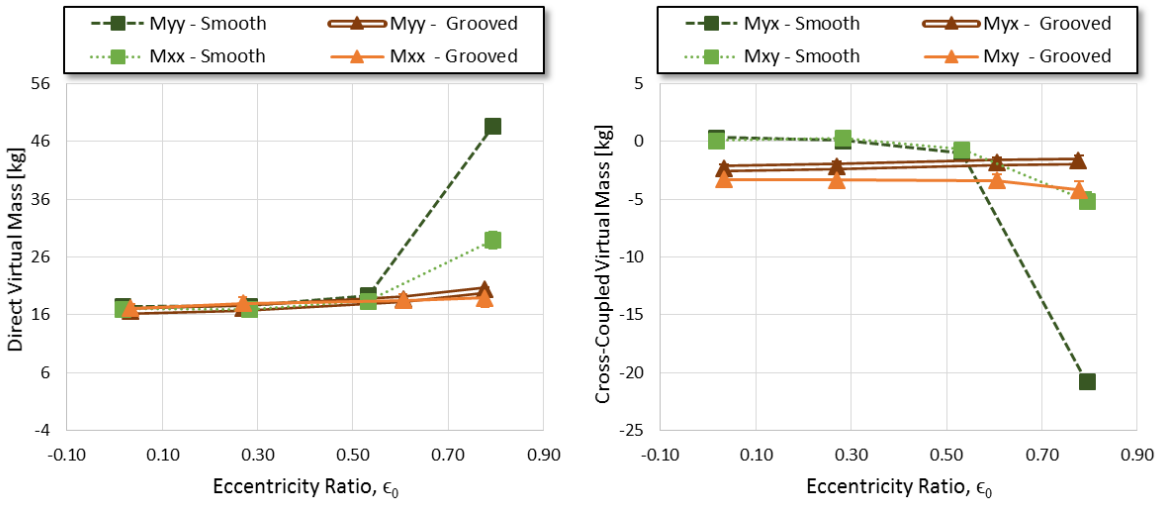

(a) **(b)**

Figure 37. Comparison between grooved and smooth seals. (a) Direct and (b) cross-coupled virtual mass versus ϵ_0 at ω = 2 krpm, and ΔP = 8.3 bar. Measured PSR values range from 0.0 to 0.11.

Next, Fig. 38a shows the direct virtual mass terms of both seals decrease with increasing ω. In Fig. 38b, the smooth seal's cross-coupled virtual mass terms increase in magnitude with increasing ω, while those from the groove seal show no clear trend.

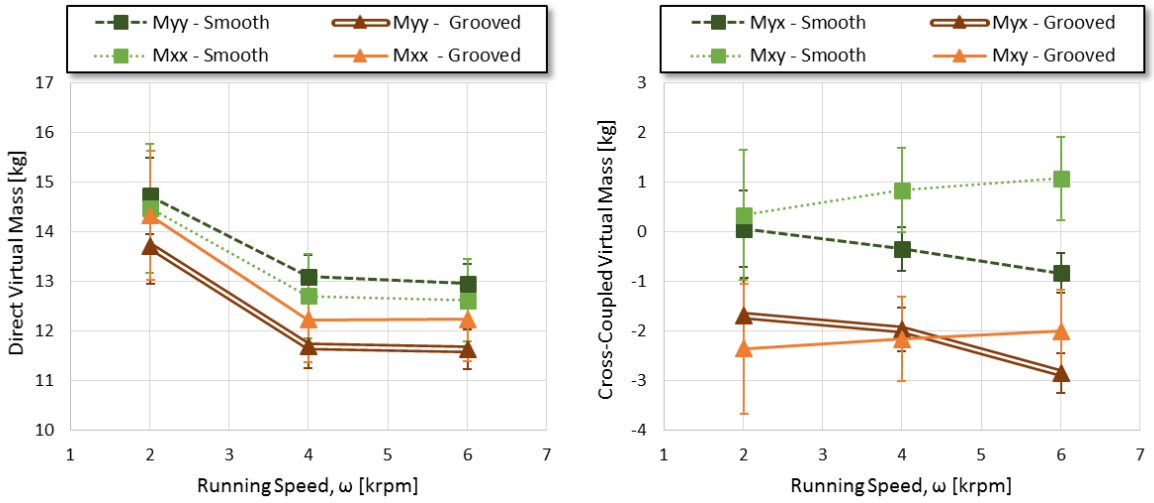

(a) **(b)**

Figure 38. Comparison between grooved and smooth seals. (a) Direct and (b) cross-coupled virtual mass versus ω at ϵ_0 = 0.00, and ΔP = 2.1 bar. Measured PSR values range from 0.0 to 0.30.

Increasing PSR had minimal impact on both seal's direct and cross-coupled virtual mass terms.

6.5 Whirl Frequency Ratio (WFR)

Displaying how ω, ΔP, and ϵ_0 affect the grooved seal's stability performance, Fig. 39a shows WFR clearly increasing with ω, while Fig. 39b shows it modestly decreasing with increasing ϵ_0. Both figures suggest that increasing ΔP benefits the seal's rotordynamics by decreasing its WFR.

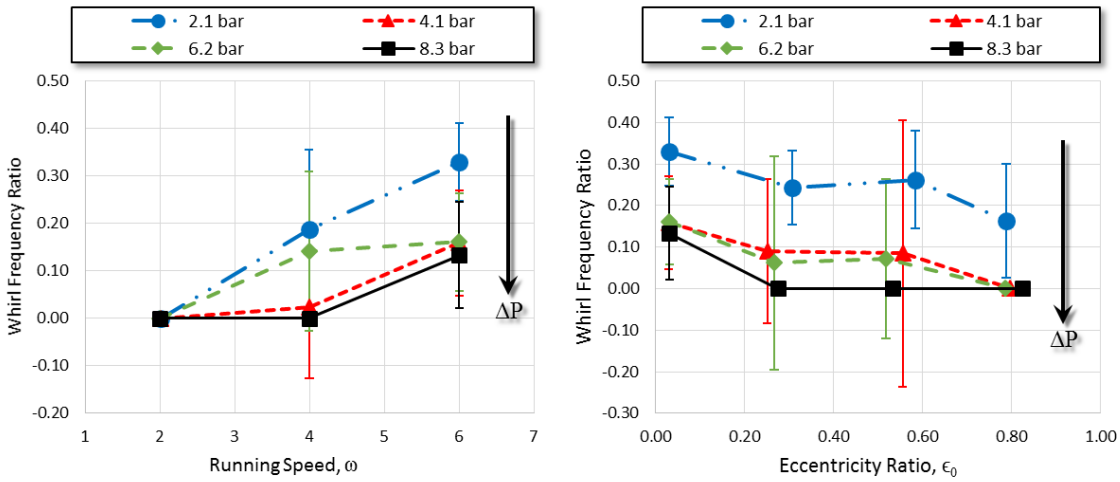

(a) **(b)**

Figure 39. Grooved seal's WFR versus (a) ω at ϵ_0 = 0.00, and (b) ϵ_0, at ω = 6 krpm. Measured PSR values range from 0.0 to 0.29.

Figure 40a shows the grooved seal's WFR clearly increasing with increasing PSR at $\boldsymbol{\omega}$ = 2 krpm. At $\boldsymbol{\omega}$ = 6 krpm, however, PSR values are lower and do not cause a clear trend on the grooved seal's WFR, as shown in Fig. 40b. In general, the grooved seal displays the lowest values of WFR at high $\boldsymbol{\Delta P}$, and low $\boldsymbol{\omega}$. Recall that these are also the operating conditions where the grooved seal develops its highest direct stiffness forces. Finally, recall

that the WFR does not provide a good basis for comparing stability performance of different seals.

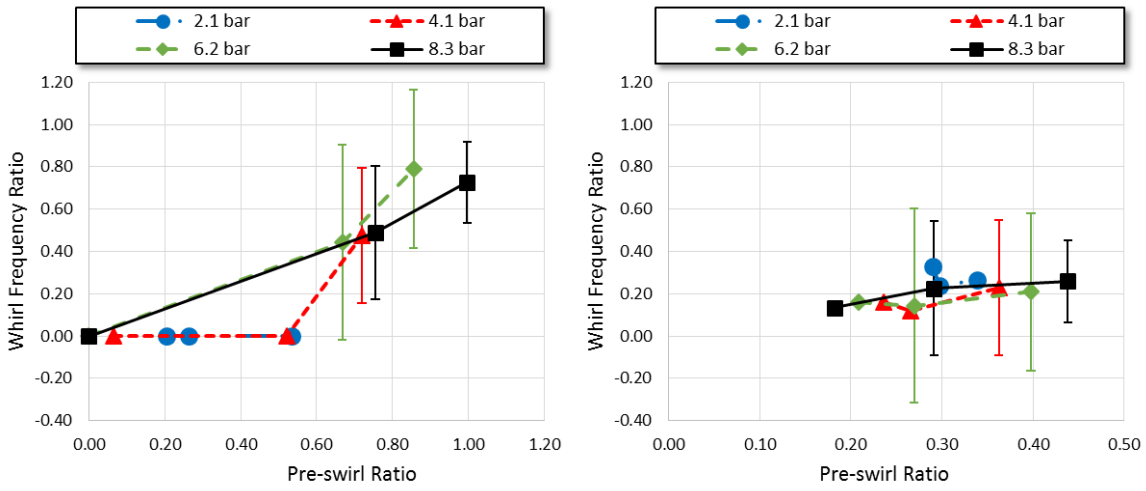

(a) **(b)**

Figure 40. Grooved seal's WFR versus measured PSR at ϵ_0 = 0.00 for (a) ω = 2 krpm, and (b) ω = 6 krpm.

6.6 Effective Stiffness Coefficients

Using Eqs. (5) and (6), the present and following sections provide a rotordynamic comparison between the grooved and smooth seals. Recall that these equations are only applicable to centered operation ($\epsilon_0 \approx 0.0$). Note that the rotordynamic coefficients in said equations are defined as the average of their two components. For example, K is defined as the average of K_{xx} and K_{yy}, c is defined as the average of C_{xy} and C_{yx}, and so on.

Figure 41 shows both seal's K_{eff} steadily dropping with increasing ω, and generally increasing with increasing ΔP. Note that the only positive effective stiffness values were produced by the smooth seal operating at ω = 2 krpm; the rest of the operating conditions result in negative K_{eff}. In general, the smooth seal's K_{eff} values are larger than those of the grooved seal by approximately 4.5 MN/m [25.6 x 10^3 lb_f/in] across the ω range. To understand the grooved seal's lower effective stiffness, recall Eqs. (5) and note that values of

positive K, negative c, and positive M all serve to decrease K_{eff}. Figure 38 shows that the grooved and smooth seal's M values are similar and thus do not play a significant role in their K_{eff} difference. Next, Section 7.2 (Rotordynamic Stiffness Coefficients) shows that the grooved seal's K values are noticeably lower than those of the smooth seal, and Figure 34 shows that the smooth seal's c values are very close to zero while those of the grooved seal are markedly negative. In short, the K-results suggest the grooved seal's K_{eff} should be greater than those of the smooth seal, but the c-results suggest the opposite. Ultimately, the effect of c overshadows the effect of K and causes higher K_{eff} for the smooth seal.

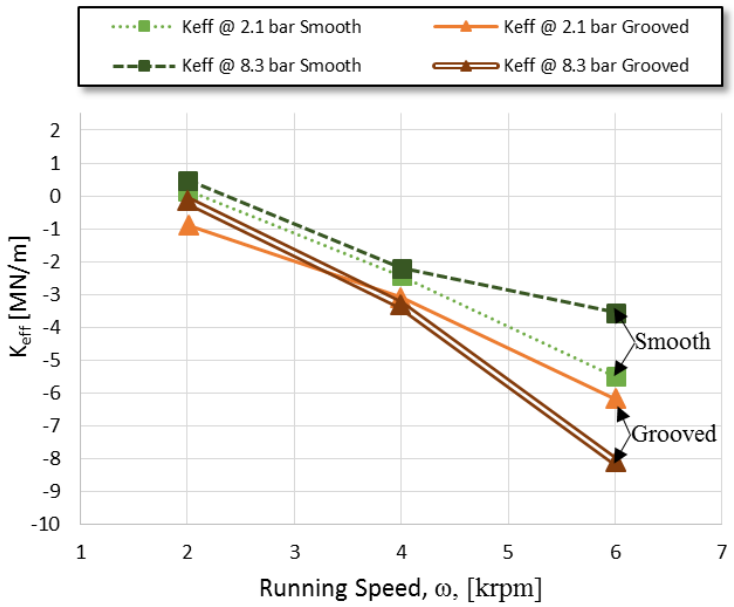

Figure 41. Comparison between grooved and smooth seals. K_{eff} versus ω for ΔP = 2.1, 8.3 bar, and ϵ_0 = 0.00. Measured PSR ranges from 0.0 to 0.30.

Figure 42a shows that the grooved seal's K_{eff} slightly decreases with increasing PSR at ω = 2 krpm. At ω = 6 krpm, increasing PSR does not produce a clear trend on the grooved and smooth seals' effective stiffness, as shown in Fig. 42b.

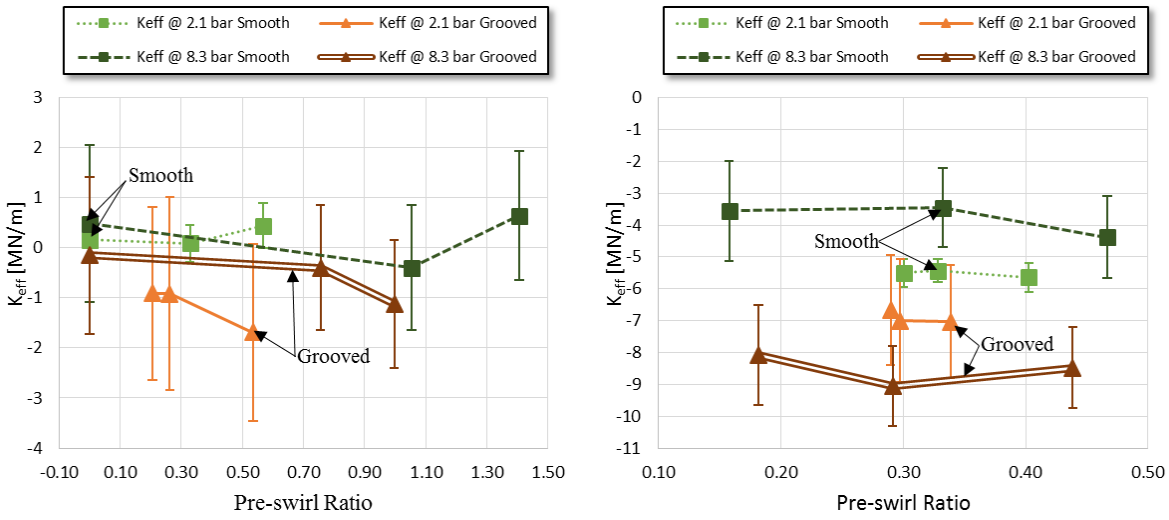

Figure 42. Comparison between grooved and smooth seals. K_{eff} versus measured PSR for ϵ_0 = 0.00, ΔP = 2.1, 8.2, and ω = (a) 2 krpm (b) 6 krpm.

6.7 Effective Damping Coefficients

Figures 43 and 44 display how seal geometry affects stability performance by plotting C_{eff} as a function of operating parameters. Specifically, Fig. 43 shows that for the same ΔP, the smooth seal develops larger C_{eff} values than the grooved seal; approximately 30% greater at ΔP = 8.3 bar [120 PSI], and 15% greater at ΔP = 2.1 bar [30 PSI].

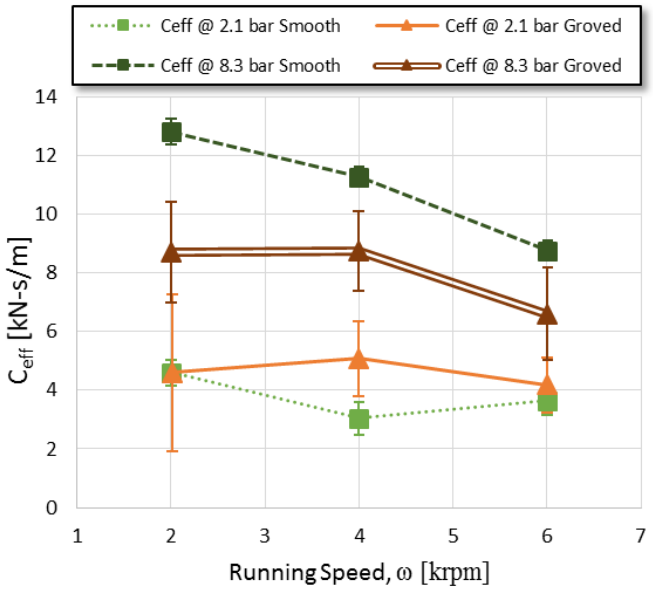

Figure 43. Comparison between grooved and smooth seals. C_{eff} versus ω for ΔP = 2.1, 8.3 bar, and ϵ_0 = 0.0. Measured PSR ranges from 0.0 to 0.30.

To continue, Fig. 43 demonstrates the stability-degrading effect of inlet-fluid rotation by showing C_{eff} decreasing with increasing PSR. Note that the C_{eff} values decrease more sharply in Fig. 43a, at ω = 2 krpm, than in Fig. 43b, at ω = 6 krpm, suggesting that the seal's stability performance suffers more with increasing PSR at low values of ω.

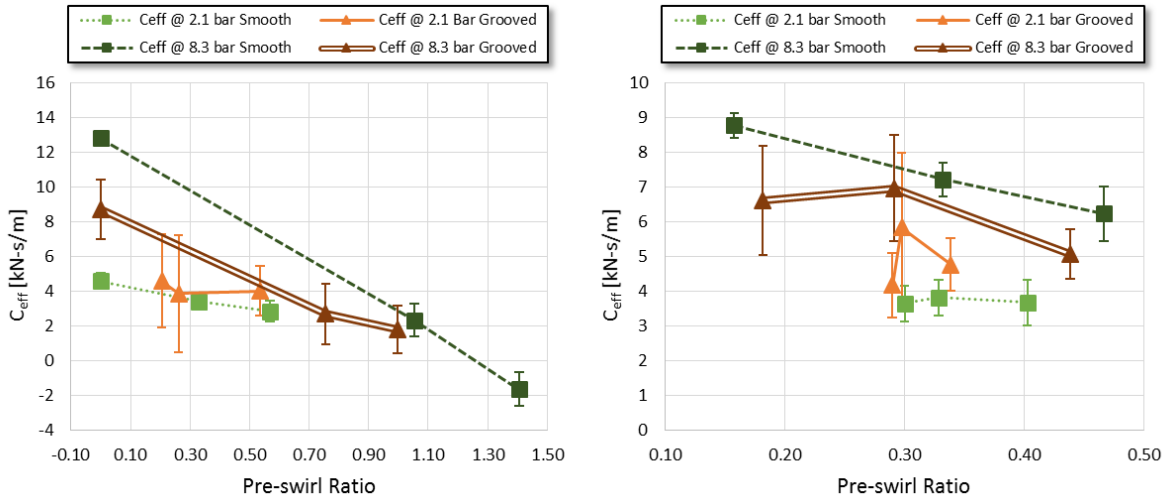

Figure 44. Comparison between grooved and smooth seals. C_{eff} versus measured PSR for ϵ_0 = 0.0, ΔP = 2.1, 8.2, and ω = (a) 2 krpm (b) 6 krpm.

7. MEASUREMENT VS. PREDICTION COMPARISON

Showing a comparison between the testing parameters of the present work and Marquette's test program [12], Fig. 45 highlights that while most of them are fairly similar, Marquette employs ΔPs approximately 10x higher than those used here.

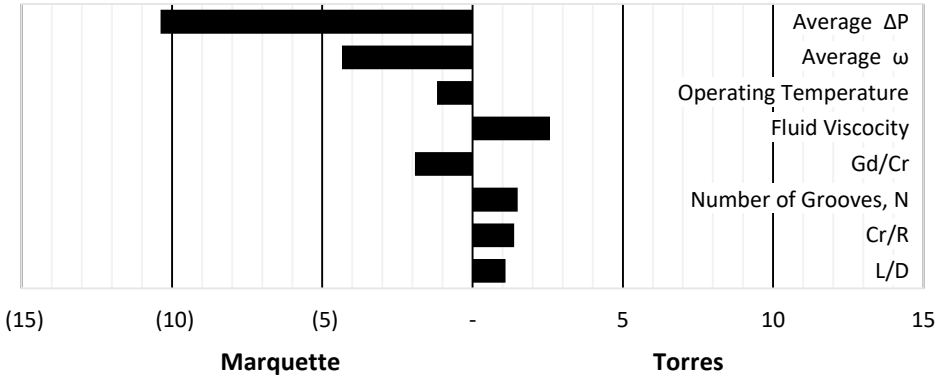

Figure 45. Testing-parameter comparison between the current test program and Marquette's experiment [12]. The x-axis represents the multiplication factor between programs. Marquette's ΔP is approximately 10 times higher than in the present study.

Next, Fig. 45 shows that the $\dot{Q}$ % deviation between measurement and prediction is significantly higher at ΔP below 10 bar [145 PSI], when compared to those at ΔP above 40 [580 PSI] bar. Additionally, increasing ω also decreases the $\dot{Q}$ % deviation.

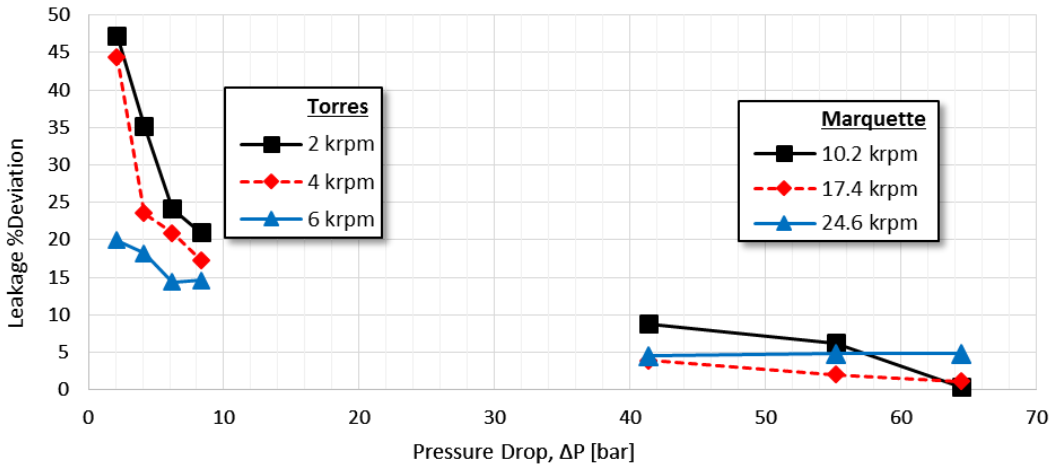

Figure 46. Percent deviation between measured and predicted $\dot{Q}$ at ϵ_0 = 0.00 for Torres' and Marquette's grooved seals.

Next, Fig. 47 shows a high percent deviation across the rotordynamic coefficients. Specifically, the code under predicts all coefficients by at least 50%. The y-direction direct stiffness suffers the highest difference of approximate 200%, on average, across the ΔP range. These results, in concert with Marquette's better agreement, suggest that the code's accuracy increases with increasing ΔP. Note that the code has default empirical parameters that affect its predictions. While modifying these parameters may have resulted in better predictions, the author used the default values to remain within the scope of this study.

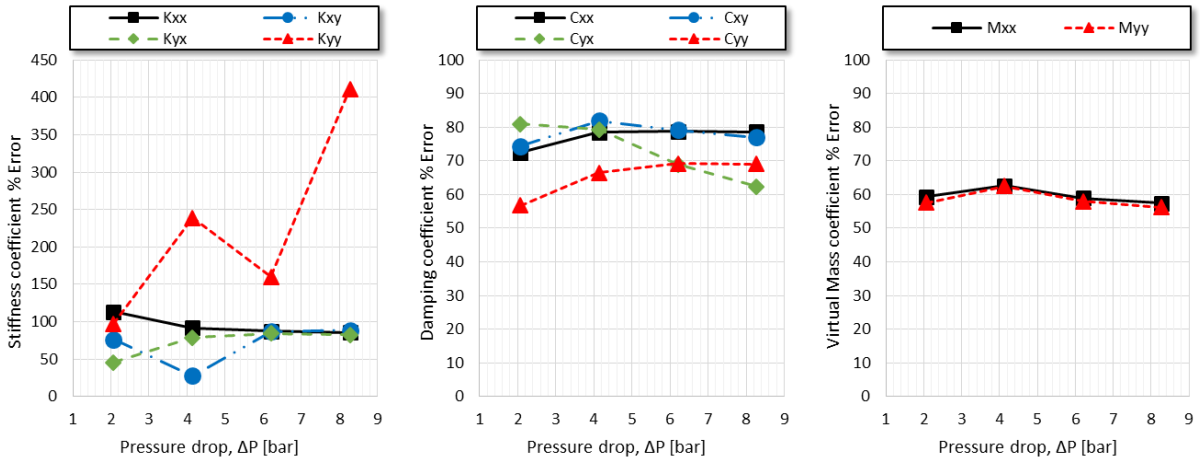

(a) **(b)** **(c)**

Figure 47. Percent deviation between measured and predicted (a) Stiffness (b) Damping (c) Virtual Mass coefficients at ϵ_0 = 0.00, and ω = 4 krpm.

8. SUMMARY AND CONCLUSIONS

8.1 Summary

While circumferentially-grooved stator (CGS) liquid annular seals have headlined some research programs [9, 12, 13, 14], none of these programs measured the fluid's circumferential velocity at the seal's outlet. Additionally, the programs [9, 13] that did induce and measure inlet-fluid rotation are limited to eccentricity ratios ϵ_0 below 0.50. As a result, the present work focuses on how a wide range of Pre-swirl Ratios (PSR) and ϵ_0 affect the static and rotordynamic performance of a CGS seal operated on a smooth rotor.

As shown in Fig. 3, the test seal features 15 equally spaced, square grooves, has a minimum radial clearance C_r of 203.2 μm (8 mil), and a length-to-diameter ratio L/D, of 0.5. To determine how seal performance depends on operating conditions, the author varies the axial pressure drop ΔP, eccentricity ratio, angular speed ω, and the pre-swirl velocities as outlined in Table 6, while measuring static and dynamic parameters.

Table 6. Variation of testing parameters.

Parameter	Values
Axial Pressure drop, ΔP	2.07, 4.14, 6.21, 8.27 bar | 30, 60, 90, 120 PSI
Eccentricity ratio, ϵ_0	0.00, 0.27, 0.53, 0.80
Shaft's angular speed, ω	2, 4, 6 krpm
Pre-swirl velocities	low, medium, high

8.2 Static Results

The results of this investigation indicate that leakage rate $\dot{Q}$ increases markedly with increasing ΔP, slightly with increasing ϵ_0, and decreases mildly with increasing ω. Moreover, the circumferential grooves provide approximately 20% reduction in $\dot{Q}$ at 2 krpm, but only approximately 6% at 6 krpm.

The measured Outlet swirl ratio (OSR) could prove useful to researchers using Computational Fluid Dynamics (CFD) calculations for predicting the static, and rotordynamic behavior of grooved seals. The data shows that OSR decreases with increasing ω, and increases with increasing ϵ_0. Also, when compared to the smooth seal, the grooved seal produces lower OSR values: approximately 10% lower at ΔP = 2.1 bar [30 PSI], and approximately 20% lower at ΔP = 8.3 bar [120 PSI]. The author suspects that the grooved seals' larger surface area, in concert with its larger average clearance, is responsible for its lower OSR values, when compared to the smooth seal.

8.3 Rotordynamic Results

As a preface to this section, recall that the applied load acts in the negative y-direction. Additionally, the component average is used to compare rotordynamic parameters and seal performance between the grooved and smooth seals. For example, the direct stiffness coefficient K refers to the average of K_{xx} and K_{yy}, the cross-coupled damping coefficient c refers to the average of C_{xy} and C_{yx}, and so on.

The grooved seal develops negative direct stiffness values for a large portion of the test program: ω > 2 krpm, and ΔP < 6.2 bar [90 PSI]. Specifically, K_{xx} and K_{yy} reach a minimum of approximately -1.9 MN/m [-1.1 x 10^4 lb_f/in] and -2.4 MN/m [-1.4 x 10^4 lb_f/in], respectively, at ω = 6 krpm, and ΔP = 2.1 bar [30 PSI]. Additionally, the grooved seal's direct stiffness are generally insensitive to increasing ϵ_0 up to 0.80. For ϵ_0 up to 0.27, the grooved and smooth seals generally produce similar direct stiffness values. However, the smooth seal's direct stiffness generally surpasses that of the grooved seal by a factor of approximately 3.5 at ϵ_0 = 0.80. Increasing ΔP from 1.2 to 8.3 bar [30 to 120 PSI] generally increases the smooth seal's direct stiffness by a factor of approximately 2.5, but does not have a significant effect on the grooved seal's direct stiffness values. Finally, increasing PSR from 0.0 to 1.2 typically causes a subtle decrease in both seal's direct stiffness values. In regards to the grooved seal's cross-coupled stiffness values, they typically increase in magnitude with increasing ω, but are largely independent of increasing ϵ_0 up to 0.80, and increasing ΔP up to 8.3 bar [120 PSI]. Generally, K_{xy} remains mostly positive, while K_{yx} remains mostly negative, and these coefficients do not always have the same magnitude. In contrast to the grooved seal's indifference to ϵ_0, the smooth seal's cross-coupled stiffness

values generally increase in magnitude with increasing eccentricity ratio, especially for $\epsilon_0 >$ 0.50. At these high eccentricities, the smooth seal's cross-coupled stiffness values are typically larger than the grooved seal's by a factor of at least 2. In contrast to its subtle effect on direct stiffness values, increasing PSR from 0.0 to 1.2 generally increases the grooved seal's cross-coupled stiffness magnitude by a factor of at least 1.5, and that of the smooth seal by a factor of approximately 2.5.

The grooved seal's direct damping coefficients increase with increasing ΔP and ω, but are generally unaffected by increasing ϵ_0 up to 0.80. The grooved seal attains its highest damping forces of approximately 17.5 kN-s/m at ω = 6 krpm and ΔP = 8.3 bar [120 PSI]. Next, the smooth seal's direct damping is also independent of ϵ_0 up to 0.50. It produces direct damping forces larger than those of the grooved seal by a factor of at least 2 for $\epsilon_0 <$ 0.50, and a factor of at least 4 for ϵ_0 = 0.80. Specifically, the smooth seal's highest direct damping value (75 kN-s/m [4.27 x 10^2 lb_f-s/m]) is greater than that of the grooved seal by a factor of approximately 4. Next, both seal's direct damping coefficients were generally unaffected by increasing PSR from 0.0 to 1.2. As for the cross-coupled damping coefficients, those of the grooved seal clearly increase with increasing ω, but are not noticeably affected by increasing ΔP up to 8.3 bar [120 PSI], and ϵ_0 up to 0.80. While C_{xy} generally remains positive and C_{yx} generally remains negative, they do not always have the same magnitude. As for the smooth seal, its cross-coupled damping terms are largely unaffected by increasing ϵ_0 up to 0.50. Then, at ϵ_0 = 0.80 both cross-coupled damping components generally take a drastic drop to the negative side, a phenomenon the author is unable to account for. In general, the smooth seal's cross-coupled damping is similar to that of the grooved seal for ϵ_0 up to 0.50, but greater by a factor of at least 4 at ϵ_0 = 0.80. Increasing the PSR from 0.0 to 1.2 generally makes the smooth seal's cross-coupled damping values clearly diverge away from zero; this trend is significantly more subtle for the grooved seal.

In general, the grooved seal's virtual mass increases with increasing ω and ϵ_0, does not show a clear trend with increasing ΔP up to 8.3 bar [120 PSI], and remains above 10 kg [22.05 lbs] for the entire range. For ϵ_0 below 0.50, the smooth seal produced very similar direct virtual mass values to those of the grooved seal. The smooth seal's direct virtual mass terms generally increase by a factor of at least 1.5 when increasing the ϵ_0 from 0.50 to 0.80.

Increasing PSR had a negligible effect on both seals' direct virtual mass. Transitioning to cross-coupled virtual mass terms, the grooved seal sometimes produces slightly negative values. Remaining above -2 kg [-4.41 lbs], they are lower than the positive, direct virtual mass terms by a factor of at least 4, and should not significantly affect the grooved seal's performance. The smooth seal's cross-coupled virtual mass terms rake a sharp drop at ϵ_0 =0.80, becoming negative. While this drop is significant, the author is unable to account for its appearance.

The grooved seal's WFR generally increases clearly with increasing ω, decreases markedly with increasing ΔP, but does not show a clear trend with increasing ϵ_0 up to 0.80. The grooved seal's WFR generally increases with increasing PSR at ω = 2 krpm. Specifically, increasing PSR from approximately 0.0 to 1.0, increases the grooved seal's WFR from approximately 0.0 to 0.75, on average, across the ΔP range. The effect of PSR diminishes with increasing ω, leading to a WFR that is indifferent to increasing PSR at ω = 6 krpm.

In general, both seal's effective stiffness increase with increasing ΔP, decrease with increasing ω, and yields positive values only for the smooth seal operating at ω = 2 krpm. Specifically, increasing ω from 2 to 6 krpm, generally drops the smooth seal's K_{eff} from approximately 0.5 MN/m [2.9 x 10^3 lb_f/in] to approximately -4.5 MN/m [-2.6 x 10^4 lb_f/in], and reduces that of the grooved seal by a factor of approximately 5. Recall that the grooved seal only produces negative effective stiffness values. In general, increasing PSR from 0.0 to 1.2 does not have a significant impact on either seal.

Similar to effective stiffness, both seal's effective damping clearly increases with increasing ΔP and slightly decreases with increasing ω. Specifically, increasing the ΔP from 2.1 to 8.3 bar [30 to 120 PSI], generally increases the smooth seal's effective damping by a factor of approximately 3, and that of the smooth seal by a factor of approximately 1.5, on average, across the ω range for ϵ_0 = 0.00. At ω = 2 krpm increasing the PSR from 0.0 to 1.2 generally decreases the smooth seal's effective damping by a factor of approximately 4. For this same PSR change, the grooved seal's effective damping is reduced by a factor of approximately 1.5. For ΔP = 8 bar [120 PSI] and $\epsilon_0 \approx 0.00$, the smooth seal's effective damping is greater than that of the grooved seal by a factor of at least 1.5.

In regards to the prediction code developed by Marquette [10], it under predicts all of the experimental rotordynamic coefficients by at least 50% when using the default empirical parameters. The author suspects that using ΔPs ~ 10x lower than those employed by Marquette is a main factor contributing to this discrepancy, and that modifying the empirical parameters could lead to improved predictions.

Serving to summarize the findings of this investigation, the following points corroborate conclusions of past relevant test programs, while contributing additional findings:

- Machining grooves into a smooth seal provide a leakage-reducing benefit at the cost of markedly lowering its direct stiffness, and damping coefficients. This investigation suggests this is specially true at high ϵ_0 values. The smooth seal's direct stiffness and damping coefficient were approximately 3.5, and 2 times greater than those of the grooved seal, respectively, at ϵ_0 = 0.80.
- Marquette and Childs reported that grooves make direct stiffness and damping coefficients independent of ϵ_0 values up to 0.50. This investigation extends this trend by showing that the grooved seal's direct *and* cross-coupled stiffness and damping coefficients are insensitive to increasing ϵ_0 up to 0.80.
- Iwatsubo et'al reported that inlet-fluid rotation strongly reduces the stability of smooth seals. This study suggests that machining circumferential grooves aggravates this effect, especially at low values of ω.
- Highlighting its better rotordynamic characteristics, the smooth seal's effective stiffness and damping coefficients are consistently larger than those of the grooved seal.
- When using the default values for empirical parameters, Marquette's code significantly under predicts experimental rotordynamic coefficients tested here at ΔPs lower than 10 bar.

To conclude, the data suggests that pump manufactures machining circumferential grooves in turbulent-fluid, annular seals, should operate them with entrance swirl brakes, especially for low ΔP, high ω applications. At the cost of reducing the seals rotordynamic performance, the circumferential grooves provide a limited leakage benefit. Finally, the

author recommends using Marquette's code with its default empirical parameters to simulate seal operation only for ΔPs exceeding 30 bar.

The development of a computer code to simulate the effectiveness of differing swirl-brake designs, accompanied by an upgraded test rig to validate such code, would further aid the industry in minimizing the fluid rotation-driven cross-coupled destabilizing forces.

REFERENCES

[1] Bremmer, C., Harris, G., and Kosmala, A., 2016, "Evolving technologies: Electrical submersible pumps," Oilfeld Rev., **18**, pp. 30–43.

[2] Childs, D. W., 2013, *Turbomachinery Rotordynamics with Case Studies*, Minter Spring, Chapter 7: Rotordynamics of Pumps. pp. 319,323, 334,343, 350-353. 354-356.

[3] Childs, D. W., Norrbin, C. S., and Phillips, S., 2014, "A lateral rotordynamics primer on electrical submersible pumps (esp's) for deep subsea applications." *Proceedings of the 30th Pump User's Symposia*, 2014.

[4] Lomakin, A., 1958, "Calculation of the critical number of revolutions and the conditions necessary for dynamic stability of rotors in high-pressure hydraulic machines when taking into account forces originating in sealings," *Journal for Power and Mechanical Engineering (In Russian)* pp. 1–5.

[5] San Andres, L., 2006, "Hydrodynamic Fluid Film Bearings and Their Effect on the Stability of Rotating Machinery" [Online]. Available: http://www.dtic.mil/dtic/tr/fulltext/u2/a476533.pdf. [Accessed: 12-Mar-2016].

[6] Salas, J. I., 2015, "Influence of Pressure-dams In Liquid Annular Seals in the Laminar Flow Regime, Measured Results for Static and Rotordyanmic Characteristics," M.S. Thesis, Texas A&M University, College Station.

[7] Lund, J., 1966, "Self-excited, Stationary Whirl Orbits of a Journal in a Sleeve Bearing," Ph.D. Thesis, Rensselaer Polytechnic Institute, Troy.

[8] San Andres, L., 1991, "Effect of Eccentricity on the Force Response of a Hybrid Bearing," *Tribology Transactions*, **34**,pp. 537–544.

[9] Florjancic, S., and McCloskey, T., 1990, "Measurement and Prediction of full scale Annular Seal coefficients," *Eighth International Pump Users Symposium*, pp. 71–87.

[10] Marquette, O. R., and Childs, D. W., 1996, "An Extended Three-Control-Volume Theory for Circumferentially-Grooved Liquid Seals," *Journal of Tribology*, **118**, pp. 277–285.

[11] Arghir, M., and Frene, J., 2004, "A Bulk-Flow Analysis of Static and Dynamic Characteristics of Eccentric Circumferentially- Grooved Liquid Annular Seals," *Journal of Tribology*, **126**, pp. 316–325.

[12] Marquette, O., and Childs, D. W., June 22-26, "Theory versus experiment for leakage and Rotordynamic coefficients of circumferentially-grooved liquid annular sealswith L/D of 0.45," in *Proceedings of the 1997 ASME Fluids Engineering Division SUmmer Meeting,* Vancouver, Canada, pp. 1-16

[13] Iwatsubo, T., Sheng, B., and Matsumoto, T., 1989, "An experimental Study on the static and dynamic characteristics of pump annular seals," in *Rotordynamic Instability Problems in High-Performance Turbomachinery,* NASA, Lewis Research Center, pp. 229–251.

[14] Kilgore, J. J., and Childs, D. W., 1990, "Rotordynamic Coefficients and Leakage Flow of Circumferentially Grooved Liquid-Seals," *Transactions of the ASME,* **112**, pp. 250–256.

[15] Childs, D. W., Graviss, M., and Rodriguez, L., 2007, "Influence of Groove Size on the Static and Rotordynamic Characteristics of Short, Laminar-Flow Annular Seals," *Transactions of the ASME,* **129**, pp. 398–406.

[16] Kaul, A., 1999, "Design and Development of a Test Setup for the Experimental Determination of the Rotordynamic and Leakage Characteristics of Annular Bushing Oil Seals," M.E. Report, Texas A&M University, College Station.

[17] Glienicke, J., 1996, "Experimental Investigation of Stiffness and Damping Coefficients of Turbine Bearings and Their Application to Instability Predictions," in *Proceedings of the Institution of Mechanical Engineers,* **181**, pp. 116–129.

[18] Kluitenberg, M., 2014, "Experimentally Determine the Impact of Inactive Jacking Ports on the Rotordynamic Characteristics of a Four-Pad, LBP, Tilting-Pad Journal Bearing," M.S. Thesis, Texas A&M University, College Station.

[19] Kulhanek, C. ., 2010, "Dynamic and Static Characteristics of a Rocker-Pivot, Tilting-Pad Bearing with 50% and 60% Offsets," M.S. Thesis, Texas A&M University, College Station.

[20] Coghlan, D. M., 2014, "Static, Rotordynamic, and Thermal Characterization of a Four Pad Spherical-Seat Tilting Pad Journal Bearing with Four Methods of Directed Lubrication," M.S. Thesis, Texas A&M University, College Station.

[21] Childs, D. W., and Hale, K., 1994, "A test apparatus and facility to identify the rotordynamic coefficients of high-speed hydrostatic bearings," *Journal of Tribology,* **166**, pp. 337–343.

[22] Childs, D. W., and Rouvas, C., 1993, “A parameter identification method for the rotordynamic coefficients of a high reynolds number hydrostatic bearing,” *Transactions of the ASME,* **115**, pp. 264–270.

[23] Beckwith, T., Marangoni, R., and Lienhard, V., 2007, *Mechanical Measurements*, Pearson Education, Inc, Upper Saddle River, NJ.

[24] Szeri, A., 1980, *Tribology: Friction, Lubrication, and Wear*, McGraw Hill Publishing, Washington.

[25] Moreland, A. J., 2016, “Moreland - Effect of Eccentricity and Pre-swirl on Smooth Stator_Grooved Rotor Liquid Annular Seals, Measured Static and Dynamic Results,” M.S. Thesis, Texas A&M University, College Station.

APPENDIX A

TABULATED RESULTS

Low PSR Assembly

Table A. 1. Static results of the grooved seal with low PSR.

#	Target			Measured					
	ω	ΔP	ϵ_0	ω	ΔP	ϵ_0	Q	φ	f_R
	[rpm]	[bar]	[-]	[rpm]	[bar]	[-]	[LPM]	[deg]	[N]
1	2000	2.068	0.00	2014.5	1.973	0.029	19.55	166.9	26.0
2	2000	2.068	0.27	2013.8	1.902	0.304	19.58	-17.1	57.4
3	2000	2.068	0.53	2013.3	1.959	0.593	20.89	-12.8	-32.6
4	2000	2.068	0.80	2012.9	2.113	0.786	23.67	-5.4	-131.5
5	2000	4.137	0.00	2012.1	3.987	0.079	31.16	-163.8	99.6
6	2000	4.137	0.27	2012.4	4.016	0.280	32.45	-17.2	197.7
7	2000	4.137	0.53	2012.1	3.967	0.580	34.62	-13.2	99.7
8	2000	4.137	0.80	2012.0	4.062	0.804	37.86	-10.2	-36.6
9	2000	6.205	0.00	2000.6	6.330	0.020	42.67	155.7	11.4
10	2000	6.205	0.27	2012.1	6.477	0.234	44.04	-9.1	-224.9
11	2000	6.205	0.53	2012.4	6.140	0.521	44.91	-6.7	-363.6
12	2000	6.205	0.80	2012.4	6.071	0.770	48.11	-5.9	-112.3
13	2000	8.274	0.00	2000.5	8.247	0.012	50.36	73.5	-11.0
14	2000	8.274	0.27	2000.3	8.170	0.271	51.33	-15.0	-84.5
15	2000	8.274	0.53	2000.4	8.043	0.564	53.71	-6.3	-111.8
16	2000	8.274	0.80	2000.5	7.762	0.795	56.36	-3.8	-231.0
17	4000	2.068	0.00	3996.1	2.066	0.009	17.93	-38.0	-21.3
18	4000	2.068	0.27	3996.7	2.025	0.287	18.03	-3.7	-49.5
19	4000	2.068	0.53	3996.7	2.089	0.588	20.14	-6.6	-201.0
20	4000	2.068	0.80	3996.8	1.927	0.794	20.23	-5.1	-313.0
21	4000	4.137	0.00	3996.9	4.212	0.009	32.13	-91.9	-30.4
22	4000	4.137	0.27	3996.7	4.170	0.289	32.24	-11.9	-8.4
23	4000	4.137	0.53	3997.0	4.123	0.532	33.76	-8.5	-213.0
24	4000	4.137	0.80	3996.8	4.217	0.807	36.75	-9.1	-278.2

Table A. 2. Static results of the grooved seal with low PSR (Continued).

#	Target			Measured					
	ω	ΔP	ϵ_0	ω	ΔP	ϵ_0	Q	φ	f_R
	[rpm]	[bar]	[-]	[rpm]	[bar]	[-]	[LPM]	[deg]	[N]
25	4000	6.205	0.00	3996.9	6.352	0.071	42.03	-168.3	67.0
26	4000	6.205	0.27	3996.9	6.160	0.288	42.43	-16.6	200.6
27	4000	6.205	0.53	3996.8	6.400	0.536	45.12	-7.6	103.4
28	4000	6.205	0.80	3996.6	6.193	0.796	47.37	-5.4	-51.6
29	4000	8.274	0.00	3996.7	8.194	0.033	49.61	-167.9	28.8
30	4000	8.274	0.27	3996.5	8.176	0.269	50.54	-15.7	184.7
31	4000	8.274	0.53	3996.5	7.851	0.606	52.81	-13.1	30.3
32	4000	8.274	0.80	3996.7	7.891	0.778	55.57	-7.1	-47.9
33	6000	2.068	0.00	6004.3	2.184	0.031	15.64	-26.1	-42.2
34	6000	2.068	0.27	6004.3	2.062	0.307	15.68	-18.9	-206.8
35	6000	2.068	0.53	6004.7	1.905	0.584	15.74	-7.3	-353.9
36	6000	2.068	0.80	6005.0	2.064	0.788	18.57	-5.3	-500.6
37	6000	4.137	0.00	6004.8	4.331	0.029	29.98	-32.1	-46.7
38	6000	4.137	0.27	6005.2	4.174	0.251	30.25	-13.0	-166.5
39	6000	4.137	0.53	6005.3	4.143	0.556	31.55	-10.2	-281.5
40	6000	4.137	0.80	6005.6	4.219	0.797	34.59	-4.4	-430.9
41	6000	6.205	0.00	6005.6	6.236	0.031	39.90	83.7	-20.9
42	6000	6.205	0.27	6005.0	6.403	0.267	41.55	-11.8	-38.6
43	6000	6.205	0.53	5993.2	6.172	0.518	42.55	-3.1	-503.4
44	6000	6.205	0.80	5992.0	5.985	0.786	44.91	-8.3	-450.9
45	6000	8.274	0.00	6004.7	8.159	0.031	48.10	-156.5	20.8
46	6000	8.274	0.27	6004.5	8.164	0.274	49.29	-15.9	103.7
47	6000	8.274	0.53	6004.7	8.190	0.532	51.43	-5.5	-62.9
48	6000	8.274	0.80	5990.1	7.955	0.826	54.82	-10.4	-430.2

Table A. 3. Static flow results of the grooved seal with low PSR.

#	PSR	OSR	Inlet Temp	Average Outlet Temp.	Re_z	Re_θ	Re
	[-]	[-]	[°C]	[°C]	[-]	[-]	[-]
1	0.205	0.245	45.4	45.0	8.59E+02	7.88E+03	7.93E+03
2	0.167	0.266	45.4	45.8	8.72E+02	7.99E+03	8.03E+03
3	0.142	0.285	45.9	46.0	9.35E+02	8.03E+03	8.08E+03
4	0.067	0.301	46.2	46.1	1.06E+03	8.05E+03	8.12E+03
5	0.064	0.271	46.8	46.5	1.41E+03	8.09E+03	8.22E+03
6	0.023	0.286	45.5	45.8	1.44E+03	7.97E+03	8.10E+03
7	0.000	0.307	46.1	46.7	1.56E+03	8.09E+03	8.24E+03
8	0.000	0.302	46.2	46.7	1.71E+03	8.10E+03	8.28E+03
9	0.000	0.245	45.5	46.1	1.91E+03	7.98E+03	8.20E+03
10	0.000	0.315	46.8	46.8	2.00E+03	8.13E+03	8.37E+03
11	0.000	0.328	46.3	46.5	2.03E+03	8.08E+03	8.33E+03
12	0.000	0.325	46.8	47.2	2.20E+03	8.18E+03	8.47E+03
13	0.000	0.273	46.2	45.8	2.25E+03	7.95E+03	8.26E+03
14	0.000	0.274	46.3	46.8	2.33E+03	8.08E+03	8.41E+03
15	0.000	0.284	46.8	46.6	2.43E+03	8.07E+03	8.43E+03
16	0.000	0.312	46.4	46.8	2.56E+03	8.08E+03	8.47E+03
17	0.259	0.237	46.7	46.5	8.12E+02	1.61E+04	1.61E+04
18	0.258	0.255	45.1	44.5	7.88E+02	1.56E+04	1.56E+04
19	0.242	0.256	44.9	45.5	8.94E+02	1.58E+04	1.58E+04
20	0.239	0.260	45.6	46.5	9.14E+02	1.61E+04	1.61E+04
21	0.196	0.237	46.6	47.0	1.47E+03	1.62E+04	1.63E+04
22	0.182	0.250	47.1	46.7	1.47E+03	1.62E+04	1.63E+04
23	0.181	0.256	46.4	47.0	1.54E+03	1.62E+04	1.63E+04
24	0.165	0.255	46.7	46.7	1.67E+03	1.61E+04	1.62E+04

Table A. 4. Static flow results of the grooved seal with low PSR (continued).

#	PSR	OSR	Inlet Temp	Average Outlet Temp.	Re_z	Re_θ	Re
	[-]	[-]	[°C]	[°C]	[-]	[-]	[-]
25	0.146	0.233	46.2	46.0	1.88E+03	1.59E+04	1.61E+04
26	0.139	0.252	46.7	47.5	1.95E+03	1.63E+04	1.65E+04
27	0.124	0.272	46.9	46.7	2.05E+03	1.62E+04	1.63E+04
28	0.097	0.286	46.6	46.0	2.12E+03	1.59E+04	1.61E+04
29	0.111	0.242	45.3	45.9	2.21E+03	1.59E+04	1.60E+04
30	0.088	0.257	45.9	46.7	2.28E+03	1.61E+04	1.62E+04
31	0.071	0.279	46.5	47.1	2.41E+03	1.62E+04	1.64E+04
32	0.000	0.285	46.1	46.4	2.50E+03	1.60E+04	1.62E+04
33	0.290	0.211	46.4	47.1	7.13E+02	2.44E+04	2.44E+04
34	0.289	0.221	46.0	47.4	7.17E+02	2.45E+04	2.45E+04
35	0.290	0.208	46.3	48.0	7.28E+02	2.47E+04	2.47E+04
36	0.267	0.222	47.1	48.4	8.68E+02	2.50E+04	2.50E+04
37	0.236	0.226	47.2	47.7	1.38E+03	2.47E+04	2.47E+04
38	0.233	0.244	46.6	48.0	1.40E+03	2.47E+04	2.48E+04
39	0.231	0.262	47.4	48.3	1.47E+03	2.49E+04	2.50E+04
40	0.218	0.272	46.5	47.0	1.57E+03	2.43E+04	2.44E+04
41	0.208	0.235	45.7	46.8	1.81E+03	2.42E+04	2.43E+04
42	0.201	0.270	46.3	47.4	1.90E+03	2.45E+04	2.45E+04
43	0.193	0.285	46.5	47.9	1.96E+03	2.46E+04	2.47E+04
44	0.188	0.291	46.7	47.7	2.07E+03	2.46E+04	2.47E+04
45	0.182	0.232	46.3	47.2	2.19E+03	2.44E+04	2.45E+04
46	0.174	0.258	46.8	48.0	2.28E+03	2.48E+04	2.49E+04
47	0.164	0.269	45.8	45.8	2.29E+03	2.38E+04	2.39E+04
48	0.157	0.264	46.8	46.6	2.48E+03	2.42E+04	2.43E+04

Table A. 5. Stiffness coefficients and uncertainties for the grooved seal with low PSR.

#	K_{xx}	K_{xy}	K_{yx}	K_{yy}	U_{Kxx}	U_{kxy}	U_{Kyx}	U_{kyy}
	[MN/m]	[MN/m]	[MN/m]	[MN/m]	[MN/m]	[MN/m]	[MN/m]	[MN/m]
1	0.69	0.65	0.09	-0.66	0.91	0.96	0.44	0.54
2	0.69	0.64	0.20	-0.53	1.23	1.00	0.59	0.48
3	1.13	0.44	-0.19	-0.70	0.96	0.66	0.35	0.37
4	1.29	0.10	-0.38	-0.36	1.40	0.72	0.58	0.42
5	1.00	0.82	0.05	-0.68	0.94	1.11	0.53	0.81
6	0.98	0.49	-0.03	-0.56	1.02	0.70	0.46	0.44
7	1.31	0.09	0.00	-0.32	1.10	0.44	0.38	0.35
8	1.34	0.01	-0.08	-0.24	1.06	0.53	0.48	0.35
9	1.72	0.06	-0.42	0.12	0.89	0.61	0.39	0.44
10	1.41	0.24	0.01	-0.11	0.83	0.61	0.30	0.43
11	1.43	-0.19	0.05	-0.25	0.99	0.65	0.43	0.49
12	1.64	-0.09	-0.09	-0.15	1.32	0.49	0.48	0.38
13	1.82	0.13	0.06	0.19	0.77	0.48	0.34	0.30
14	2.20	-0.25	-0.29	0.38	0.87	0.54	0.36	0.32
15	1.75	-0.51	-0.09	0.02	0.83	0.47	0.36	0.27
16	1.80	-0.09	-0.05	-0.01	1.91	0.72	0.90	0.37
17	0.19	1.07	-0.47	-0.86	0.61	0.45	0.24	0.31
18	0.77	0.86	-0.34	-0.83	0.80	0.42	0.39	0.30
19	1.08	0.61	-0.47	-0.77	0.64	0.43	0.28	0.36
20	0.96	0.52	-0.29	-0.74	0.75	0.39	0.36	0.38
21	0.62	0.14	-0.82	-0.04	1.45	1.51	0.71	0.79
22	1.00	0.41	-0.40	-0.52	0.88	0.47	0.38	0.35
23	1.39	0.17	-0.48	-0.42	0.71	0.43	0.34	0.26
24	1.36	0.09	-0.31	-0.53	1.01	0.65	0.45	0.42

Table A. 6. Stiffness coefficients and uncertainties for the grooved seal with low PSR (Continued).

#	K_{xx}	K_{xy}	K_{yx}	K_{yy}	U_{Kxx}	U_{kxy}	U_{Kyx}	U_{kyy}
	[MN/m]	[MN/m]	[MN/m]	[MN/m]	[MN/m]	[MN/m]	[MN/m]	[MN/m]
25	0.87	0.80	-0.68	-0.18	0.67	0.56	0.45	0.33
26	1.04	0.82	-0.04	-0.58	1.50	1.13	0.82	0.70
27	1.55	0.09	-0.33	-0.23	1.06	0.46	0.40	0.26
28	1.50	-0.37	-0.23	-0.23	1.17	0.63	0.50	0.45
29	1.08	0.55	-0.35	-0.05	0.52	0.44	0.30	0.31
30	1.75	0.29	-0.37	-0.07	0.78	0.45	0.31	0.26
31	1.68	-0.03	-0.20	-0.06	0.76	0.40	0.34	0.34
32	1.71	-0.37	-0.13	-0.36	1.16	0.55	0.39	0.33
33	-0.04	1.77	-0.98	-0.89	0.59	0.30	0.31	0.28
34	0.42	1.50	-0.96	-1.23	0.44	0.18	0.35	0.28
35	0.32	1.69	-1.01	-1.58	0.64	0.28	0.49	0.36
36	0.28	1.37	-0.73	-1.64	0.46	0.32	0.43	0.38
37	0.56	1.39	-1.01	-1.02	0.81	0.51	0.63	0.42
38	0.81	1.23	-0.91	-1.09	0.78	0.45	0.74	0.33
39	0.93	1.77	-0.91	-1.64	0.97	0.59	0.91	0.49
40	0.91	1.31	-0.61	-1.39	0.68	0.57	0.55	0.48
41	0.63	1.59	-0.77	-0.90	0.43	0.59	0.50	0.49
42	1.06	1.34	-0.79	-1.06	0.67	0.42	0.64	0.25
43	0.70	0.94	-0.92	-1.09	0.67	0.48	0.57	0.26
44	1.01	0.85	-0.65	-0.98	0.67	0.26	0.52	0.22
45	0.68	1.09	-1.02	-0.63	0.76	0.77	0.57	0.52
46	1.10	0.94	-0.91	-0.92	0.66	0.52	0.61	0.44
47	1.62	0.47	-0.88	-0.91	0.89	0.93	0.56	0.49
48	1.06	0.93	-0.33	-1.24	0.54	0.59	0.35	0.44

Table A. 7. Damping coefficients and uncertainties for the grooved seal with low PSR.

#	C_{xx} [MN-s/m]	C_{xy} [MN-s/m]	C_{yx} [MN-s/m]	C_{yy} [MN-s/m]	U_{Cxx} [MN-s/m]	U_{Cxy} [MN-s/m]	U_{Cyx} [MN-s/m]	U_{Cyy} [MN-s/m]
1	7.59	0.68	-3.52	5.14	1.68	1.71	0.83	0.93
2	7.64	0.81	-3.78	4.87	1.51	1.87	0.81	1.14
3	7.67	0.58	-3.80	5.09	1.19	1.35	0.62	0.64
4	7.04	0.57	-3.64	4.56	1.91	1.51	1.12	0.51
5	8.70	0.06	-3.58	6.38	1.38	1.91	0.75	0.92
6	8.61	0.14	-3.53	6.40	1.33	1.29	0.67	0.73
7	8.39	0.12	-3.70	6.10	1.76	1.45	0.79	0.66
8	7.94	0.45	-3.73	5.18	1.88	1.90	0.89	0.99
9	9.59	0.37	-3.75	7.17	1.90	1.34	0.65	0.68
10	9.42	0.27	-3.52	6.96	1.54	1.71	0.69	0.91
11	9.44	0.46	-3.80	6.64	1.66	1.78	0.68	1.01
12	8.39	0.66	-3.54	5.46	2.23	1.64	1.03	1.01
13	10.45	-0.13	-3.89	7.84	1.84	1.45	0.55	0.90
14	10.45	0.21	-4.06	7.26	2.14	1.40	0.70	0.78
15	9.60	0.39	-3.83	6.73	1.96	1.25	0.86	0.75
16	9.09	0.38	-3.85	5.60	3.05	1.41	1.92	0.78
17	8.45	1.83	-4.97	5.39	2.20	1.42	0.47	0.47
18	8.21	1.78	-5.34	5.67	1.36	1.64	0.56	0.60
19	8.00	2.07	-5.75	5.66	1.58	1.00	0.69	0.76
20	7.85	2.20	-6.38	5.27	1.28	1.37	0.54	0.66
21	10.29	1.64	-5.73	6.59	2.86	2.80	1.47	1.96
22	9.63	1.92	-5.73	6.37	1.63	1.33	0.65	0.68
23	9.00	2.57	-5.62	5.83	1.66	1.47	0.61	0.66
24	8.45	2.59	-6.08	5.23	2.03	1.55	0.74	0.65

Table A. 8. Damping coefficients and uncertainties for the grooved seal with low PSR (Continued).

#	C_{xx} [MN-s/m]	C_{xy} [MN-s/m]	C_{yx} [MN-s/m]	C_{yy} [MN-s/m]	U_{Cxx} [MN-s/m]	U_{Cxy} [MN-s/m]	U_{Cyx} [MN-s/m]	U_{Cyy} [MN-s/m]
25	10.65	1.37	-5.17	7.36	2.18	1.49	0.65	0.74
26	10.04	1.86	-5.48	7.06	2.07	1.82	1.13	1.28
27	10.01	1.79	-5.72	6.93	2.12	1.47	0.52	0.66
28	9.61	2.31	-6.30	5.88	2.01	1.55	0.67	0.54
29	11.64	1.20	-5.34	8.02	2.26	1.56	0.48	0.76
30	10.75	1.81	-5.43	7.61	1.62	1.34	0.54	0.74
31	10.30	1.68	-5.94	7.15	1.51	1.31	0.55	0.60
32	10.09	2.33	-6.15	6.21	1.73	1.37	0.63	0.57
33	8.30	3.75	-6.89	4.42	1.65	1.34	0.55	0.53
34	8.19	3.69	-6.86	4.53	1.45	0.86	0.62	0.53
35	8.03	3.29	-7.39	5.12	1.18	0.94	0.57	0.49
36	8.22	3.20	-8.29	5.25	1.03	0.87	0.59	0.49
37	11.89	3.25	-8.19	7.26	1.80	1.23	0.82	0.91
38	13.30	2.88	-9.53	7.15	1.80	1.23	0.99	0.67
39	13.31	2.92	-10.30	6.77	2.13	1.11	1.45	0.70
40	11.08	3.09	-9.88	6.18	2.24	1.34	0.97	0.65
41	10.70	3.70	-7.33	7.06	1.32	1.86	0.80	0.60
42	11.26	3.76	-7.79	7.07	1.29	1.64	0.63	0.83
43	11.01	3.34	-8.03	7.10	1.89	2.24	0.81	0.78
44	9.88	3.47	-8.48	6.27	1.36	1.55	0.69	0.85
45	12.30	2.25	-7.44	8.28	2.50	2.41	1.37	1.11
46	11.85	3.26	-7.69	7.85	1.66	2.30	0.77	1.34
47	11.53	3.32	-8.32	7.80	1.69	1.76	1.08	0.86
48	11.48	3.33	-9.27	6.51	1.74	1.95	0.60	1.12

Table A. 9. Virtual mass coefficients and uncertainties for the grooved seal with low PSR.

#	M_{xx}	M_{xy}	M_{yx}	M_{yy}	U_{Mxx}	U_{Mxy}	U_{Myx}	U_{Myy}
	[kg]	[kg]	[kg]	[kg]	[kg]	[kg]	[kg]	[kg]
1	14.33	-2.36	-1.69	13.71	1.30	1.37	0.63	0.77
2	13.96	-2.30	-1.73	13.87	1.74	1.41	0.83	0.68
3	14.95	-2.35	-1.63	15.30	1.33	0.93	0.49	0.52
4	16.13	-3.08	-1.98	18.26	1.84	0.95	0.76	0.56
5	15.72	-2.30	-1.94	14.74	1.34	1.58	0.76	1.15
6	15.55	-2.05	-1.66	15.08	1.42	0.97	0.64	0.61
7	16.31	-2.32	-1.62	16.74	1.49	0.59	0.51	0.48
8	16.99	-2.75	-1.52	19.53	1.51	0.75	0.69	0.51
9	17.13	-2.71	-2.77	15.66	1.20	0.82	0.53	0.60
10	16.65	-2.60	-1.87	16.28	1.12	0.82	0.41	0.58
11	17.01	-3.07	-1.68	17.71	1.35	0.88	0.58	0.67
12	17.69	-3.04	-1.60	19.82	1.79	0.67	0.66	0.51
13	17.32	-2.43	-2.08	16.36	1.10	0.68	0.48	0.43
14	17.85	-2.92	-2.23	17.04	1.22	0.76	0.50	0.45
15	17.92	-3.26	-1.86	18.61	1.18	0.68	0.51	0.39
16	19.16	-3.41	-2.09	20.63	2.72	1.02	1.28	0.53
17	12.22	-2.16	-1.97	11.69	0.85	0.62	0.34	0.44
18	13.28	-2.79	-1.92	12.57	1.08	0.57	0.52	0.41
19	15.12	-3.15	-1.99	15.17	0.92	0.62	0.41	0.52
20	15.26	-3.29	-1.71	17.85	1.05	0.55	0.50	0.52
21	15.56	-3.60	-2.75	15.47	2.08	2.16	1.01	1.13
22	16.16	-3.39	-2.26	15.44	1.23	0.66	0.53	0.49
23	17.06	-3.57	-2.34	16.71	0.99	0.60	0.47	0.37
24	17.72	-3.66	-1.93	19.53	1.36	0.88	0.60	0.57

Table A. 10. Virtual mass coefficients and uncertainties for the grooved seal with low PSR (Continued).

#	M_{xx}	M_{xy}	M_{yx}	M_{yy}	U_{Mxx}	U_{Mxy}	U_{Myx}	U_{Myy}
	[kg]	[kg]	[kg]	[kg]	[kg]	[kg]	[kg]	[kg]
25	16.13	-2.43	-2.70	15.77	0.93	0.77	0.63	0.46
26	17.07	-2.95	-1.91	16.47	2.14	1.62	1.17	0.99
27	17.61	-3.50	-1.74	17.44	1.43	0.63	0.54	0.36
28	17.88	-4.29	-1.56	20.32	1.53	0.83	0.66	0.59
29	17.14	-3.32	-2.37	16.63	0.72	0.62	0.41	0.43
30	18.00	-3.34	-2.14	17.14	1.08	0.62	0.43	0.36
31	18.49	-3.38	-1.84	18.68	1.05	0.55	0.47	0.47
32	18.95	-4.19	-1.73	20.32	1.52	0.72	0.52	0.44
33	12.23	-2.00	-2.85	11.62	0.84	0.43	0.45	0.40
34	13.06	-2.31	-2.62	11.75	0.62	0.24	0.48	0.39
35	13.30	-2.37	-2.48	13.32	0.89	0.39	0.68	0.50
36	13.54	-2.65	-1.85	15.92	0.65	0.45	0.60	0.53
37	16.15	-3.75	-2.86	14.77	1.13	0.72	0.88	0.58
38	18.17	-5.16	-3.91	16.02	1.07	0.62	1.01	0.45
39	19.49	-5.17	-4.27	17.53	1.32	0.80	1.24	0.67
40	18.66	-5.09	-2.99	20.07	0.98	0.82	0.80	0.70
41	16.73	-2.66	-3.14	15.43	0.58	0.80	0.67	0.67
42	18.33	-3.38	-3.21	15.88	0.91	0.57	0.87	0.34
43	17.21	-4.08	-2.66	17.16	0.91	0.64	0.77	0.36
44	18.04	-3.71	-1.90	19.56	0.93	0.36	0.71	0.30
45	16.93	-2.85	-3.11	15.83	1.02	1.04	0.77	0.70
46	17.75	-3.71	-2.63	16.36	0.89	0.71	0.83	0.59
47	18.80	-3.76	-2.58	17.55	1.20	1.25	0.76	0.66
48	19.00	-3.60	-2.17	20.37	0.74	0.80	0.48	0.59

Table A. 11. WFR, K_{eff}, C_{eff}, and uncertainties for the grooved seal with low PSR.

#	ω	ΔP	ϵ_0	*WFR*	U_{WFR}	K_{eff}	U_{Keff}	C_{eff}	U_{Ceff}
	[rpm]	[bar]	[-]	[kg]	[kg]	[MN/m]	[MN/m]	[kN-s/m]	[kN-s/m]
1	2000	2.068	0.00	0.00	0.00	-0.90	0.98	4.60	2.69
2	2000	2.068	0.27	0.00	0.00	-0.85	0.93	4.25	2.91
3	2000	2.068	0.53	0.00	0.00	-0.79	0.56	4.88	1.91
4	2000	2.068	0.80	0.00	0.00	-0.63	1.03	4.64	2.41
5	2000	4.137	0.00	0.00	0.00	-0.88	1.26	5.48	3.03
6	2000	4.137	0.27	0.00	0.00	-0.83	0.75	6.27	2.13
7	2000	4.137	0.53	0.00	0.00	-0.61	0.42	7.03	1.66
8	2000	4.137	0.80	0.00	0.00	-0.60	0.58	6.35	2.00
9	2000	6.205	0.00	0.00	0.00	-0.15	0.77	7.24	2.00
10	2000	6.205	0.27	0.00	0.00	-0.42	0.74	7.60	1.84
11	2000	6.205	0.53	0.00	0.00	-0.54	0.61	7.47	2.08
12	2000	6.205	0.80	0.00	0.00	-0.39	0.71	6.49	2.05
13	2000	8.274	0.00	0.00	0.00	-0.15	0.69	8.71	1.73
14	2000	8.274	0.27	0.00	0.00	0.12	0.82	7.55	1.93
15	2000	8.274	0.53	0.00	0.00	-0.27	0.51	6.72	1.76
16	2000	8.274	0.80	0.00	0.00	-0.34	1.25	7.00	3.16
17	4000	2.068	0.00	0.19	0.17	-3.09	0.38	5.08	1.28
18	4000	2.068	0.27	0.00	0.00	-3.04	0.28	5.50	1.01
19	4000	2.068	0.53	0.00	0.00	-3.27	0.40	5.54	1.07
20	4000	2.068	0.80	0.00	0.00	-3.66	0.33	5.59	0.96
21	4000	4.137	0.00	0.02	2.35	-3.28	0.67	7.30	2.64
22	4000	4.137	0.27	0.00	0.00	-3.32	0.31	7.03	1.14
23	4000	4.137	0.53	0.00	0.00	-3.11	0.28	6.64	1.11
24	4000	4.137	0.80	0.00	0.00	-3.58	0.45	6.36	1.42

Table A. 12. WFR, K_{eff}, C_{eff}, and uncertainties for the grooved seal with low PSR (Continued).

#	ω	ΔP	ϵ_0	*WFR*	U_{WFR}	K_{eff}	U_{Keff}	C_{eff}	U_{Ceff}
	[rpm]	[bar]	[-]	[kg]	[kg]	[MN/m]	[MN/m]	[kN-s/m]	[kN-s/m]
25	4000	6.205	0.00	0.14	0.17	-3.25	1.28	7.25	1.43
26	4000	6.205	0.27	0.00	0.00	-3.46	2.48	7.52	2.07
27	4000	6.205	0.53	0.00	0.00	-3.23	1.37	7.97	1.33
28	4000	6.205	0.80	0.00	0.00	-3.55	2.03	7.03	1.42
29	4000	8.274	0.00	0.00	0.00	-3.31	1.99	8.75	1.35
30	4000	8.274	0.27	0.00	0.00	-3.00	1.21	8.39	1.10
31	4000	8.274	0.53	0.00	0.00	-3.34	1.52	8.45	1.02
32	4000	8.274	0.80	0.00	0.00	-3.56	1.46	7.56	1.21
33	6000	2.068	0.00	0.33	0.08	-6.17	0.88	4.18	0.93
34	6000	2.068	0.27	0.24	0.09	-6.31	0.81	4.40	0.83
35	6000	2.068	0.53	0.26	0.12	-7.18	1.13	4.43	0.78
36	6000	2.068	0.80	0.16	0.14	-8.11	0.95	5.07	0.71
37	6000	4.137	0.00	0.16	0.11	-7.90	1.75	7.66	1.20
38	6000	4.137	0.27	0.09	0.17	-8.99	1.28	8.53	1.18
39	6000	4.137	0.53	0.08	0.32	-10.00	1.57	7.91	1.41
40	6000	4.137	0.80	0.00	0.00	-10.04	1.49	7.11	1.33
41	6000	6.205	0.00	0.16	0.10	-7.64	0.96	7.01	0.95
42	6000	6.205	0.27	0.06	0.26	-8.03	0.90	7.48	0.98
43	6000	6.205	0.53	0.07	0.19	-8.44	1.70	7.58	1.18
44	6000	6.205	0.80	0.00	0.00	-8.96	0.80	6.88	0.92
45	6000	8.274	0.00	0.13	0.11	-8.08	1.99	8.61	1.57
46	6000	8.274	0.27	0.00	0.00	-8.04	1.37	8.38	1.24
47	6000	8.274	0.53	0.00	0.00	-8.41	1.05	8.60	1.28
48	6000	8.274	0.80	0.00	0.00	-9.70	1.08	7.99	1.17

Medium PSR Assembly

Table A. 13. Static results of the grooved seal with medium PSR.

#	Target			Measured					
	ω	ΔP	ϵ_0	ω	ΔP	ϵ_0	Q	φ	f_R
	[rpm]	[bar]	[-]	[rpm]	[bar]	[-]	[LPM]	[deg]	[N]
1	2000	2.068	0.00	2013.6	1.863	0.024	17.53	-115.4	-284.6
2	2000	2.068	0.27	1996.4	2.302	0.303	22.54	-22.0	-326.6
3	2000	2.068	0.53	1996.7	2.218	0.576	22.68	-16.5	-409.9
4	2000	2.068	0.80	2001.3	2.129	0.784	23.97	-7.1	-243.5
5	2000	4.137	0.00	2001.2	4.298	0.040	33.01	-47.6	-302.2
6	2000	4.137	0.27	2001.1	4.364	0.281	33.87	-14.7	-62.7
7	2000	4.137	0.53	2001.3	4.307	0.552	35.67	-8.6	-46.0
8	2000	4.137	0.80	2001.2	4.304	0.801	38.22	-7.0	-116.8
9	2000	6.205	0.00	2001.4	6.329	0.028	42.57	-21.7	-294.2
10	2000	6.205	0.27	2001.6	6.379	0.273	43.56	-11.3	-219.7
11	2000	6.205	0.53	2001.3	6.346	0.544	44.95	-8.0	-247.5
12	2000	6.205	0.80	2001.4	6.419	0.779	48.76	-9.6	-348.2
13	2000	8.274	0.00	2001.2	8.348	0.018	49.17	73.3	-284.5
14	2000	8.274	0.27	2001.5	8.249	0.279	51.04	-11.1	-66.8
15	2000	8.274	0.53	2001.8	8.133	0.523	52.95	-12.4	-88.4
16	2000	8.274	0.80	2001.8	7.813	0.770	54.69	-2.1	-100.2
17	4000	2.068	0.00	3992.7	2.135	0.018	20.11	-55.5	-283.3
18	4000	2.068	0.27	3992.7	1.858	0.279	18.02	-13.7	-184.1
19	4000	2.068	0.53	4032.4	1.915	0.536	19.21	-11.7	-494.3
20	4000	2.068	0.80	4032.0	1.907	0.811	20.67	-11.1	-487.0
21	4000	4.137	0.00	3992.0	4.060	0.054	30.95	179.7	-317.5
22	4000	4.137	0.27	3991.6	3.875	0.261	31.18	-22.8	-136.4
23	4000	4.137	0.53	3991.7	3.914	0.561	32.89	-12.8	-98.8
24	4000	4.137	0.80	3991.8	3.895	0.845	34.70	-11.7	-221.6

Table A. 14. Static results of the grooved seal with medium PSR (Continued).

#	Target			Measured					
	ω	ΔP	ϵ_0	ω	ΔP	ϵ_0	Q	φ	f_R
	[rpm]	[bar]	[-]	[rpm]	[bar]	[-]	[LPM]	[deg]	[N]
`25	4000	6.205	0.00	3991.4	6.084	0.011	40.79	4.1	-277.2
26	4000	6.205	0.27	3991.7	5.977	0.315	41.13	-20.0	-176.2
27	4000	6.205	0.53	3991.9	6.095	0.548	43.79	-15.0	-213.2
28	4000	6.205	0.80	3992.1	6.162	0.803	46.58	-9.4	-258.3
29	4000	8.274	0.00	3992.2	8.204	0.029	49.22	-173.5	-301.6
30	4000	8.274	0.27	3992.3	8.251	0.278	50.19	-15.8	-54.2
31	4000	8.274	0.53	3992.6	8.031	0.552	51.92	-7.7	-67.2
32	4000	8.274	0.80	3992.8	7.920	0.767	53.98	-2.8	-193.0
33	6000	2.068	0.00	5983.8	2.158	0.068	16.13	2.3	-330.1
34	6000	2.068	0.27	5985.8	2.021	0.292	16.19	-14.9	-239.8
35	6000	2.068	0.53	5988.6	1.893	0.523	16.25	-8.3	-302.6
36	6000	2.068	0.80	5991.0	2.018	0.735	18.13	-7.9	-425.8
37	6000	4.137	0.00	5991.0	4.004	0.030	28.97	-151.3	-284.3
38	6000	4.137	0.27	5991.8	4.124	0.258	30.16	-8.7	-258.6
39	6000	4.137	0.53	5991.8	3.877	0.591	30.53	-12.8	-326.4
40	6000	4.137	0.80	5991.6	3.876	0.750	31.41	-11.2	-400.9
41	6000	6.205	0.00	6012.4	5.860	0.040	37.56	18.1	-298.2
42	6000	6.205	0.27	5992.7	6.061	0.268	39.87	-24.7	-205.9
43	6000	6.205	0.53	5991.7	6.303	0.497	42.47	-12.5	-319.2
44	6000	6.205	0.80	5992.1	6.202	0.798	45.29	-13.4	-353.2
45	6000	8.274	0.00	5992.4	8.065	0.045	47.24	65.9	-308.4
46	6000	8.274	0.27	5962.6	8.216	0.260	48.93	-14.1	-290.8
47	6000	8.274	0.53	5962.2	7.994	0.517	49.90	-9.6	-356.4
48	6000	8.274	0.80	5963.1	7.936	0.784	53.25	-10.5	-397.6

Table A. 15. Static flow results of the grooved seal with medium PSR.

#	PSR	OSR	Inlet Temp	Average Outlet Temp.	Re_z	Re_θ	Re
	[-]	[-]	[°C]	[°C]	[-]	[-]	[-]
1	0.262	0.219	45.4	46.4	7.88E+02	1.60E+04	1.56E+04
2	0.311	0.280	48.1	48.4	1.05E+03	8.30E+03	8.22E+03
3	0.308	0.291	46.1	43.8	9.81E+02	7.67E+03	7.92E+03
4	0.333	0.289	45.2	44.7	1.05E+03	7.79E+03	7.84E+03
5	0.520	0.260	46.1	47.0	1.50E+03	8.09E+03	8.01E+03
6	0.494	0.283	47.1	46.7	1.54E+03	8.09E+03	8.17E+03
7	0.496	0.284	46.8	46.7	1.62E+03	8.06E+03	8.14E+03
8	0.526	0.247	46.6	45.9	1.71E+03	7.97E+03	8.14E+03
9	0.668	0.250	47.4	48.1	1.98E+03	8.26E+03	8.30E+03
10	0.644	0.280	46.8	47.4	2.00E+03	8.16E+03	8.22E+03
11	0.635	0.298	46.0	44.4	1.97E+03	7.77E+03	8.11E+03
12	0.668	0.339	47.1	47.1	2.23E+03	8.13E+03	8.32E+03
13	0.755	0.248	46.2	44.2	2.15E+03	7.76E+03	8.19E+03
14	0.720	0.300	45.5	46.1	2.29E+03	7.97E+03	8.12E+03
15	0.647	0.304	46.9	47.5	2.43E+03	8.17E+03	8.35E+03
16	0.685	0.333	44.7	45.0	2.40E+03	7.82E+03	8.05E+03
17	0.261	0.227	46.0	46.9	9.15E+02	1.61E+04	1.57E+04
18	0.262	0.245	47.5	48.3	8.42E+02	1.66E+04	1.62E+04
19	0.256	0.260	45.4	46.2	8.61E+02	1.61E+04	1.57E+04
20	0.253	0.265	46.8	47.8	9.55E+02	1.65E+04	1.61E+04
21	0.297	0.211	47.4	46.8	1.41E+03	1.62E+04	1.61E+04
22	0.289	0.251	46.0	46.4	1.41E+03	1.60E+04	1.58E+04
23	0.291	0.253	46.8	47.7	1.52E+03	1.63E+04	1.60E+04
24	0.296	0.257	46.8	45.5	1.55E+03	1.58E+04	1.60E+04

Table A. 16. Static flow results of the grooved seal with medium PSR (Continued).

#	PSR	OSR	Inlet Temp	Average Outlet Temp.	Re_z	Re_θ	Re
	[-]	[-]	[°C]	[°C]	[-]	[-]	[-]
25	0.347	0.235	45.2	46.1	1.83E+03	1.59E+04	1.56E+04
26	0.339	0.255	46.2	46.2	1.85E+03	1.60E+04	1.59E+04
27	0.346	0.266	46.6	47.3	2.01E+03	1.62E+04	1.60E+04
28	0.350	0.287	46.9	45.9	2.09E+03	1.59E+04	1.61E+04
29	0.405	0.245	46.3	46.9	2.24E+03	1.61E+04	1.59E+04
30	0.387	0.254	46.9	46.8	2.28E+03	1.61E+04	1.61E+04
31	0.378	0.279	46.5	46.7	2.35E+03	1.61E+04	1.60E+04
32	0.376	0.298	45.9	45.2	2.38E+03	1.57E+04	1.58E+04
33	0.298	0.209	46.8	47.0	7.36E+02	2.43E+04	2.39E+04
34	0.297	0.221	45.7	46.8	7.34E+02	2.41E+04	2.34E+04
35	0.294	0.217	47.0	48.8	7.65E+02	2.50E+04	2.40E+04
36	0.284	0.219	46.9	47.8	8.39E+02	2.46E+04	2.40E+04
37	0.265	0.221	47.1	47.8	1.34E+03	2.46E+04	2.41E+04
38	0.261	0.236	45.1	45.2	1.33E+03	2.35E+04	2.32E+04
39	0.255	0.254	45.3	46.5	1.38E+03	2.40E+04	2.33E+04
40	0.256	0.261	46.5	46.2	1.41E+03	2.39E+04	2.38E+04
41	0.269	0.226	46.6	45.9	1.68E+03	2.38E+04	2.40E+04
42	0.275	0.256	47.4	48.6	1.87E+03	2.49E+04	2.42E+04
43	0.276	0.273	46.7	47.9	1.96E+03	2.46E+04	2.39E+04
44	0.279	0.277	47.5	48.5	2.12E+03	2.49E+04	2.43E+04
45	0.291	0.225	44.8	46.1	2.11E+03	2.38E+04	2.32E+04
46	0.204	0.256	47.3	48.5	2.28E+03	2.47E+04	2.41E+04
47	0.127	0.264	45.8	46.8	2.26E+03	2.40E+04	2.35E+04
48	0.083	0.266	46.8	48.0	2.46E+03	2.45E+04	2.39E+04

Table A. 17. Stiffness coefficients and uncertainties for the grooved seal with medium PSR.

#	K_{xx}	K_{xy}	K_{yx}	K_{yy}	U_{Kxx}	U_{kxy}	U_{Kyx}	U_{kyy}
	[MN/m]	[MN/m]	[MN/m]	[MN/m]	[MN/m]	[MN/m]	[MN/m]	[MN/m]
1	0.43	-0.04	-0.81	-0.52	0.36	1.35	0.28	0.86
2	0.38	-0.01	-0.53	-0.51	0.57	0.57	0.25	0.34
3	0.37	0.13	-0.58	-0.45	0.58	0.40	0.26	0.44
4	0.47	-0.36	-0.59	-0.32	1.17	0.54	0.78	0.52
5	1.09	-0.05	-1.04	-0.38	0.62	0.64	0.39	0.59
6	1.18	-0.09	-1.25	-0.11	0.54	0.37	0.30	0.44
7	0.90	-0.41	-1.32	-0.02	0.49	0.47	0.34	0.55
8	1.08	-0.59	-1.27	0.03	0.40	0.53	0.30	0.47
9	1.30	0.71	-1.42	-0.10	0.63	0.57	0.43	0.59
10	1.12	0.13	-1.32	0.06	0.34	0.55	0.21	0.47
11	1.19	-0.04	-1.55	-0.07	0.65	0.48	0.43	0.46
12	1.27	-0.14	-1.47	-0.10	0.50	0.44	0.36	0.40
13	1.43	0.68	-1.74	0.07	0.49	0.45	0.29	0.37
14	2.03	0.53	-1.91	0.14	0.67	0.48	0.39	0.40
15	1.60	0.24	-1.73	-0.05	0.50	0.42	0.31	0.35
16	1.53	-0.13	-1.65	0.01	0.30	0.25	0.17	0.29
17	0.40	0.71	-1.20	-0.88	0.21	0.30	0.20	0.45
18	0.26	-0.09	-0.82	-0.38	0.78	0.61	0.55	0.54
19	0.28	0.69	-0.91	-0.87	0.59	0.48	0.33	0.51
20	0.40	0.23	-0.82	-0.70	0.44	0.39	0.24	0.38
21	0.86	0.44	-1.10	-0.52	0.28	0.20	0.22	0.42
22	0.93	0.39	-1.16	-0.51	0.35	0.27	0.21	0.38
23	0.85	0.08	-1.29	-0.43	0.53	0.42	0.45	0.48
24	0.87	-0.17	-1.08	-0.42	0.28	0.29	0.18	0.36

Table A. 18. Stiffness coefficients and uncertainties for the grooved seal with medium PSR (Continued).

#	K_{xx}	K_{xy}	K_{yx}	K_{yy}	U_{Kxx}	U_{kxy}	U_{Kyx}	U_{kyy}
	[MN/m]	[MN/m]	[MN/m]	[MN/m]	[MN/m]	[MN/m]	[MN/m]	[MN/m]
25	1.20	0.74	-1.57	-0.49	0.27	0.32	0.26	0.43
26	0.97	0.51	-1.41	-0.46	0.34	0.60	0.19	0.50
27	1.02	0.28	-1.46	-0.29	0.26	0.27	0.25	0.34
28	1.06	-0.11	-1.33	-0.37	0.27	0.31	0.21	0.40
29	1.39	0.98	-1.59	-0.44	0.43	0.37	0.30	0.36
30	1.85	0.15	-1.90	0.09	0.69	0.68	0.44	0.51
31	1.42	0.24	-1.67	-0.25	0.31	0.26	0.28	0.32
32	1.25	0.00	-1.55	-0.41	0.31	0.24	0.24	0.37
33	-0.34	0.71	-1.58	-0.68	1.18	0.87	0.49	0.53
34	-0.11	1.07	-1.61	-1.03	1.03	0.97	0.72	0.68
35	-0.11	1.40	-1.24	-1.49	1.25	1.06	0.97	0.70
36	-0.38	0.62	-1.20	-1.09	0.88	0.93	0.61	0.61
37	-0.21	0.63	-1.44	-0.98	0.76	0.93	0.45	0.51
38	-0.04	0.68	-1.34	-0.83	0.56	0.74	0.44	0.63
39	0.14	1.10	-1.49	-1.14	0.70	0.75	0.60	0.68
40	0.73	0.54	-1.75	-0.79	0.59	0.88	0.74	0.67
41	0.80	1.11	-1.39	-0.69	1.01	0.79	0.77	0.61
42	0.31	0.56	-1.59	-0.55	0.75	0.83	0.61	0.63
43	0.69	0.56	-1.62	-0.90	0.52	0.74	0.48	0.57
44	0.83	0.35	-1.57	-0.76	0.73	0.90	0.58	0.70
45	0.25	1.82	-1.60	-1.19	0.80	0.39	0.47	0.43
46	0.65	3.73	-1.54	-2.82	0.61	2.98	0.57	2.17
47	0.60	0.94	-1.77	-1.07	0.83	0.78	0.63	0.51
48	0.97	0.96	-1.66	-1.14	0.85	0.62	0.53	0.38

Table A. 19. Damping coefficients and uncertainties for the grooved seal with medium PSR.

#	C_{xx}	C_{xy}	C_{yx}	C_{yy}	U_{Cxx}	U_{Cxy}	U_{Cyx}	U_{Cyy}
	[MN-s/m]	[MN-s/m]	[MN-s/m]	[MN-s/m]	[MN-s/m]	[MN-s/m]	[MN-s/m]	[MN-s/m]
1	6.87	1.86	-4.94	4.91	1.06	1.38	0.58	1.18
2	6.51	0.63	-3.39	4.95	2.07	1.33	1.14	1.20
3	6.21	0.74	-3.39	4.66	2.29	1.77	1.29	1.35
4	5.76	0.30	-3.49	4.62	2.48	1.16	1.34	0.95
5	7.53	0.40	-3.69	6.21	2.50	2.05	0.99	1.25
6	7.60	0.32	-3.86	6.33	1.87	1.24	0.92	1.09
7	7.36	0.52	-3.97	5.97	2.05	0.85	0.87	0.87
8	7.34	0.11	-4.43	5.55	2.20	0.98	0.98	0.98
9	8.63	0.35	-4.16	7.03	2.06	1.39	0.72	1.15
10	9.39	0.15	-4.52	7.11	1.49	0.82	0.79	1.08
11	8.46	0.41	-4.49	6.72	1.93	0.97	0.75	1.10
12	8.49	0.44	-4.97	5.88	1.03	0.65	0.57	1.04
13	9.13	0.34	-4.33	7.82	2.01	1.26	0.82	1.15
14	9.38	0.43	-4.81	7.38	1.96	0.81	0.87	0.94
15	9.04	0.52	-4.82	6.91	1.65	0.66	0.68	0.97
16	8.91	0.42	-5.42	6.20	2.00	0.89	0.98	0.99
17	7.61	1.61	-5.35	5.49	1.76	1.50	1.00	1.31
18	7.32	1.73	-5.38	5.15	1.25	1.09	0.72	0.88
19	7.58	1.39	-5.89	5.84	1.45	1.10	0.71	1.10
20	6.39	2.12	-6.12	5.03	1.36	0.89	0.69	0.95
21	8.57	1.99	-5.79	6.10	1.56	0.69	0.77	0.81
22	8.53	1.99	-5.85	6.09	1.37	0.67	0.61	0.77
23	8.21	2.21	-6.08	5.78	2.14	1.60	1.13	1.27
24	7.84	1.99	-6.76	5.50	1.45	0.93	0.68	0.86

Table A. 20. Damping coefficients and uncertainties for the grooved seal with medium PSR (Continued).

#	C_{xx}	C_{xy}	C_{yx}	C_{yy}	U_{Cxx}	U_{Cxy}	U_{Cyx}	U_{Cyy}
	[MN-s/m]	[MN-s/m]	[MN-s/m]	[MN-s/m]	[MN-s/m]	[MN-s/m]	[MN-s/m]	[MN-s/m]
25	9.59	1.65	-5.72	7.08	1.52	0.63	0.64	0.86
26	9.75	1.77	-6.21	7.08	1.82	0.82	0.76	1.02
27	9.42	1.88	-6.42	6.93	1.63	0.96	0.67	1.07
28	9.07	2.11	-7.12	6.12	1.62	0.94	0.71	0.96
29	10.57	1.43	-6.05	8.00	1.99	1.58	1.09	1.24
30	10.49	1.67	-6.51	7.80	1.81	0.95	0.97	1.07
31	9.98	2.06	-6.76	7.25	1.71	0.63	0.57	0.81
32	9.68	2.23	-7.21	6.54	1.66	0.85	0.79	0.91
33	11.09	3.75	-9.09	4.24	3.65	2.52	2.83	1.60
34	11.29	3.19	-9.43	4.70	3.36	3.06	2.60	2.03
35	11.29	2.80	-9.90	5.23	3.66	3.13	2.81	2.18
36	12.82	2.18	-11.63	5.93	3.33	2.94	2.68	2.13
37	16.66	0.47	-11.80	9.11	4.14	3.46	2.85	2.72
38	17.76	0.80	-13.23	8.71	4.83	3.21	3.37	2.42
39	16.21	1.01	-13.16	8.12	4.33	3.06	3.14	2.40
40	15.43	1.10	-13.41	7.73	4.94	3.81	3.25	2.89
41	15.53	1.43	-12.03	8.71	4.34	2.96	3.12	2.17
42	17.94	-0.20	-13.36	9.59	4.40	3.74	2.97	2.40
43	17.47	-0.17	-13.56	9.70	4.64	4.08	3.06	2.90
44	16.74	0.08	-14.27	8.84	4.67	4.00	3.22	2.85
45	14.44	1.75	-9.78	8.93	2.59	2.18	1.59	1.32
46	15.23	1.99	-10.89	9.11	5.07	3.18	3.74	2.26
47	15.15	1.10	-11.41	9.32	3.22	3.03	1.80	2.09
48	14.46	1.63	-12.39	8.46	2.86	2.12	1.94	1.74

Table A. 21. Virtual mass coefficients and uncertainties for the grooved seal with medium PSR.

#	M_{xx}	M_{xy}	M_{yx}	M_{yy}	U_{Mxx}	U_{Mxy}	U_{Myx}	U_{Myy}
	[kg]	[kg]	[kg]	[kg]	[kg]	[kg]	[kg]	[kg]
1	12.60	-2.17	-1.76	11.96	0.50	1.87	0.39	1.20
2	14.84	-1.44	-1.90	13.84	0.83	0.82	0.36	0.49
3	15.32	-1.21	-1.78	15.03	0.84	0.58	0.37	0.63
4	14.72	-1.71	-1.20	17.14	1.58	0.73	1.05	0.70
5	16.49	-2.33	-2.68	14.72	0.82	0.84	0.51	0.78
6	16.17	-1.83	-2.32	15.31	0.75	0.51	0.42	0.61
7	16.55	-2.35	-2.50	16.81	0.68	0.65	0.47	0.76
8	16.77	-2.63	-1.99	19.20	0.56	0.74	0.41	0.66
9	16.96	-1.63	-2.92	15.54	0.89	0.80	0.60	0.83
10	16.37	-2.22	-2.33	16.58	0.49	0.79	0.30	0.68
11	17.00	-2.39	-2.33	17.81	0.92	0.69	0.61	0.66
12	17.53	-2.37	-2.01	19.76	0.70	0.62	0.50	0.56
13	17.13	-1.90	-2.51	16.21	0.70	0.65	0.42	0.53
14	18.17	-2.33	-2.73	17.14	0.96	0.68	0.56	0.57
15	17.72	-2.41	-2.08	18.24	0.71	0.60	0.44	0.50
16	18.00	-3.19	-2.23	20.44	0.43	0.36	0.25	0.41
17	13.83	-2.12	-2.53	12.88	0.30	0.42	0.28	0.63
18	12.80	-2.47	-1.81	12.95	1.11	0.87	0.78	0.76
19	13.51	-1.88	-1.43	14.22	0.83	0.68	0.46	0.71
20	14.68	-2.03	-1.04	17.37	0.61	0.54	0.34	0.54
21	16.08	-2.51	-2.27	15.09	0.39	0.28	0.31	0.59
22	16.34	-2.25	-2.40	15.07	0.49	0.37	0.29	0.53
23	16.42	-2.61	-2.23	16.64	0.75	0.60	0.65	0.68
24	16.76	-2.55	-1.46	19.31	0.40	0.40	0.25	0.50

Table A. 22. Virtual mass coefficients and uncertainties for the grooved seal with medium PSR (Continued).

#	M_{xx}	M_{xy}	M_{yx}	M_{yy}	U_{Mxx}	U_{Mxy}	U_{Myx}	U_{Myy}
	[kg]	[kg]	[kg]	[kg]	[kg]	[kg]	[kg]	[kg]
25	16.97	-2.06	-3.06	15.62	0.38	0.45	0.36	0.60
26	16.90	-2.68	-2.34	16.50	0.48	0.84	0.26	0.70
27	17.33	-2.62	-2.21	17.56	0.37	0.38	0.35	0.48
28	17.75	-3.09	-1.85	19.97	0.38	0.43	0.29	0.55
29	17.71	-2.27	-2.61	16.23	0.59	0.52	0.42	0.50
30	18.32	-3.18	-2.69	17.62	0.99	0.97	0.63	0.73
31	18.35	-3.05	-2.57	18.44	0.43	0.36	0.39	0.45
32	18.21	-3.57	-2.31	20.21	0.43	0.33	0.33	0.51
33	14.96	-5.71	-4.79	14.69	1.64	1.21	0.68	0.74
34	14.75	-6.31	-4.53	15.57	1.43	1.35	1.00	0.95
35	15.54	-7.25	-4.05	16.94	1.78	1.51	1.39	0.99
36	16.20	-8.75	-3.90	20.35	1.25	1.32	0.86	0.87
37	17.88	-9.10	-4.35	18.77	1.03	1.25	0.61	0.69
38	18.61	-10.20	-4.62	20.59	0.78	1.03	0.61	0.88
39	19.83	-10.17	-5.11	22.62	0.98	1.04	0.83	0.94
40	20.58	-11.05	-4.93	24.72	0.83	1.22	1.04	0.93
41	20.44	-8.44	-5.08	20.26	1.39	1.08	1.06	0.84
42	19.54	-10.16	-5.13	21.79	1.06	1.19	0.88	0.89
43	20.28	-10.34	-4.65	22.69	0.72	1.03	0.66	0.79
44	20.84	-10.79	-3.99	25.85	1.02	1.25	0.81	0.97
45	17.90	-3.98	-3.48	17.43	1.05	0.51	0.61	0.56
46	19.08	-3.49	-3.48	17.46	0.80	3.94	0.76	2.87
47	18.27	-5.84	-3.15	19.90	1.13	1.06	0.86	0.70
48	20.43	-5.50	-3.19	22.35	1.20	0.87	0.74	0.54

Table A. 23. WFR, K_{eff}, C_{eff}, and uncertainties for the grooved seal with medium PSR.

#	ω	ΔP	ϵ_0	*WFR*	U_{WFR}	K_{eff}	U_{Keff}	C_{eff}	U_{Ceff}
	[rpm]	[bar]	[-]	[kg]	[kg]	[MN/m]	[MN/m]	[kN-s/m]	[[kN-s/m]
1	2000	2.068	0.00	0.00	0.00	-0.91	0.72	3.87	3.36
2	2000	2.068	0.27	0.00	0.00	-0.98	0.38	4.44	1.91
3	2000	2.068	0.53	0.00	0.00	-0.98	0.38	3.74	1.75
4	2000	2.068	0.80	0.00	0.00	-0.96	0.43	2.92	2.62
5	2000	4.137	0.00	0.00	0.00	-0.68	0.49	4.25	2.26
6	2000	4.137	0.27	0.00	0.00	-0.53	0.34	3.77	1.57
7	2000	4.137	0.53	0.00	0.00	-0.65	0.29	2.53	1.77
8	2000	4.137	0.80	0.00	0.00	-0.69	0.34	1.99	1.89
9	2000	6.205	0.00	0.44	0.46	-0.52	0.42	2.76	2.08
10	2000	6.205	0.27	0.00	0.00	-0.59	0.35	4.79	1.68
11	2000	6.205	0.53	0.00	0.00	-0.63	0.36	3.78	1.89
12	2000	6.205	0.80	0.00	0.00	-0.71	0.27	3.33	1.53
13	2000	8.274	0.00	0.49	0.32	-0.40	0.34	2.70	1.73
14	2000	8.274	0.27	0.21	0.95	-0.15	0.32	2.54	1.83
15	2000	8.274	0.53	0.00	0.00	-0.47	0.29	3.28	1.57
16	2000	8.274	0.80	0.00	0.00	-0.60	0.27	3.32	1.33
17	4000	2.068	0.00	0.25	0.14	-3.35	0.25	4.26	1.18
18	4000	2.068	0.27	0.00	0.00	-3.07	0.23	5.15	1.24
19	4000	2.068	0.53	0.21	0.21	-3.72	0.18	4.82	1.15
20	4000	2.068	0.80	0.00	0.00	-3.85	0.20	4.47	0.99
21	4000	4.137	0.00	0.07	0.29	-3.35	0.16	5.49	0.94
22	4000	4.137	0.27	0.00	0.00	-3.34	0.16	5.46	0.88
23	4000	4.137	0.53	0.00	0.00	-3.49	0.30	5.36	1.45
24	4000	4.137	0.80	0.00	0.00	-3.92	0.21	5.18	0.93

Table A. 24. WFR, K_{eff}, C_{eff}, and uncertainties for the grooved seal with medium PSR (Continued).

#	ω	ΔP	ϵ_0	*WFR*	U_{WFR}	K_{eff}	U_{Keff}	C_{eff}	U_{Ceff}
	[rpm]	[bar]	[-]	[kg]	[kg]	[MN/m]	[MN/m]	[kN-s/m]	[kN-s/m]
25	4000	6.205	0.00	0.20	0.14	-3.34	0.99	5.57	1.00
26	4000	6.205	0.27	0.14	0.28	-3.59	1.03	6.12	1.29
27	4000	6.205	0.53	0.02	0.87	-3.63	1.21	6.10	1.07
28	4000	6.205	0.80	0.00	0.00	-4.00	1.09	5.88	1.04
29	4000	8.274	0.00	0.22	0.13	-3.46	1.37	6.21	1.31
30	4000	8.274	0.27	0.00	0.00	-3.18	1.53	6.70	1.43
31	4000	8.274	0.53	0.00	0.00	-3.61	0.95	6.33	1.05
32	4000	8.274	0.80	0.00	0.00	-3.98	1.12	6.25	1.03
33	6000	2.068	0.00	0.24	0.18	-8.01	2.40	5.83	2.14
34	6000	2.068	0.27	0.27	0.20	-8.48	2.12	5.86	2.18
35	6000	2.068	0.53	0.25	0.23	-9.41	2.30	6.15	2.42
36	6000	2.068	0.80	0.15	0.17	-10.89	1.84	7.92	2.16
37	6000	4.137	0.00	0.12	0.12	-11.36	2.82	11.24	2.61
38	6000	4.137	0.27	0.12	0.10	-12.05	2.79	11.62	2.79
39	6000	4.137	0.53	0.17	0.12	-12.67	2.56	10.10	2.59
40	6000	4.137	0.80	0.09	0.23	-12.81	3.30	9.76	3.00
41	6000	6.205	0.00	0.14	0.13	-11.35	2.71	10.14	2.58
42	6000	6.205	0.27	0.11	0.12	-12.52	2.51	12.06	2.64
43	6000	6.205	0.53	0.07	0.17	-12.87	3.24	11.85	2.82
44	6000	6.205	0.80	0.00	0.00	-13.60	2.98	11.26	2.87
45	6000	8.274	0.00	0.23	0.07	-9.95	1.27	8.97	1.53
46	6000	8.274	0.27	0.27	0.30	-10.99	4.09	7.95	3.69
47	6000	8.274	0.53	0.14	0.13	-10.89	1.71	10.06	2.08
48	6000	8.274	0.80	0.11	0.16	-11.78	1.89	9.36	1.80

High PSR Assembly

Table A. 25. Static results of the grooved seal with high PSR.

#	Target			Measured					
	ω	ΔP	ϵ_0	ω	ΔP	ϵ_0	Q	φ	f_R
	[rpm]	[bar]	[-]	[rpm]	[bar]	[-]	[LPM]	[deg]	[N]
1	2000	2.068	0.00	1996.2	2.165	0.051	21.42	-12.9	-268.8
2	2000	2.068	0.27	1995.7	2.296	0.266	23.31	-10.9	2.4
3	2000	2.068	0.53	1995.8	1.927	0.533	21.99	-4.9	-127.9
4	2000	2.068	0.80	1996.0	2.279	0.784	25.78	-3.1	-282.9
5	2000	4.137	0.00	1999.4	4.216	0.032	32.16	-142.7	-156.9
6	2000	4.137	0.27	1999.1	4.414	0.289	33.27	-14.7	47.4
7	2000	4.137	0.53	1999.0	4.248	0.537	34.80	-9.3	-136.1
8	2000	4.137	0.80	1998.9	4.183	0.747	35.57	-11.6	-339.7
9	2000	6.205	0.00	1995.7	6.116	0.052	40.14	-101.7	-180.9
10	2000	6.205	0.27	1996.3	6.329	0.266	42.27	-4.5	-126.0
11	2000	6.205	0.53	1996.0	6.335	0.525	44.20	-7.3	-296.7
12	2000	6.205	0.80	1996.0	6.351	0.788	47.20	-4.7	-474.4
13	2000	8.274	0.00	1999.2	8.387	0.017	48.48	-144.7	-133.1
14	2000	8.274	0.27	1999.1	8.315	0.275	49.36	-18.1	3.5
15	2000	8.274	0.53	1999.2	8.260	0.550	51.43	-14.1	-138.0
16	2000	8.274	0.80	1999.0	8.085	0.784	53.05	-10.4	-336.8
17	4000	2.068	0.00	3999.3	2.348	0.020	21.21	-153.1	117.9
18	4000	2.068	0.27	3999.4	2.021	0.291	20.34	-25.9	-11.1
19	4000	2.068	0.53	3999.0	2.054	0.554	21.70	-28.0	-225.1
20	4000	2.068	0.80	3999.4	2.069	0.792	23.03	-17.7	-363.3
21	4000	4.137	0.00	3999.2	4.240	0.047	31.75	115.7	-177.8
22	4000	4.137	0.27	4002.8	4.263	0.270	33.10	-12.9	-22.5
23	4000	4.137	0.53	4004.3	4.093	0.534	33.38	-4.6	-157.8
24	4000	4.137	0.80	4005.3	4.080	0.826	35.72	-5.9	-390.8

Table A. 26. Static results of the grooved seal with high PSR (Continued).

#	Target			Measured					
	ω	ΔP	ϵ_0	ω	ΔP	ϵ_0	Q	φ	f_R
	[rpm]	[bar]	[-]	[rpm]	[bar]	[-]	[LPM]	[deg]	[N]
25	4000	6.205	0.00	4000.9	6.405	0.015	40.60	-30.0	-135.5
26	4000	6.205	0.27	4000.4	6.147	0.292	40.96	-13.0	-44.0
27	4000	6.205	0.53	4000.6	6.232	0.518	42.96	-1.7	-114.3
28	4000	6.205	0.80	4000.1	6.164	0.780	45.40	-6.8	-309.4
29	4000	8.274	0.00	3999.6	8.365	0.006	48.29	-177.4	-123.7
30	4000	8.274	0.27	3999.8	8.220	0.275	48.71	-12.2	-23.8
31	4000	8.274	0.53	3999.5	8.239	0.533	50.79	-2.5	-161.1
32	4000	8.274	0.80	3999.5	7.979	0.809	53.08	-4.5	-361.8
33	6000	2.068	0.00	5998.2	2.158	0.022	17.92	-171.4	-143.4
34	6000	2.068	0.27	5998.8	2.131	0.314	17.97	-10.6	-92.1
35	6000	2.068	0.53	5998.5	2.043	0.527	18.37	-3.0	-210.7
36	6000	2.068	0.80	5998.6	2.032	0.818	20.13	-4.8	-455.5
37	6000	4.137	0.00	5999.6	4.078	0.011	29.07	-98.7	-131.6
38	6000	4.137	0.27	6000.6	4.276	0.293	30.94	-10.4	36.9
39	6000	4.137	0.53	6001.3	4.086	0.537	31.19	-4.5	-80.6
40	6000	4.137	0.80	6001.3	4.133	0.789	33.12	-5.5	-305.4
41	6000	6.205	0.00	6002.2	6.165	0.045	38.90	-12.6	-174.6
42	6000	6.205	0.27	6002.1	6.182	0.286	39.29	-11.8	-56.9
43	6000	6.205	0.53	6002.9	6.244	0.541	41.55	-7.9	-177.5
44	6000	6.205	0.80	6003.1	6.222	0.789	44.08	-10.0	-401.5
45	6000	8.274	0.00	6001.4	8.205	0.007	46.74	-162.5	-125.5
46	6000	8.274	0.27	6000.8	8.278	0.274	47.78	-15.1	-84.1
47	6000	8.274	0.53	6000.3	8.233	0.544	49.69	-8.0	-230.2
48	6000	8.274	0.80	6000.0	8.129	0.791	51.77	-8.1	-450.9

Table A. 27. Static flow results of the grooved seal with high PSR.

#	PSR	OSR	Inlet Temp	Average Outlet Temp.	Re_z	Re_θ	Re
	[-]	[-]	[°C]	[°C]	[-]	[-]	[-]
1	0.535	0.238	45.3	42.2	9.37E+02	7.75E+03	7.81E+03
2	0.564	0.282	46.1	46.3	1.03E+03	7.86E+03	7.93E+03
3	0.522	0.283	47.1	47.1	9.93E+02	8.00E+03	8.06E+03
4	0.568	0.304	47.0	47.3	1.16E+03	7.99E+03	8.08E+03
5	0.720	0.268	47.4	46.8	1.46E+03	8.06E+03	8.20E+03
6	0.715	0.285	47.2	45.1	1.51E+03	8.04E+03	8.18E+03
7	0.708	0.292	45.2	46.1	1.52E+03	7.75E+03	7.90E+03
8	0.685	0.285	46.6	43.8	1.59E+03	7.94E+03	8.10E+03
9	0.856	0.252	46.6	45.1	1.80E+03	7.93E+03	8.13E+03
10	0.842	0.289	46.0	46.3	1.87E+03	7.85E+03	8.07E+03
11	0.832	0.303	46.7	47.0	1.98E+03	7.94E+03	8.19E+03
12	0.835	0.326	46.2	46.6	2.10E+03	7.87E+03	8.15E+03
13	0.997	0.245	46.8	45.1	2.18E+03	7.98E+03	8.27E+03
14	0.963	0.295	47.2	46.0	2.23E+03	8.03E+03	8.33E+03
15	0.951	0.301	46.9	46.2	2.32E+03	7.99E+03	8.32E+03
16	0.925	0.323	45.7	42.9	2.33E+03	7.81E+03	8.15E+03
17	0.376	0.216	47.5	45.7	9.65E+02	1.62E+04	1.62E+04
18	0.371	0.239	44.8	44.6	8.83E+02	1.54E+04	1.54E+04
19	0.377	0.263	46.3	47.4	9.65E+02	1.58E+04	1.58E+04
20	0.380	0.272	47.6	48.4	1.05E+03	1.62E+04	1.62E+04
21	0.447	0.218	45.2	43.3	1.39E+03	1.55E+04	1.56E+04
22	0.448	0.251	45.7	46.5	1.46E+03	1.57E+04	1.57E+04
23	0.442	0.253	46.7	47.2	1.50E+03	1.59E+04	1.60E+04
24	0.453	0.262	46.4	46.6	1.59E+03	1.59E+04	1.60E+04

Table A. 28. Static flow results of the grooved seal with high PSR (Continued).

#	PSR	OSR	Inlet Temp	Average Outlet Temp.	Re_z	Re_θ	Re
	[-]	[-]	[°C]	[°C]	[-]	[-]	[-]
25	0.536	0.231	46.4	43.6	1.81E+03	1.58E+04	1.59E+04
26	0.526	0.250	44.5	44.8	1.77E+03	1.53E+04	1.54E+04
27	0.530	0.263	45.3	46.1	1.88E+03	1.55E+04	1.56E+04
28	0.539	0.286	46.7	47.4	2.03E+03	1.59E+04	1.60E+04
29	0.600	0.236	47.0	46.3	2.18E+03	1.60E+04	1.62E+04
30	0.589	0.254	46.2	46.4	2.16E+03	1.58E+04	1.59E+04
31	0.589	0.281	46.4	46.6	2.26E+03	1.58E+04	1.60E+04
32	0.590	0.294	46.6	46.8	2.37E+03	1.59E+04	1.61E+04
33	0.339	0.225	47.0	48.0	8.07E+02	2.40E+04	2.40E+04
34	0.338	0.212	46.5	47.1	8.03E+02	2.38E+04	2.38E+04
35	0.336	0.214	46.4	47.6	8.19E+02	2.38E+04	2.38E+04
36	0.337	0.231	46.8	47.8	9.03E+02	2.39E+04	2.39E+04
37	0.362	0.214	46.4	46.2	1.29E+03	2.37E+04	2.38E+04
38	0.366	0.242	46.1	47.0	1.37E+03	2.36E+04	2.37E+04
39	0.362	0.255	46.7	47.6	1.40E+03	2.39E+04	2.39E+04
40	0.368	0.267	46.7	46.6	1.48E+03	2.39E+04	2.39E+04
41	0.398	0.227	46.4	47.2	1.74E+03	2.38E+04	2.38E+04
42	0.396	0.262	46.5	46.2	1.76E+03	2.38E+04	2.39E+04
43	0.401	0.278	46.2	47.1	1.84E+03	2.37E+04	2.37E+04
44	0.411	0.281	46.7	47.6	1.98E+03	2.39E+04	2.40E+04
45	0.438	0.220	46.0	46.7	2.07E+03	2.36E+04	2.37E+04
46	0.437	0.253	46.4	47.3	2.13E+03	2.38E+04	2.38E+04
47	0.438	0.265	46.8	47.6	2.23E+03	2.39E+04	2.40E+04
48	0.444	0.267	46.7	46.4	2.32E+03	2.39E+04	2.40E+04

Table A. 29. Stiffness coefficients and uncertainties for the grooved seal with high PSR.

#	K_{xx}	K_{xy}	K_{yx}	K_{yy}	U_{Kxx}	U_{kxy}	U_{Kyx}	U_{kyy}
	[MN/m]	[MN/m]	[MN/m]	[MN/m]	[MN/m]	[MN/m]	[MN/m]	[MN/m]
1	-0.95	-0.09	-0.76	-0.54	0.49	0.44	0.23	0.45
2	-0.64	-0.61	-1.00	0.02	1.09	0.63	0.68	0.66
3	-1.02	-0.18	-0.63	-0.34	0.74	0.54	0.52	0.41
4	-0.39	-0.47	-1.24	-0.22	0.72	0.47	0.32	0.44
5	-0.50	0.44	-1.15	-0.37	0.30	0.54	0.34	0.47
6	-0.22	0.06	-1.54	-0.20	0.75	0.36	0.42	0.45
7	-0.45	-0.34	-1.35	-0.02	0.29	0.34	0.21	0.36
8	-0.78	-0.16	-1.01	-0.27	0.56	0.39	0.29	0.39
9	-0.26	0.99	-1.82	-0.49	0.98	0.82	0.27	0.49
10	-0.02	0.28	-2.04	0.07	2.03	1.04	1.42	1.15
11	-0.11	0.15	-1.70	-0.13	0.56	0.40	0.20	0.40
12	0.01	0.12	-2.14	-0.17	0.69	0.44	0.60	0.38
13	0.17	0.81	-2.25	0.04	0.32	0.39	0.24	0.33
14	0.06	0.82	-2.04	0.01	0.52	1.49	0.66	1.61
15	0.39	0.26	-2.46	0.10	0.38	0.40	0.18	0.38
16	0.05	0.17	-1.95	0.00	0.41	0.45	0.20	0.33
17	-0.96	0.37	-0.99	-0.76	0.31	0.49	0.25	0.40
18	-0.94	0.32	-1.08	-0.59	0.33	0.65	0.16	0.29
19	-0.97	0.11	-1.07	-0.55	0.31	0.38	0.27	0.43
20	-0.87	-0.08	-0.92	-0.69	0.33	0.35	0.20	0.36
21	-0.75	0.38	-1.29	-0.53	0.29	0.55	0.25	0.26
22	-0.71	0.38	-1.30	-0.47	0.34	0.39	0.21	0.38
23	-0.85	0.17	-1.18	-0.58	0.44	0.39	0.45	0.39
24	-0.92	-0.14	-1.05	-0.56	0.33	0.41	0.36	0.41

Table A. 30. Stiffness coefficients and uncertainties for the grooved seal with high PSR (Continued).

#	K_{xx}	K_{xy}	K_{yx}	K_{yy}	U_{Kxx}	U_{kxy}	U_{Kyx}	U_{kyy}
	[MN/m]	[MN/m]	[MN/m]	[MN/m]	[MN/m]	[MN/m]	[MN/m]	[MN/m]
25	-0.31	0.51	-1.89	-0.17	0.85	0.82	0.59	0.68
26	-0.64	0.28	-1.45	-0.35	0.36	0.37	0.23	0.33
27	-0.55	0.23	-1.49	-0.38	0.43	0.54	0.39	0.49
28	-0.63	-0.11	-1.31	-0.49	0.86	0.53	0.66	0.47
29	-0.17	0.88	-1.93	-0.18	0.52	0.50	0.28	0.39
30	-0.10	0.66	-1.97	-0.31	0.52	0.39	0.49	0.35
31	-0.48	0.44	-1.82	-0.39	1.01	0.50	0.69	0.37
32	-0.27	0.01	-1.68	-0.58	0.41	0.50	0.18	0.31
33	-1.36	0.88	-1.18	-1.00	0.43	0.61	0.43	0.52
34	-1.41	0.89	-1.27	-0.98	0.36	0.53	0.20	0.43
35	-1.20	0.93	-1.44	-1.15	0.53	0.54	0.41	0.48
36	-1.55	0.45	-1.24	-1.18	0.45	0.43	0.25	0.36
37	-1.21	1.02	-1.72	-1.00	0.35	0.52	0.36	0.49
38	-1.20	0.46	-1.46	-0.89	0.29	0.42	0.39	0.22
39	-0.87	0.68	-1.69	-1.06	0.42	0.37	0.44	0.29
40	-0.87	0.72	-1.51	-1.08	0.56	0.46	0.52	0.37
41	-0.79	0.82	-1.89	-0.64	0.42	0.47	0.35	0.34
42	-0.64	0.80	-1.92	-0.90	0.36	0.37	0.43	0.31
43	-0.85	0.55	-1.84	-0.95	0.40	0.38	0.28	0.34
44	-1.00	0.66	-1.58	-1.01	0.24	0.41	0.20	0.35
45	-0.63	1.18	-1.95	-0.70	0.21	0.44	0.27	0.31
46	-0.33	0.84	-2.22	-0.64	0.29	0.38	0.32	0.27
47	-0.73	1.04	-1.82	-1.06	0.29	0.43	0.18	0.42
48	-0.66	0.69	-1.86	-1.04	0.38	0.43	0.25	0.37

Table A. 31. Damping coefficients and uncertainties for the grooved seal with high PSR.

#	C_{xx}	C_{xy}	C_{yx}	C_{yy}	U_{Cxx}	U_{Cxy}	U_{Cyx}	U_{Cyy}
	[MN-s/m]	[MN-s/m]	[MN-s/m]	[MN-s/m]	[MN-s/m]	[MN-s/m]	[MN-s/m]	[MN-s/m]
1	6.44	-0.10	-3.10	5.66	1.40	1.25	0.88	0.84
2	7.18	-0.59	-3.60	6.09	0.84	1.46	0.85	0.99
3	6.74	-0.50	-3.42	5.62	1.63	1.25	1.20	0.89
4	6.48	-0.71	-3.66	5.67	2.45	1.84	1.80	1.49
5	7.91	-0.38	-3.89	6.81	1.98	1.91	1.36	1.41
6	8.13	-0.52	-4.01	7.12	1.15	1.30	0.93	1.13
7	8.05	-0.44	-4.30	6.96	0.98	1.31	0.77	1.29
8	8.05	-0.72	-4.52	6.74	1.09	1.40	0.84	1.25
9	9.02	-0.22	-4.64	7.67	2.67	2.25	1.86	1.61
10	7.16	0.91	-2.72	6.50	5.49	4.31	5.60	4.13
11	8.76	-0.13	-4.69	7.50	1.83	1.61	1.48	1.38
12	8.51	-0.14	-5.18	6.72	2.65	1.88	1.55	1.58
13	9.73	-0.22	-4.68	8.53	1.23	1.35	0.69	1.14
14	8.70	0.73	-3.85	7.42	3.54	2.71	3.73	2.65
15	9.63	-0.30	-5.50	8.03	1.49	1.46	0.97	1.28
16	8.89	0.54	-5.57	6.82	1.18	1.36	0.85	1.06
17	8.52	0.12	-5.97	6.79	1.06	1.63	0.75	1.24
18	7.77	0.74	-5.55	6.09	1.00	1.20	0.96	1.12
19	7.68	1.01	-5.92	6.06	0.75	1.42	0.70	1.12
20	7.61	0.38	-6.60	6.35	0.95	1.82	0.95	1.41
21	9.20	0.63	-6.27	7.41	0.98	1.19	0.92	1.07
22	9.53	0.26	-6.60	7.84	1.18	1.90	0.96	1.40
23	9.56	0.24	-6.64	7.56	1.35	1.97	0.78	1.30
24	9.88	-0.02	-7.83	7.30	1.26	2.04	1.10	1.54

Table A. 32. Damping coefficients and uncertainties for the grooved seal with high PSR (Continued).

#	C_{xx}	C_{xy}	C_{yx}	C_{yy}	U_{Cxx}	U_{Cxy}	U_{Cyx}	U_{Cyy}
	[MN-s/m]	[MN-s/m]	[MN-s/m]	[MN-s/m]	[MN-s/m]	[MN-s/m]	[MN-s/m]	[MN-s/m]
25	9.60	1.18	-6.14	7.97	1.31	1.55	1.03	1.23
26	9.46	1.50	-6.10	7.65	1.20	1.56	0.63	1.12
27	9.88	1.57	-6.64	7.59	1.50	1.46	1.05	1.19
28	9.61	1.50	-7.24	7.09	1.02	1.60	0.71	1.19
29	10.51	1.12	-6.43	8.57	1.85	2.11	1.32	1.44
30	10.40	1.43	-6.55	8.25	1.51	1.45	0.75	1.12
31	10.45	1.40	-7.06	8.07	1.79	1.96	1.09	1.33
32	9.90	1.99	-7.66	7.03	1.34	1.56	0.86	1.25
33	7.63	2.71	-6.88	5.17	0.77	1.20	0.45	0.56
34	7.42	2.69	-6.75	5.24	0.67	1.14	0.69	0.67
35	8.42	1.76	-7.76	6.04	0.88	1.50	0.89	0.97
36	8.66	1.66	-9.04	6.57	1.07	1.90	1.10	1.33
37	11.11	1.46	-8.32	8.54	1.24	2.01	0.74	1.68
38	11.39	1.97	-9.06	7.82	1.75	2.03	1.14	1.40
39	11.29	1.01	-9.34	8.13	1.53	2.63	1.19	1.96
40	11.08	1.91	-10.61	7.18	1.78	2.26	1.35	1.63
41	11.74	2.24	-9.03	8.27	1.04	1.52	0.91	1.01
42	11.70	2.08	-9.24	8.24	1.53	2.23	0.87	1.32
43	10.78	2.95	-8.81	7.56	1.12	1.91	0.68	1.17
44	9.51	3.28	-9.01	6.82	0.83	1.52	0.53	1.10
45	10.76	2.82	-7.86	8.35	0.62	1.49	0.39	1.03
46	10.89	3.32	-8.28	8.21	1.13	1.53	0.62	1.09
47	10.60	3.15	-8.71	8.17	0.79	1.43	0.51	1.16
48	10.32	3.56	-9.40	7.20	0.88	1.62	0.51	1.25

Table A. 33. Virtual mass coefficients and uncertainties for the grooved seal with high PSR.

#	M_{xx}	M_{xy}	M_{yx}	M_{yy}	U_{Mxx}	U_{Mxy}	U_{Myx}	U_{Myy}
	[kg]	[kg]	[kg]	[kg]	[kg]	[kg]	[kg]	[kg]
1	14.26	-1.81	-1.96	13.63	0.74	0.66	0.34	0.69
2	14.79	-2.58	-2.33	14.90	1.65	0.96	1.03	1.00
3	13.75	-2.13	-1.79	14.93	1.10	0.80	0.78	0.62
4	15.23	-2.71	-2.20	17.97	1.09	0.72	0.48	0.66
5	15.18	-1.74	-2.00	14.92	0.45	0.82	0.51	0.72
6	15.58	-1.82	-2.31	15.42	1.14	0.54	0.63	0.68
7	15.49	-2.28	-2.10	16.70	0.44	0.52	0.31	0.54
8	15.35	-2.32	-1.41	18.31	0.84	0.58	0.44	0.58
9	15.67	-1.80	-2.87	15.30	1.33	1.12	0.36	0.67
10	15.98	-1.85	-2.36	15.91	2.98	1.53	2.09	1.69
11	16.42	-2.64	-1.99	17.83	0.84	0.60	0.30	0.61
12	17.09	-2.87	-2.49	20.13	1.04	0.67	0.92	0.58
13	16.26	-1.78	-2.39	16.16	0.49	0.58	0.36	0.50
14	15.85	-1.23	-1.55	15.78	0.73	2.10	0.93	2.27
15	17.02	-2.40	-2.02	18.55	0.58	0.61	0.28	0.58
16	17.04	-2.16	-1.49	19.88	0.60	0.65	0.29	0.48
17	13.36	-2.94	-1.97	13.94	0.44	0.71	0.36	0.58
18	13.18	-2.29	-1.92	13.89	0.48	0.94	0.23	0.42
19	14.15	-2.50	-1.47	15.22	0.45	0.54	0.39	0.62
20	14.49	-2.92	-0.93	17.81	0.47	0.49	0.28	0.51
21	15.35	-2.90	-2.18	15.49	0.41	0.77	0.35	0.37
22	15.30	-3.18	-2.12	16.21	0.49	0.55	0.30	0.53
23	15.14	-3.80	-2.06	17.23	0.63	0.54	0.63	0.55
24	15.56	-4.86	-1.70	20.64	0.47	0.57	0.50	0.58

Table A. 34. Virtual mass coefficients and uncertainties for the grooved seal with high PSR (Continued).

#	M_{xx}	M_{xy}	M_{yx}	M_{yy}	U_{Mxx}	U_{Mxy}	U_{Myx}	U_{Myy}
	[kg]	[kg]	[kg]	[kg]	[kg]	[kg]	[kg]	[kg]
25	16.15	-2.53	-2.84	16.17	1.24	1.18	0.86	0.98
26	15.91	-2.98	-1.98	16.63	0.51	0.53	0.32	0.47
27	15.97	-2.96	-1.91	17.30	0.60	0.77	0.54	0.68
28	16.21	-3.68	-1.40	19.76	1.21	0.75	0.93	0.67
29	16.24	-2.43	-2.04	16.50	0.76	0.72	0.41	0.56
30	16.73	-2.90	-2.13	17.08	0.75	0.57	0.71	0.51
31	15.64	-2.96	-1.41	18.15	1.43	0.70	0.97	0.52
32	17.16	-3.62	-1.79	20.35	0.58	0.70	0.25	0.44
33	11.32	-1.77	-2.06	11.70	0.62	0.88	0.62	0.75
34	11.14	-1.82	-1.86	12.08	0.51	0.75	0.29	0.61
35	11.68	-3.11	-1.87	13.71	0.75	0.77	0.58	0.67
36	11.76	-4.20	-1.42	17.69	0.64	0.61	0.35	0.51
37	14.46	-4.14	-2.40	15.35	0.51	0.76	0.52	0.71
38	15.12	-5.56	-2.69	16.99	0.42	0.61	0.57	0.32
39	16.08	-5.86	-3.20	18.31	0.58	0.52	0.61	0.40
40	17.21	-6.08	-3.04	20.89	0.80	0.67	0.75	0.53
41	16.58	-4.70	-3.29	17.03	0.60	0.68	0.51	0.49
42	16.84	-4.80	-3.20	17.18	0.52	0.53	0.63	0.44
43	16.43	-4.23	-2.57	17.74	0.58	0.56	0.41	0.49
44	16.07	-3.08	-1.43	19.29	0.35	0.60	0.29	0.51
45	15.55	-2.49	-2.15	16.00	0.31	0.63	0.39	0.45
46	16.47	-3.31	-2.13	16.52	0.42	0.55	0.46	0.39
47	16.10	-2.67	-1.56	17.32	0.42	0.63	0.27	0.60
48	16.72	-3.42	-1.55	19.84	0.55	0.63	0.37	0.54

Table A. 35. WFR, K_{eff}, C_{eff}, and uncertainties for the grooved seal with high PSR.

#	ω	ΔP	ϵ_0	*WFR*	U_{WFR}	*Keff*	U_{Keff}	C_{eff}	U_{Ceff}
	[rpm]	[bar]	[-]	[kg]	[kg]	[MN/m]	[MN/m]	[kN-s/m]	[kN-s/m]
1	2000	2.068	0.00	0.00	0.00	-1.69	0.27	4.02	1.43
2	2000	2.068	0.27	0.00	0.00	-1.39	0.25	2.78	2.31
3	2000	2.068	0.53	0.00	0.00	-1.72	0.37	4.24	2.02
4	2000	2.068	0.80	0.00	0.00	-1.49	0.32	1.98	1.98
5	2000	4.137	0.00	0.48	0.32	-1.54	0.40	3.57	1.95
6	2000	4.137	0.27	0.20	0.59	-1.36	0.31	3.82	1.54
7	2000	4.137	0.53	0.00	0.00	-1.43	0.29	3.47	1.26
8	2000	4.137	0.80	0.00	0.00	-1.81	0.26	4.61	1.43
9	2000	6.205	0.00	0.79	0.37	-1.56	0.32	1.63	2.59
10	2000	6.205	0.27	0.55	1.06	-0.86	0.35	1.29	5.44
11	2000	6.205	0.53	0.31	0.41	-1.37	0.35	3.70	1.56
12	2000	6.205	0.80	0.34	0.64	-1.45	0.35	2.21	2.36
13	2000	8.274	0.00	0.73	0.19	-1.12	0.40	1.82	1.37
14	2000	8.274	0.27	0.78	0.75	-0.99	0.32	1.24	4.47
15	2000	8.274	0.53	0.45	0.36	-1.14	0.43	2.33	1.44
16	2000	8.274	0.80	0.37	0.48	-1.31	0.29	2.78	1.42
17	4000	2.068	0.00	0.20	0.15	-4.48	0.31	6.03	1.05
18	4000	2.068	0.27	0.20	0.23	-4.15	0.28	5.26	1.09
19	4000	2.068	0.53	0.11	0.25	-4.36	0.40	5.46	0.87
20	4000	2.068	0.80	0.00	0.00	-4.92	0.44	5.79	0.98
21	4000	4.137	0.00	0.21	0.16	-4.53	0.27	6.32	1.02
22	4000	4.137	0.27	0.20	0.11	-4.69	0.34	6.68	1.06
23	4000	4.137	0.53	0.12	0.16	-4.90	0.42	6.95	1.17
24	4000	4.137	0.80	0.00	0.00	-5.57	0.41	7.17	1.18

Table A. 36. WFR, K_{eff}, C_{eff}, and uncertainties for the grooved seal with high PSR (Continued).

#	ω	ΔP	ϵ_0	*WFR*	U_{WFR}	*Keff*	U_{Keff}	C_{eff}	U_{Ceff}
	[rpm]	[bar]	[-]	[kg]	[kg]	[MN/m]	[MN/m]	[kN-s/m]	[kN-s/m]
25	4000	6.205	0.00	0.27	0.23	-4.12	1.11	5.92	1.50
26	4000	6.205	0.27	0.18	0.13	-4.32	0.91	6.49	0.97
27	4000	6.205	0.53	0.17	0.19	-4.44	0.82	6.69	1.24
28	4000	6.205	0.80	0.00	0.00	-4.92	1.04	6.64	1.28
29	4000	8.274	0.00	0.34	0.11	-4.16	1.18	6.19	1.36
30	4000	8.274	0.27	0.30	0.10	-4.24	1.27	6.19	1.20
31	4000	8.274	0.53	0.24	0.15	-4.58	1.27	6.56	1.51
32	4000	8.274	0.80	0.04	0.84	-4.90	1.06	6.45	1.11
33	6000	2.068	0.00	0.26	0.11	-7.03	1.00	4.76	0.76
34	6000	2.068	0.27	0.28	0.10	-7.05	1.31	4.61	0.65
35	6000	2.068	0.53	0.28	0.10	-8.07	1.42	5.34	0.85
36	6000	2.068	0.80	0.17	0.09	-9.49	1.44	6.26	0.94
37	6000	4.137	0.00	0.23	0.07	-9.14	1.21	7.65	1.16
38	6000	4.137	0.27	0.14	0.07	-9.61	1.29	8.08	1.21
39	6000	4.137	0.53	0.19	0.07	-10.38	1.10	7.83	1.33
40	6000	4.137	0.80	0.20	0.09	-11.23	1.07	7.36	1.33
41	6000	6.205	0.00	0.21	0.07	-9.49	0.97	7.84	0.86
42	6000	6.205	0.27	0.21	0.06	-9.74	1.40	7.81	1.11
43	6000	6.205	0.53	0.18	0.07	-9.49	1.26	7.27	0.90
44	6000	6.205	0.80	0.21	0.07	-9.79	1.08	6.39	0.78
45	6000	8.274	0.00	0.26	0.06	-8.47	1.18	7.07	0.72
46	6000	8.274	0.27	0.23	0.06	-8.56	0.81	7.11	0.88
47	6000	8.274	0.53	0.24	0.06	-9.24	0.82	7.11	0.80
48	6000	8.274	0.80	0.21	0.07	-9.90	0.93	6.73	0.86

Measurement vs. Predictions

Table A. 37 – Stiffness coefficient measurement-vs.-prediction % deviation values

#	ω	ΔP	ϵ_0	Measurement-vs.-prediction % deviation			
				K_{xx}	K_{xy}	K_{yx}	K_{yy}
	[rpm]	[bar]	[-]	--	--	--	--
1	2000	2.068	0.00	93.64	93.89	142.06	106.72
2	2000	4.137	0.00	90.40	97.20	147.94	114.22
3	2000	6.205	0.00	90.72	74.57	96.24	37.37
4	2000	8.274	0.00	87.51	91.94	118.44	17.65
5	4000	2.068	0.00	113.18	76.11	45.48	97.08
6	4000	4.137	0.00	91.45	27.94	78.50	239.07
7	4000	6.205	0.00	87.61	86.52	84.10	159.70
8	4000	8.274	0.00	85.50	88.78	82.38	410.91
9	6000	2.068	0.00	538.98	66.22	38.99	72.86
10	6000	4.137	0.00	119.22	61.66	47.36	89.43
11	6000	6.205	0.00	100.92	72.52	43.10	99.36
12	6000	8.274	0.00	89.54	69.11	66.80	111.37

Table A. 38 – Damping coefficient measurement-vs.-prediction % deviation values

#	ω	ΔP	ϵ_0	Measurement-vs.-prediction % deviation			
				C_{xx}	C_{xy}	C_{yx}	C_{yy}
	[rpm]	[bar]	[-]	--	--	--	--
1	2000	2.068	0.00	82.00	41.95	72.50	73.43
2	2000	4.137	0.00	77.30	2241.90	59.53	69.05
3	2000	6.205	0.00	72.91	346.57	55.57	63.74
4	2000	8.274	0.00	70.04	1474.06	54.71	60.06
5	4000	2.068	0.00	72.45	48.37	80.98	56.79
6	4000	4.137	0.00	78.55	27.98	79.39	66.48
7	4000	6.205	0.00	78.73	17.27	68.87	69.25
8	4000	8.274	0.00	78.67	66.88	62.35	69.06
9	6000	2.068	0.00	60.96	52.96	74.42	26.67
10	6000	4.137	0.00	71.83	54.29	81.87	53.89
11	6000	6.205	0.00	69.79	58.87	79.23	54.22
12	6000	8.274	0.00	74.53	23.67	76.93	62.16

Table A. 39 – Virtual mass coefficient measurement-vs.-prediction % deviation values

#	ω	ΔP	ϵ_0	Measurement-vs.-prediction % deviation			
				M_{xx}	M_{xy}	M_{yx}	M_{yy}
	[rpm]	[bar]	[-]	--	--	--	--
1	2000	2.068	0.00	49.55	--	--	47.28
2	2000	4.137	0.00	45.26	--	--	41.63
3	2000	6.205	0.00	46.48	--	--	41.48
4	2000	8.274	0.00	45.62	--	--	42.42
5	4000	2.068	0.00	59.41	--	--	57.57
6	4000	4.137	0.00	62.69	--	--	62.46
7	4000	6.205	0.00	58.87	--	--	57.95
8	4000	8.274	0.00	57.48	--	--	56.18
9	6000	2.068	0.00	61.87	--	--	59.87
10	6000	4.137	0.00	69.73	--	--	66.89
11	6000	6.205	0.00	68.54	--	--	65.89
12	6000	8.274	0.00	66.51	--	--	64.19

APPENDIX B

UNCERTAINTY ANALYSIS

The author used the same testing apparatus, instrumentation, procedure, and data analysis tools that Alex J. Moreland used in his test program [25]. Consequently, the author uses Moreland's same uncertainty analysis, adapting it, where needed, to the current study as follows:

"Instrument error is assumed to be negligible and only repeatability is calculated for the uncertainty of measurements. A 95% confidence interval is used to calculate the uncertainties for static measurements and the dynamic stiffness values. The true mean, μ, of a set of sample measurements, x_i, lies within the confidence interval

$$\tilde{x} - t_{\alpha/2,v}\frac{S_x}{\sqrt{n}} < \mu < \tilde{x} + t_{\alpha/2,v}\frac{S_x}{\sqrt{n}} \quad \text{(B.1)}$$

where $\tilde{x}$ is the sample mean, $t_{\alpha/2,v}$ is the Student's t-distribution value, the level of significance is $\alpha = 1 - c$, c = 0.95 is the level of confidence, the degrees of freedom are v = 1 - n, and n is the number of samples. The standard deviation is

$$S_x = \sqrt{\left(\frac{\sum_{i=1}^{n} x_i^2 - n\bar{x}^2}{n-1}\right)} \quad \text{(B.2)}$$

Recalling Eqs.(17)-(20) of Section 4.3 (Measuring Impedances) used to calculated the rotordynamic coefficients from curve fits to the dynamic stiffness data, the confidence intervals on the rotordynamic coefficients are determined using a statistical test described in [23]. The true slope of a least-squares regression lies within the c% confidence interval

$$b \pm t_{\alpha/2,v}\frac{S_{y/x}}{S_{xx}} \quad \text{(B.3)}$$

where the standard error of the y-data about the curve fit is

$$S_{y/x} = \left(\frac{1}{n-2}\sum_{i=1}^{n}[y_i - y(x_i)]^2\right) \quad \text{(B.4)}$$

and the total squared variation of the independent variable, x_i, is

$$S_{xx}^2 = \sum_{i=1}^{n}(x_i - \bar{x})^2 \quad \text{(B.5)}$$

Finally, the true intercept lies within the interval

$$a \pm t_{\alpha/2,v} S_{y/x}\sqrt{\frac{1}{n} + \frac{\overline{x^2}}{S_{xx}^2}} \quad \text{(B.6)}$$

Confidence intervals of the rotordynamic coefficients are propagated into the confidence intervals on the WFR, K_{eff} and C values. Uncertainty propagation is defined as"

$$u_y = \sqrt{\left(\frac{\partial y}{\partial x_1}u_1\right)^2 + \left(\frac{\partial y}{\partial x_2}u_2\right)^2 + \cdots + \left(\frac{\partial y}{\partial x_n}u_n\right)^2} \quad \text{(B.7)}$$